CRACK INITIATION AND GROWTH BEHAVIOR AT CORROSION PIT IN 7075-T6 HIGH STRENGTH ALUMINUM ALLOY

THESIS

Eric M. Hunt, Second Lieutenant, USAF

AFIT-ENY-13-J-01

DEPARTMENT OF THE AIR FORCE
AIR UNIVERSITY

AIR FORCE INSTITUTE OF TECHNOLOGY

Wright-Patterson Air Force Base, Ohio

The views expressed in this thesis are those of the author and do not reflect the official policy or position of the United States Air Force, the Department of Defense, or the United States Government.

AFIT-ENY-13-J-01

CRACK INITIATION AND GROWTH BEHAVIOR AT CORROSION PIT IN 7075-T6 HIGH STRENGTH ALUMINUM ALLOY

THESIS

Presented to the Faculty

Department of Aerospace and Astronautical Engineering

Graduate School of Engineering and Management

Air Force Institute of Technology

Air University

Air Education and Training Command

in Partial Fulfillment of the Requirements for the

Degree of Master of Science in Materials Science

Eric M. Hunt, B.S.

Second Lieutenant, USAF

June 2013

AFIT-ENY-13-J-01

CRACK INITIATION AND GROWTH BEHAVIOR AT CORROSION PIT IN 7075-T6 HIGH STRENGTH ALUMINUM ALLOY

Eric M. Hunt, B.S.
Second Lieutenant, USAF

Approved:

Shankar N. Mall, PhD (Chairman)	Date
Lt Col Timothy C. Radsick, PhD (Member)	Date
Vinod K. Jain, PhD (Member)	Date

AFIT-ENY-13-J-01

Abstract

Research on fatigue crack formation from two types corrosion pits tangent to a circular hole in a 7075-T6 aluminum alloy subjected to uni-axial loads ($R = 0.5$, $\lambda = 0$) in both an air and saltwater environment provides a method for exploring crack initiation and initial growth rates. This work focuses on a fracture mechanics approach to explore the transition from corrosion pit to crack growth. Specimens with a cylinder shaped through-pit tangent to a circular hole have a closed form solution to predict this ΔK that closely resembles the finite element solutions. Specimens with a semi-circular corner-pit tangent to hole lack a closed form solution and finite element modeling was used to determine ΔK of these specimens. Optical and electron microscopy provided an accurate way to measure and observe the crack growth rate ($\frac{da}{dN}$) and the cycles until initiation of the fatigue cracks. This research shows that corner-pit specimens initially have a slower crack growth rate than through-pit specimens due to the propagation of a quarter-circular crack front through the thickness of the sample. After initial crack growth, both corner-pit and through-pit samples have the same growth rate as their machine notched counterparts exposed air and saltwater environments.

Acknowledgments

I would like to acknowledge the Office of Corrosion policy and Oversight, OSD, Washington DC for their support in this work. I would also like to thank Dr. Volodymyr Sabelkin for taking the time to show me how to properly prepare specimens and execute fatigue experiments, Dr. Victor Perel for his help in developing the finite element models, and Dr. Heath Misak for showing me how to capture the beautiful SEM images of the fatigue specimens. I would also like to acknowledge Jay Anderson, Barry Page, and Christopher Zickefoose for their expertise in using the laboratory equipment. Brian Crabtree provided excellent machine shop support. I also greatly appreciate the knowledge and guidance provided by Dr. Shankar Mall.

Eric M. Hunt

Table of Contents

Page

List of Figures

List of Tables

List of Symbols

Symbol	Definition
Q	charge (coulombs)
F	Faraday's Constant (C/mol)
Δ	change in a variable (unit less)
n	number of moles (moles)
I	current (amps)
E	electric potential (volts)
R	universal gas constant ($\frac{J}{Kmol}$)
T	temperature (Kelvin)
$Q_{reaction}$	reaction quotient (unit less)
K	stress intensity factor ($MPa * m^{\frac{1}{2}}$)
σ	stress (MPa)
a	crack length (meters)
C	constant for Paris law (unit less)
$\frac{da}{dN}$	rate of crack growth per cycle (unit less)
R	ratio of minimum to maximum loads (unit less)
b	width of specimen (mm)
t	thickness of specimen (mm)
P	applied load (Newtons)
c	hole radius (mm)
F	applied load (Newtons)
w	width of specimen (mm)

Subscripts

Symbol	Definition
cell	electrochemical cell
cathode	cathodic reaction
anode	anodic reaction
1	mode one (opening)
max	maximum load values
min	minimum load values
t	designates stress concentration factor

Superscripts

n+	cathode
−	anode
∘	initial state of reaction
m	constant for Paris law (unit less)

CRACK INITIATION AND GROWTH BEHAVIOR AT CORROSION PIT
IN 7075-T6 HIGH STRENGTH ALUMINUM ALLOY

I. Introduction

1.1 Corrosion and Fatigue Concerns

Corrosion is an indiscriminate problem in nearly all industries and infrastructures. From ships to aircraft and everywhere in between, corrosion plays constant role in the efficiency, cost, and longevity of any given platform/system. Corrosion costs the United States approximately 3.1% of its GNP yearly, roughly $276 billon [36]. This estimate, though impressive, ignores the immeasurable cost loss of life resulting from the effects of corrosion. Damage is not limited to the humans that use these structures, but also applies to the overall ecosystem or environment surrounding these structures. Structures that corrode and leak hazardous material into the environment present a danger that may have consequences for many years. Physical effects from corrosion on infrastructure ranges from aestheic concerns to flaws that can cause unexpected failures. It is a topic of great concern for nearly every industry as shown in Fig. 1.1.

The United States Air Force also has a great deal of interest in the effects and implications of corrosion because they must extend the service life of the current fleet and associated infrastructure, while at the same time, reducing operating costs. However, corrosion is not the only area of concern for fleet reliability and longevity. Fatigue, including corrosion assisted fatigue, is also of great concern because aircraft are dynamic structures which experience many load cycles.

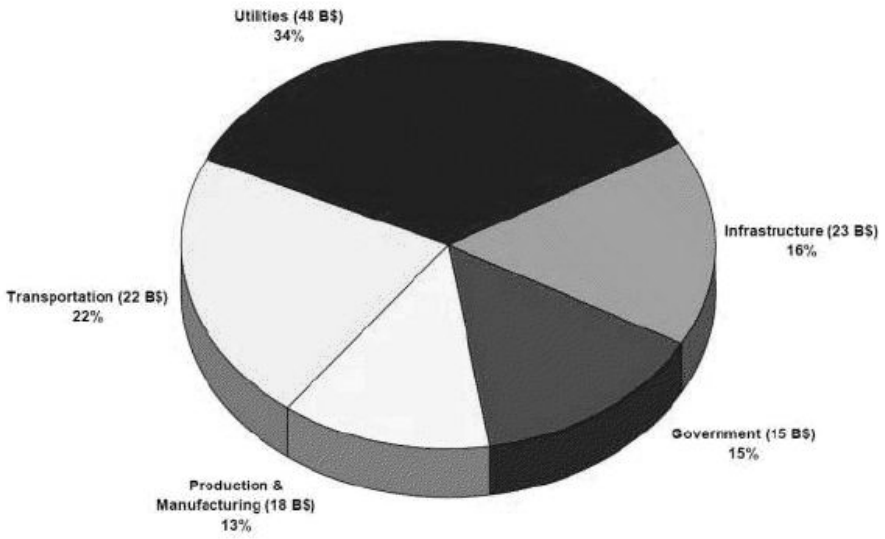

Figure 1.1: Cost of corrosion across many industrial sectors. [36]

Fatigue is defined as the damage and fracture of materials exposed to cyclic or repeated loads [3]. This cyclic loading causes fatigue cracks to nucleate and grow in the material until the strength is reduced to a point of failure [12]. Fatigue is great concern because often fatigue cracks are not readily detected until a failure occurs. Fatigue is such a highly studied area of research that the American Society for Testing and Materials have published over 25 volumes with regard to fracture and over half of them dealt with fatigue [3]. A proper understanding of the mechanisms of corrosion and fatigue life is essential for aircraft survivability because this information is vital in determining accurate service intervals, as well as reliable total life estimates for the aircraft. Currently, the service intervals for corrosion/ crack growth are too conservative for some platforms and too aggressive for others. An overly conservative service plan results in excessive cost while an aggressive service plan may result in unsafe operating conditions. Therefore, it is crucial to have an understanding of corrosion and its components of pitting, crack initiation, and crack growth

along with an understanding of fatigue to give an accurate estimate of the factors that affect aircraft lifetimes.

While corrosion itself is a very important issue, corrosion in combination with fatigue, which is commonly known as corrosion fatigue, draws an even greater amount of interest. During all active portions of an aircraft's life, it experiences fatigue. Takeoff and landing generally have the largest loads, while in flight, the aircraft experiences smaller cyclical loads for extended periods of time. Assuming atmospheric flight, the aircraft is in a corrosive environment during the entirety of the cyclical loads [29]. As a result, the interaction between the environment and the fatigue life of a structure is of great importance. It is understood that a corrosive environment reduces the fatigue life of structural materials, but the specifics associated with each material have yet to be fully explored.

1.2 Types of Corrosion

Failure due to corrosion occurs in a variety of different ways. Corrosion is generally broken down into generalized and localized corrosion conditions. Generalized corrosion attacks the entire surface of a structure in a uniform manner. This type of corrosion is seen many instances, such as the Statue of Liberty. The uniform green hue results from the oxidation of the copper structure. Uniform corrosion results in a loss of mass in the structure which has the potential to weaken the structure to the point of failure over time. In general, however, this corrosion is easily monitored to avoid sudden failures.

In addition to general corrosion, corrosion also occurs in a localized manner [36]. Localized corrosion is corrosion that occurs in a non-uniform manner in discrete sections of a structure. As a result, some portions of the structure are weakened while others remain at full strength. Pitting, crevice corrosion, inter-granular corrosion, and galvanic corrosion are different forms of localized corrosion. This type of degradation is particularly dangerous because it is difficult to detect these flaws as they can be very small and/or hidden beneath

the surface [36]. These localized flaws often lead to stress corrosion cracking (SCC) or corrosion fatigue because they act as a flaw that increases the stress intensity factor in the material. As the stress intensity factor increases, the fatigue life decreases. As a result, local corrosion can reach critical dimensions before detection which may ultimately lead to failure. The focus of this research is the effect of localized corrosion (pitting) on the nucleation and growth of fatigue cracks.

1.3 Background

A great deal of fatigue and corrosion research has been conducted with all structural materials [23]. However, many of these materials (i.e. iron, brass, etc.) have a very small impact in the aerospace industry. In other words, their usage is limited in aerospace systems, which at present are primarily composed of aluminum and its various compositions. Not only does aluminum make up a large percentage of an aircraft's structure, but it also demonstrates unique behavior when subjected to cyclic loading. Most importantly, unlike steels, aluminum has no fatigue limit and under cyclical loading, its fatigue strength continues to decrease until failure [12]. This is important for aircraft aluminum alloys because, as previously mentioned, they are constantly exposed to cyclic loading. Consequently, a great deal of research involves corrosion and/or fatigue in aluminum alloys. Much of this research deals with the growth of fatigue cracks after they formed from the corrosion sites– research pioneered by McEvily. McEvily focused on the propagation of fatigue cracks in various aluminum alloys and helped to formulate the Paris law of fracture mechanics [24]. He, along with Endo, researched methods of predicting crack growth behavior in materials [14]. Forman studied the fatigue crack growth initiating from flaws. He successfully determined, that fatigue cracks do originate from natural or man-made flaws in the material. He also determined that the stress intensity range, as discussed in Chapter II, is the main contributor in determining crack growth [15].

Along with fracture mechanics research, a great deal of research has been conducted with regard to corrosion and pitting. The formation of pitting due to corrosion may seem more like an art than a science at times because of the large number of variables that are at play in this process. Szklarska-Smialowska defines the four stages of pit growth as: "(1) processes occurring on the passive film, (2) processes occurring within the passive film, (3) formation of so-called metastable pits and (4) stable pit growth" [39]. She then explored the specific electro-chemistry involved in various structural aluminum alloys. Similarly, Wei, studied how pits are created in aluminum alloys in addition to the reactions involved in the formations of these pits [44]. Additionally, there has been a great deal of research conducted on the effects of salt sprays on structural materials. While the present study in corrosion did not specifically investigate corrosion pit life, there are a large number of studies that have investigated the relationship between corrosion and fatigue life.

While it is important to know about fatigue and corrosion individually, it is especially useful to explore how both processes work together during crack growth. Research from numerous research laboratories used aircraft-type loading (tension-tension loading) to determine that, not surprisingly, fatigue life decreases in the presence of a corrosive environment [13, 19, 23, 37, 46]. While this information is useful, these studies focus primarily on the crack growth after the initiation of a man-made crack. In other words, they focus on the crack growth after the crack has formed. Some research in this area has been conducted, but the extent of this research is limited with respect to a fracture mechanics approach.

The transition from pit to fatigue crack is a very important area of research because it connects the information about fatigue crack growth in terms of fracture mechanics to the formation of corrosion pits in terms of an electro-chemical research. Some notable research on this topic comes from Burns et al. They used extensive scanning electron microscopy to investigate the transition from pit to crack growth in aircraft grade aluminum

alloys. They attributed crack growth to the presence of small stress concentrations that exist within the pit [5]. Similar research was conducted by Kim et al. [22]. The results from this research showed that the shape of the micro-pits has a great deal to do with the formation of cracks in aluminum [22]. Both of these studies involved the use of marker bands (a change in load ratio to create lines on fracture surface) and of scanning electron microscopes to examine this pit-to-crack transition. Besides these studies, there have been several studies where crack initiation from a corrosion pit or multiple pits have been studied [5, 6, 8, 9, 16, 22, 26, 28, 37, 43, 45] In these studies, fracture mechanics has not been used. As an example, Lee et al. studied the growth rates from a corner pit on a hole and the cycles required to create a crack of 1 mm [25]. In this research, however, Lee et al. only used fracture mechanics to estimate initial the ΔK values. The rest of the crack growth is given only as a function of the number load cycles. As result, there is a need to investigate not only the transition from corrosion pit to fatigue crack growth, but to also investigate this transition using fracture mechanics principles at every step of the process.

1.4 Problem Statement

An understanding of the transition from a corrosion pit to a fatigue crack is necessary to determine what mechanisms are responsible for this progression. This is the area of focus for the present study. With a great deal of research already completed individually for crack growth and for pit formation, further research is required to better understand the interactions between these two phenomena using the fracture mechanics principles, as such an understanding is presently lacking. Also, more research is required to understand the crack growth in specimens that contain pits located at holes in the specimen. This type of testing mimics real-world scenarios because a high percentage of aircraft panels have rivet holes [7]. To fill this void in research, aluminum specimens measuring approximately 50 mm wide and 3 mm thick with 3 mm radius circular holes at the center were machined. Two types of corrosion pits were electrochemically created at the hole edge and subjected

to uni-axial loading (tension-tension, $R = 0.5$, $\lambda = 0$) in both saltwater(3.5%) and air environments. This test setup allowed the study of the transition from pit to crack growth. As in the previous studies [5, 22], marker bands were created by variations in the load and measured with scanning electron microscopy during all stages of crack growth. A high magnification camera was used to measure the crack growth as it progressed through the specimen to estimate the crack growth per cycle rate. Additionally, the scanning electron microscope was used to examine how cracks initiated and propagated from the experimentally-created pits. This investigation shed light on the mechanisms responsible for the pit to crack growth transition. Two-dimensional and three-dimensional finite element analyses of crack growth from a corrosion pit at a hole were conducted to calculate the crack driving forces (stress intensity range). These models were then correlated with the measured crack initiation and crack growth rates. This approach provided understanding of transition from corrosion pit to long crack in both laboratory and saltwater environments. This research yielded a great deal of useful information for crack initiation and growth from a corrosion pit, will help fill the void that exists from previous crack growth studies, and will provide useful data that can be used to better predict the lifetimes of an aging fleet of aircraft.

II. Background

2.1 Theories of Corrosion

Corrosion is problematic, in part, because it is energetically favorable for a metal to return to its natural state from its refined state since the creation of useful and refined structural metal requires the input of energy. As thermodynamics demonstrates, systems tend toward states of increased entropy or disorder and lower energy. So, any metallic part will constantly progress toward a corroded state and the most that the user can do is try to delay the corrosion or be ready to replace corroded parts before a catastrophic failure occurs. Since corrosion is a natural process, electrochemical and thermodynamic laws readily explain its behavior.

Electrochemical reactions account for a great deal of the corrosion process. An electrochemical reaction is defined as a chemical reaction involving the transfer of electrons. As a result, these chemical reactions involve the oxidation and reduction of the materials. Oxidation refers to the material that loses electrons during a reaction, while reduction refers to the material that gains electrons during a reaction. The coupling of separate reduction and oxidation reactions is known as an electrochemical cell. In corrosion, an oxidation reaction is known as an anodic reaction and a reduction reaction is known as a cathodic reaction [1]. General forms of these reactions are shown in Equations 2.1 and 2.2.

$$M(s) \rightarrow M^{n+} + ne^{-} \tag{2.1}$$

$$M^{n+} + ne^{-} \rightarrow M(s) \tag{2.2}$$

These equations show that electrons are transferred between the metal and its environment to create ions and excess electrons. These reactions must occur in an electrolytic solution to allow for the transfer of electrons. For this process to perpetuate, there must be an anodic surface which will donate the electrons and a cathodic surface

which accepts these electrons. These surfaces can exist on the same piece of metal as long as there is an electrolyte solution to complete the electrochemical circuit. In fact, these surfaces can be neighboring grains on a given piece of metal, Fig. 2.1.

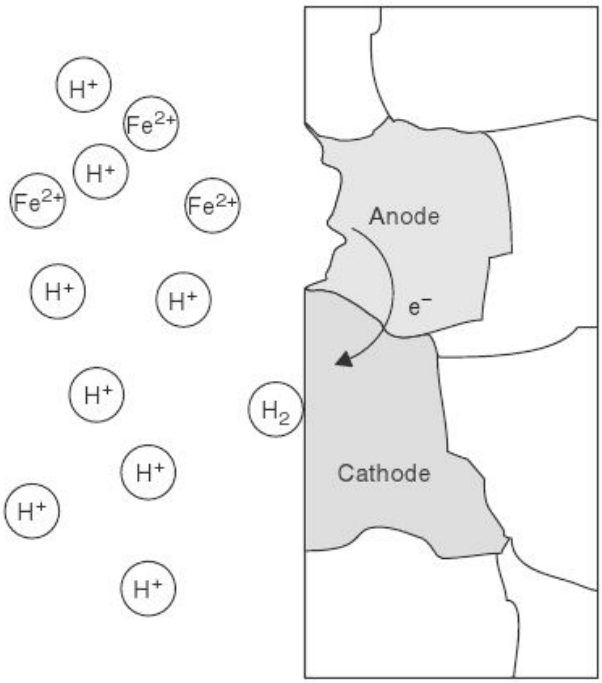

Figure 2.1: Local anodes and cathodes in neighboring grain boundaries during an electrochemical reaction. [36]

During the process of corrosion, the anodic and cathodic regions may shift and change as the reaction progresses. Similarly, corrosion can occur between two dissimilar metals that are in close proximity to one another. This type of corrosion is known as galvanic corrosion. The transfer of electrons that takes place during this reaction generates a current and by using Faraday's law, the mass loss and corrosion rate are easily determined.

Faraday's law relates moles of the corroded material to the total charge carried by a mole of that material, as shown in equation 2.3.

$$Q = F\Delta Nn \tag{2.3}$$

In this equation, F is Faraday's constant, delta N is the change in the number of moles of a material, and n is the number of electrons per mole of material. The time and/or current is then solved by using the total charge (Q) in equation 2.4, where I is the total current in amperes and t is the duration of the electrochemical process in seconds.

$$Q = \int_0^t Idt \tag{2.4}$$

This equation is useful in determining how long a corrosive reaction should take place to achieve a given amount of corrosion in an experimental setting. Along with the current and corrosion rate, the potential of an electrochemical cell is also an important parameter.

The change in free energy is the underlying concept that allowed Nernst to develop his equation for the electric potential of an electrochemical cell (equation 2.5) [36].

$$E_{cell} = (E^o_{cathode} - E^o_{anode}) - \frac{RT}{nF} \ln Q_{reaction} \tag{2.5}$$

The E^o values represent the electric potential of the cathodic and anodic reactions individually. R is the universal gas constant. T is the temperature in Kelvin. n is the number of moles being reacted. F is Faraday's constant, and Q is the reaction quotient which is related to the equilibrium constant of the reaction. Again, this information is useful in determining the necessary voltage to experimentally cause corrosion in a timely manner. This is especially important for electrolytic cells since they are not spontaneous reactions as is the case for galvanic cells.

2.2 Pitting

Pitting is the most common type of localized corrosion. A pit consists of a small volume of material being removed to form a cavity or pit in the surface. If left unresolved,

pits can travel completely through a material causing a hole. Due to the difficulty in predicting and detecting pits, it is one of the more dangerous forms of corrosion. Part of this danger lies in the fact that a small pit in a key area of a structure could cause catastrophic failure. This is especially true of pits that have undercutting or that occur below the surface (Fig. 2.2).

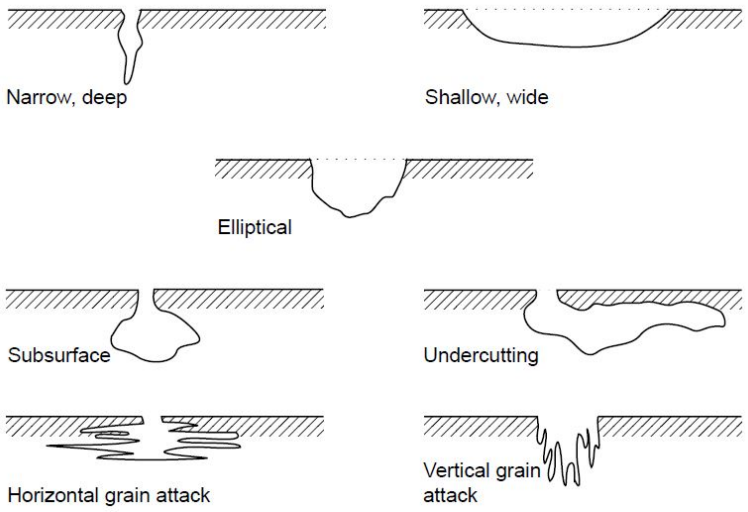

Figure 2.2: Common pit shapes in structural materials, [36]

Pits frequently form in areas where a protective coating has been scratched off or removed. This in itself presents a problem because a small area of unprotected surface leads to an increased corrosion current density. As a result, the rate at which the pit forms will increase. However, as the number of pits increases, the rate of penetration for each of the pits decreases. This is due, in part, to the increase of corrosion products that can fill the pit and cause a break in the electrochemical circuit. These pits act as the nucleation site for fatigue cracks. This is true for most structural materials including steel, aluminum, and even titanium in certain situations. There appears to be critical or threshold values for the pit size, below which, a fatigue crack will not nucleate [8]. Though a pit may be

below a threshold value for crack growth, it may still develop into a crack depending on the surrounding defects. Pits that are in close proximity may coalesce into a larger pit which may increase the size of the pit enough to cause a fatigue crack to nucleate [37].

Pits also readily form in sections of a material that have anodic and cathodic regions in contact with one another. In fact, pits may be detected by looking for the cathodic region (un-corroded region) surrounding the pit, Fig. 2.3. This may be difficult, however, because a film can cover this cathodic region causing it to change its location or shape. This localized cathodic reaction often results in the formation of hydrogen ions at the surface of the material. This excess hydrogen can travel to pit or similar flaw and enter into the lattice structure of the material causing embrittlement [23]. This hydrogen embrittlement, not surprisingly, results in a material that is more brittle and more likely to initiate cracks from cyclical loading. In other words, hydrogen embrittlement is a fundamental mechanism in corrosion fatigue.

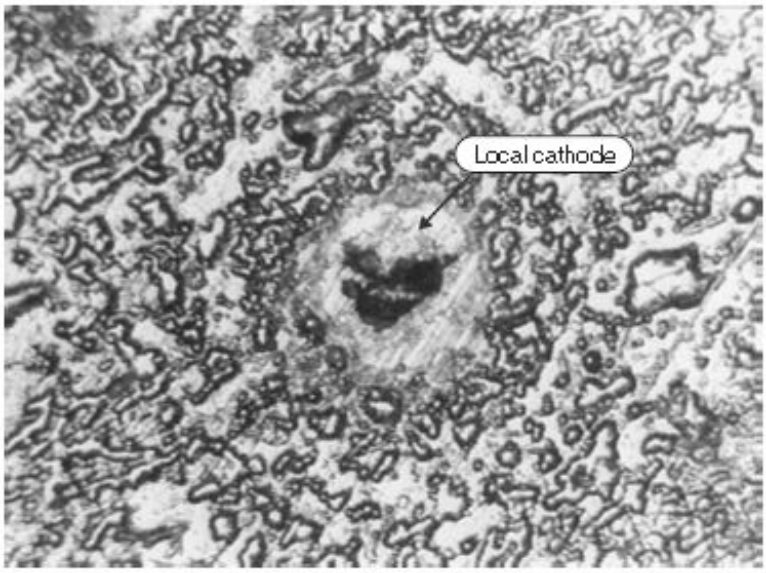

Figure 2.3: Local cathode on the surface of an aluminum plate exposed to 3.5% NaCl, [36]

2.3 Corrosion Fatigue

Corrosion fatigue is defined as the failure of metal due to a cyclical load in combination with exposure to a caustic environment; either gaseous or aqueous. The result is a reduction in the number of required cycles until failure when compared to the cycles required if the metal were not exposed to a corrosive environment. In most cases, the corrosion forms defects in the material which nucleate and subsequently propagate fatigue cracks throughout a given specimen. Though there is a minimum size to cause crack growth, the pit size larger than this critical dimension has less of an effect on the crack growth. For example in several studies [13] and [19], larger pits were found to be no more likely to cause a fatigue crack to propagate than smaller pits. As a result, the average sized pits are equally likely to produce a crack that will continue to propagate through a material. This is only true when there is widespread pitting on the surface (Fig. 2.4) of the material with no other flaws present.

The transition from pit to fatigue crack growth is affected by pit shape. Pits that have a higher aspect ratio, deep and narrow are more likely to form fatigue cracks than wide shallow pits [23]. Pit shape may be a material-dependent property and may vary according to the fracture toughness of a given material. The rolling direction of the material has a profound impact on the growth of the pits. The pits have anisotropy and the largest dimension occurs along the grains in the rolling direction. This means that the pits grow along the grain directions over the surface of the given material [19].

2.4 Effect of Corrosion Fatigue on Fatigue Life

Once the transition from pit to crack occurs, corrosion still continues to play a role in propagation of the crack. A material experiencing corrosion fatigue has a different crack growth rate when compared to a material with only a fatigue loading condition. As

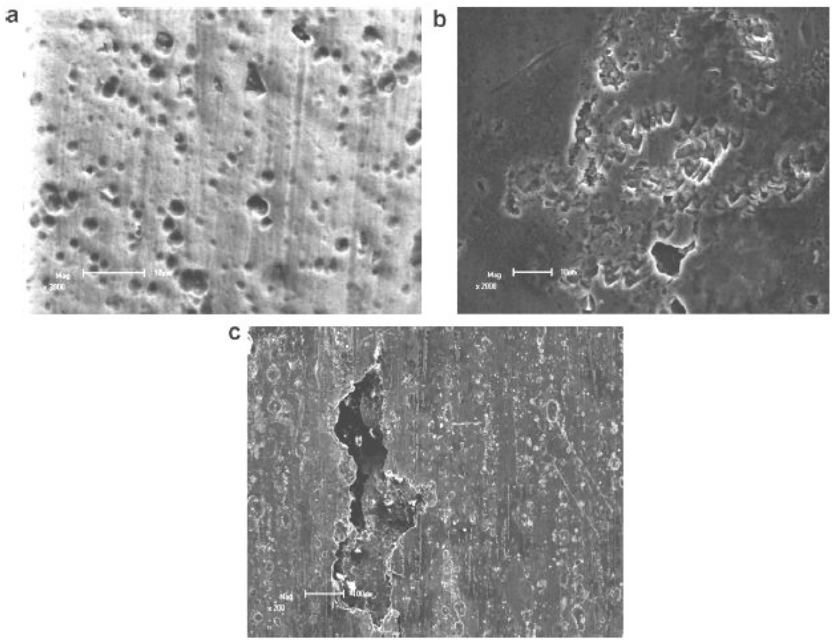

Figure 2.4: Three examples of surface corrosion on 6151-T6 aluminum. Larger pits do not necessarily form fatigue cracks more than averaged sized pits. [13]

expected, the crack growth rate of corrosion fatigue is larger than that of fatigue alone. A schematic of life reduction due to corrosion is shown in Fig. 2.5

Before the crack nucleates, the pit from corrosion must form. The study by Chen et al., [8] notes that the formation of the pit dominates the early stages of the crack growth process. This is analogous to the nucleation of a fatigue crack without corrosion present. The majority of the cyclic lifetime is spent creating the crack while the actual crack growth makes up a smaller portion of the total lifetime. With corrosion fatigue however, the pit nucleation takes less time than a load-only fatigue crack to nucleate. In fact, in the study by DuQuesnay and Underhill, [13], specimens that were not exposed to a corrosive environment did not experience failures in the time it took the corrosive specimens to fail. The corroded specimens failed up to 13 times faster than their un-corroded counterparts. The longer the specimen was exposed to the corrosive environment, the shorter the fatigue

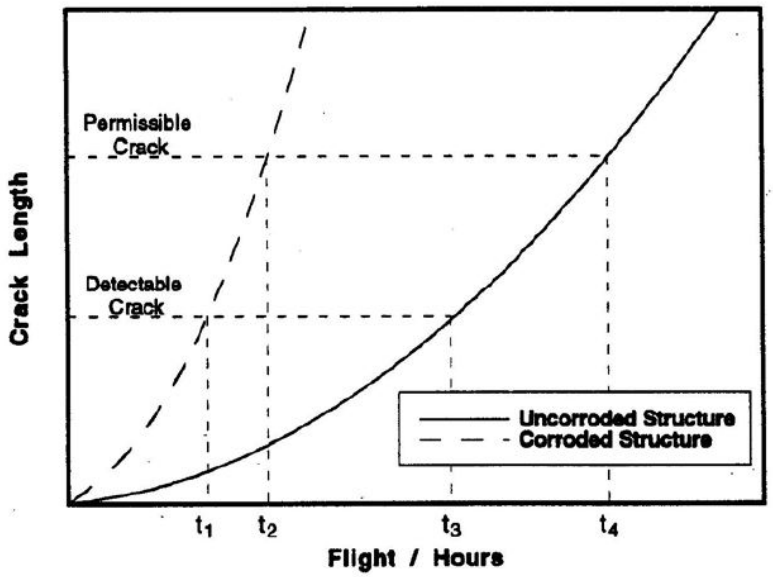

Figure 2.5: Plot showing the reduction of life due to corrosion in terms of real-world flight hours, [23]

life. This is due to the fact that the pits became deeper and longer as corrosion proceeded. The initial pit size is an important factor in determining the growth rate of the crack.

In estimating the life of the specimen with the pit/crack, the specimen is just treated as though it has a surface crack. As a result, a stress intensity factor (K, $MPa * m^{1/2}$) is calculated using the initial pit size, shape, and loading direction. Unfortunately, with tunneling, the formation of a pit beneath the surface, the exact dimensions of the pit are difficult to achieve which can make accurate K and Δ K calculations difficult [19]. These parameters are best calculated after failure by inspecting the initial corrosion dimensions to obtain an accurate geometry of the specimen. However, once the initial crack is assumed, the $\frac{da}{dN}$ versus ΔK curves can be generated and the fatigue life can be predicted.

2.5 Fracture Mechanics

Fracture mechanics is the study of the propagation of cracks through a material [1]. This field uses solid mechanics to determine crack growth through the relationship between an applied load and the material's resistance to fracture. Crack driving force is broken down into three different modes. Mode I is known as the opening mode and it is a result of a force normal to the direction of crack growth. Mode II is known as the sliding mode and it is caused by an in-plane shear stress. Mode III is known as the tearing mode and it is a result of out of plane shear stress [1]. Fig. 2.6 illustrates all three modes and the forces which cause them. Since the current research involves tensile testing, mode I is the mode of primary concern.

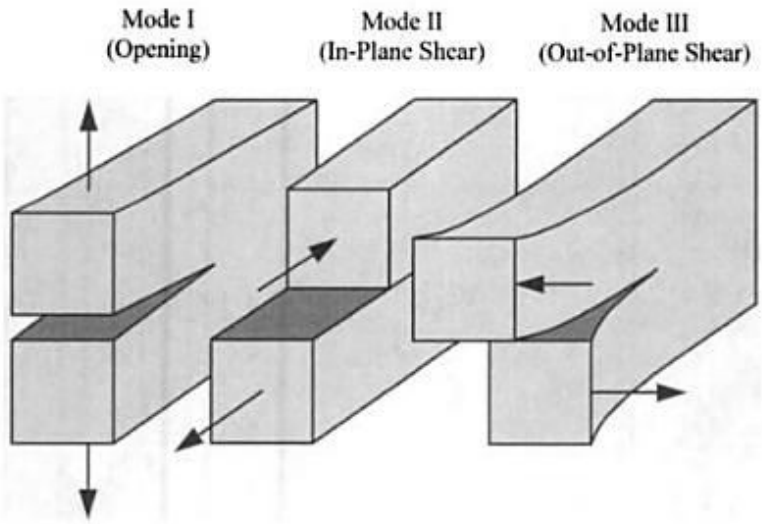

Figure 2.6: The three modes shapes referred to in fracture mechanics. Mode I is the mode of concern for the current research. [1]

For each of these modes, the effect on an applied force on crack growth has a unique relationship. For mode I, the primary measure of the effect of the load on crack growth is

known as a stress intensity factor K_1, eq. 2.6, where σ is the applied stress and a is the crack length [12].

$$K_1 = \sigma \sqrt{} \tag{2.6}$$

This stress intensity factor accounts for the flaw in a given specimen so that as the flaw, in this case a crack, grows the stress intensity factor will continue to grow as well. In the case of cyclical loading, the stress intensity factor is modified to account for the maximum and minimum stresses. The range of the stress intensity factor ΔK, eq. 2.7, is used in the Paris law, eq. 2.8, to define the rate of the crack growth as a function of ΔK, [12].

$$\Delta K = K_{max} - K_{min} \tag{2.7}$$

$$\frac{da}{dN} = C * \Delta K^m \tag{2.8}$$

In eq. 2.8, m and C are material constants that are determined empirically. The Paris law states that as the stress intensity factor increases, the rate of the crack growth will also increase. So, if either the crack size or the loading changes, the rate of the crack growth will also change. The rate of crack growth, $\frac{da}{dN}$, is a derivative of the crack length with respect to the applied cycles. This is easily calculated from a plot of the crack length versus the number of cycles. Such a curve is a necessity in a fracture mechanics study of fatigue crack growth.

Using equations 2.6, 2.7, and 2.8, the crack growth as a function of the stress intensity factor can be studied. This way, results from different test setups may be compared because the stress intensity factor accounts for the specimen's size, shape, crack size, and loading conditions.

2.6 Previous Research

Fatigue and corrosion have been popular areas of research in recent history. This research generally employs a fracture mechanics approach to crack growth after initiation in structural materials. Both McEvily and Paris laid the foundation for how cracks grow and the fundamentals of fracture mechanics [2, 24]. This research is extremely valuable for the current research because it provides methods to predict and interpret crack growth rates given a cyclic load through the Paris law and other fracture mechanics tools. As discussed previously, the Paris law uses the load ratio and stress intensity range to determine the crack growth rate per loading cycle ($\frac{da}{dN}$). More recently, research has been extended to test the validity of these mathematical concepts at the microscopic level. White and Wright studied a method of variable amplitude loading to create marker bands in cracks growing from laser pits in 7075 aluminum specimens that could be examined with a scanning electron microscope [27, 45]. This method of creating bands on the fracture surface was also used by Burns et al. in their fatigue crack growth research [5, 6]. These marker bands allow the actual crack growth rates to be compared and correlated to the predicted $\frac{da}{dN}$ values.

In addition to long crack growth research, Forman's work in the study of how and where cracks initiate in aluminum specimens spawned a totally new area of research that concerned itself with the crack initiation [15, 16, 19]. Forman's work confirmed that the stress intensity factor range was a primary factor in crack growth rate. He also determined that cracks more easily initiated from engineering defects such as scratches or nicks in the surface. He performed his experimental testing using uni-axial cyclic loading in 7075-T6 aluminum specimens in a non-corrosive environment. He found that these flaws did have an effect on the fatigue life if they were longer than 0.013 mm [15]. If a given flaw was smaller than 0.013 mm, Forman was unable to measure the flaw's effect on the fatigue life. However, for flaws greater than 0.013mm, the larger the flaw the shorter the fatigue lifetime [19].

Another study by Wang et al. investigated the effect of pitting and corrosion on fatigue life, but, like Forman, not the transition from the flaw to crack specifically [43]. Unlike Forman, this research did not use fracture mechanics. This study found that pitting resulted in overall decrease in the fatigue life in 7075-T6 aluminum. The main cause being that corrosion flaws may create stress concentrations surrounding the pit [43]. Other studies found similar results using similar techniques [8, 9, 22, 45]. This transition between flaw and crack growth has also been investigated by many researchers [6, 26].

To continue this idea of crack formation, Lukas et al. studied micro crack formation in flaws when they were subjected to cyclic loads. They found that there is some effect of these micro cracks on the fatigue crack growth initiation, but that there is no conclusive method for characterizing these phenomena [26]. Additionally, they found the cracks always initiated from the pits and that those specimens without pits did not have a specific, repeated area from which the cracks grew. This research was continued by Burns et al. to better determine the mechanisms responsible for this initial crack growth [6]. They found that the topography near the edges of the pits had a large effect on the rate of crack initiation and this effect can vary a great deal depending on the pit shape. They also noted that the current software models are not sufficiently validated to predict crack growth from pitted surfaces [6]. Each of these studies used test specimens of 7075-T6 aluminum with uni-axial testing, but without applying fracture mechanics to the entire crack growth regime. Sankaran et al. also investigated the effect on corrosion pits on the fatigue life. They found that accurate lifetime predictions could be made while using the average pit size as the initial flaw size in existing closed form solutions [37]. There are several studies involving the transition from pit to crack [30, 31, 35, 46]. The author is not aware of any such study in highly corrosive environments as all previous studies using fracture mechanics involved the laboratory air environment.

Intuition says that a corrosive environment will result in a decreased fatigue life. While this corrosion would result in a shorter fatigue life, it is important to quantify this effect so that accurate lifetime predictions can be made. Work done by Pao et al. revealed that a corrosive environment reduced the fatigue life by a factor of two or three and reduced the crack initiation load threshold by approximately 50 percent [31]. Ro et al. also examined the effect and mechanisms of corrosion fatigue in aluminum samples [35]. This research shows that a corrosive environment (saltwater) does reduce the fatigue life, however, other factors and parameters are involved. These factors include the stress intensity range, load ratio, and environment composition. These factors all work together, but their exact contributions need further investigation. Similar research investigates similar structural alloys in saltwater environments with similar results [30, 46]. Much of this corrosion testing research has occurred at other institutions, some fatigue testing has been conducted by the Air Force Institute of Technology (AFIT).

Misak et al. have already conducted a series of tests in-house related to fatigue crack growth [28]. Their research involved both uni-axial and bi-axial test specimens machined out of aircraft grade aluminum alloys. Similarly, the tests involved the specimens being exposed to both air and saltwater solutions and thier crack growth behavior being explained using fracture mechanics. In each of these tests, however, machined notches were present. Initiation of the fatigue cracks took place by creating a pre-crack from a machined notch. This pre-cracking was caused by applying low loads over a high number of cycles. Figure 2.7 shows all the $\frac{da}{dN}$ vs. ΔK from these previous experiments. These experiments also investigate the different crack growth rates that result from the different grain orientations in the specimen. This crack growth information will be used as a baseline to compare the current research's crack growth rates due to the similar approach to the research.

There has also been a tremendous amount of research and experimentation in the field of elasticity, specifically stress intensity and stress concentration factors for a wide range of

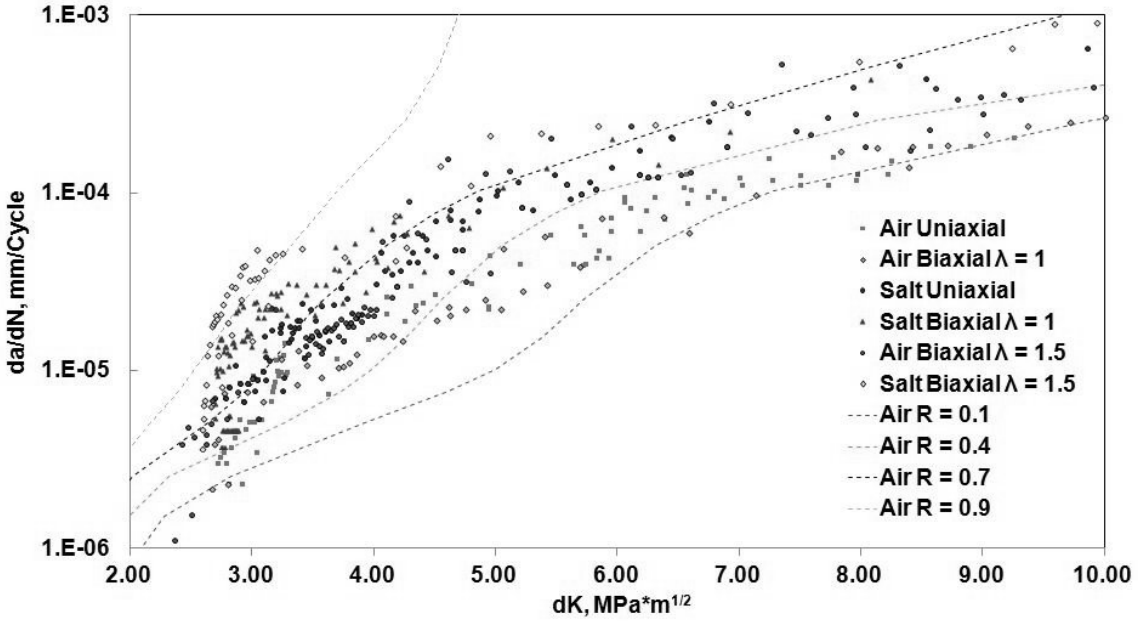

Figure 2.7: Plot showing the crack growth rate as a function of the stress intensity factor from the previous fatigue cracking experiments conducted at AFIT by Misak et al. [28].

shapes and geometries. There already exists a solution for calculating the stress intensity factor of a circular hole with one radial crack at the hole boundary in an infinite plane. However, there is no solution for a circular hole with one radial quarter-circular crack from the hole boundary in a uni-axial specimen [20, 21, 34, 47]. Misak et al. developed finite element models to predict the stress intensity factor for a circular hole with a radial crack from a rectangular notch, but not for specimens with corner corrosion pits [28].

2.7 Why This Thesis?

The above literature review revealed the following observations:

- There have been several studies involving the transition from pit to crack.
- Most of these studies did not use a fracture mechanics approach.

- Previous studies involved transition from pit to crack in the ambient air environment, not in a corrosive environment.
- None of the studies compare different shaped pits.
- There is no closed form solution for predicting stress intensity values for complex crack, pit, and hole geometries.

The following studies, [4, 6, 25] offer some insight into the pit-to-crack transition, but the research is lacking in some crucial areas. For example, the study by Lee et al. involving fatiguing aluminum specimens in a corrosive environment, did not use fracture mechanics nor did it attempt to quantify the crack growth rate during the corrosion pit to crack transition [25]. The results of this study are demonstrated by showing the final pit size and aspect ratio and how many cycles required to reach this pit size. These results are shown in Table 2.1.

Table 2.1: Results from the study by Lee et al. where fracture mechanics was not used to measure the transition from corrosion pit to long crack [25].

Environment	Frequency (Hz)	Pit Radius (mm)	Initial Pit Aspect Ratio	Final Crack Aspect Ratio	Cycles to Detect Crack Propagation
Dry N_2	20	0.17	1.62	1.26	30,000
90-95 % RH N_2	20	0.22	0.92	1.18	35,000
0.06 M NaCl	20	0.29	1.26	1.35	45,000
0.06 M NaCl	20	0.24	0.86	1.20	85,000
0.06 M NaCl	0.1	0.29	0.67	1.28	10,000
0.06 M NaCl	0.1	0.27	2.53	1.39	51,000
Pure H_2O	0.1	0.25	0.93	1.39	40,000 (at 5 Hz)
Pure H_2O	0.1	0.23	1.86	1.03	40,000

Similarly, in a study by Burns et al. the crack growth in a corrosive environment was only shown as a function of the cycles applied to the specimen and not explained using fracture mechanics [6]. Conversely, in another study, Burns et al. investigated the crack growth transition, but did not use fracture mechanics or determine the cycles required for a crack to initiate from a pit [4]. Additionally, this investigation did not take place in a

saltwater environment [4]. Another difference is that each of these studies used a different pit shape. Lee et al. used quarter-circular corner pits, Burns used ellipse shaped corrosion pits [4, 6, 25]. None of these studies compared initiation or propagation for different pit shapes nor did they examine the difference in the stress intensity factor for these different geometries.

As a result of these observations, the author determined that there is a need for additional understanding of the transition from pit to crack and then crack growth. This understanding should involve fracture mechanics, the rate of crack growth, and the cycles required for initiation in laboratory air and corrosive saltwater environments. This is the objective of the present thesis.

2.8 Approach

This research determines the crack initiation and growth properties from a pit made through electrochemical corrosion on the edge of a hole in a common aircraft grade aluminum (7075-T6). The specimens were thin (3.2 mm) and had a center hole (6.28 mm) that mimics a rivet hole that is common in most aircraft skins where corrosion fatigue is prevalent [10, 29]. Two types of corrosion pits were created in the aluminum specimens: through-pits and corner-pits. Their differences are explicitly defined in the latter chapters of this thesis. The primary result from this research is a relationship of the crack initiation lifetime verses the stress intensity factor for specimens with each pit type exposed to air and saltwater. To accomplish this, two- and three-dimensional finite element models for determining the stress intensity factor of a hole with a corrosion pit and crack in a thin plate were created. This is because there are no closed form solutions or any widely distributed finite element models with the aforementioned geometry available to determine these parameters . Another important result from this research is the crack growth rate ($\frac{da}{dN}$) with respect to the stress intensity factor for the aforementioned test specimens. Each test was done using cyclic (tension-tension, $R = 0.5$) loading to create a fatigue environment.

This research is unique and useful because though there is data on the nucleation and growth of fatigue cracks from electrochemical pitting, few of these research studies use fracture mechanics to explain and predict the results. Similarly, there is currently no uniform model for determining the stress intensity factor for specimens containing a crack originating from a corrosion pit. This method of developing a finite element model and then correlating this model to experimental testing while incorporating fracture mechanics will yield accurate, useful, and reliable results to extend the life of the Air Force's aging fleet to save money and, more importantly, lives.

III. Methodology

3.1 Material

Research was conducted using 7075-T6 aluminum. This alloy is commonly used in aerospace applications and as a result, information regarding its resistance to corrosion fatigue is highly desired. Tables 3.1 and 3.2 shows the typical chemical composition and material properties of this alloy. It is important to note that these properties were also used in all finite element models.

Table 3.1: Composition of a typical sample of 7075-T6 aluminum [41].

Element	**% Comp.**
Aluminum, Al	87.1-91.4
Chromium, Cr	0.18-0.280
Copper, Cu	1.20-2.0
Iron, Fe	$\leq$ 0.50
Magnesium, Mg	2.10-2.90
Manganese, Mn	$\leq$ 0.30
Other, each	$\leq$ 0.050
Other, total	$\leq$ 0.15
Silicon, Si	$\leq$ 0.40
Titanium, Ti	$\leq$ 0.20
Zinc, Zn	5.10-6.10

Table 3.2: Mechanical properties of a typical sample of 7075-T6 aluminum [41].

Material Property	**Value**
Ultimate Strength	572 MPa
Yield Strength	503 MPa
Young's Modulus	71.1 GPa
Shear Modulus	26.9 GPa
Poisson's Ratio	0.33

This alloy of aluminum is considered a very high strength aluminum alloy suitable for use in high stress applications. While this alloy has higher strength than both 2000 and 6000 series aluminums, it is also more brittle. As a result, its fatigue resistance will vary greatly from other aluminum alloys [15]. Similarly, the T6 temper offers greater resistance to corrosion when compared to other tempers such as T3.

3.2 Test Specimens

The uni-axial specimens have very simple geometry which made it simple to fabricate the test specimens. Each specimen was cut from 3.22 mm thick 7075-T6 rolled aluminum sheets by the AFIT machine shop using a Flow Corporation water-jet machine. The center hole for each specimen measured 6.28 mm in diameter. Figure 3.1 shows the dimensions for the uni-axial specimens. For the uni-axial tests, the grain orientation was parallel to the direction of the applied load. As a result, crack growth occurred in the L-T direction.

After the specimens were machined, the surfaces surrounding the hole on both faces of the specimen were polished using 1000 grit sandpaper. This polishing allowed for easier identification of surface imperfections caused by the crack initiation because the surfaces, after polishing, are smooth and uniform. The specimens were then prepared to undergo the electrochemical corrosion procedure as outlined by Burns [4]. To begin, the corners of the holes' bore were filleted using an Exacto knife by hand. The radius of the fillet should be approximately 0.2 mm. The fillet radius was checked with a magnifying lens to ensure the correct size. The fillet is necessary because without it, E-470 electroplating tape would not adhere well to the corner of the bore because of the 90 degree angle. The electroplating tape was used to create the shape of the corrosion pit. In other words, the areas not covered by the tape would be exposed to the electrochemical solution and, consequently, would be corroded. To ensure strong adhesion, all surfaces that would be in contact with the tape were cleaned with isopropyl alcohol. Since through pits and corner pits have different

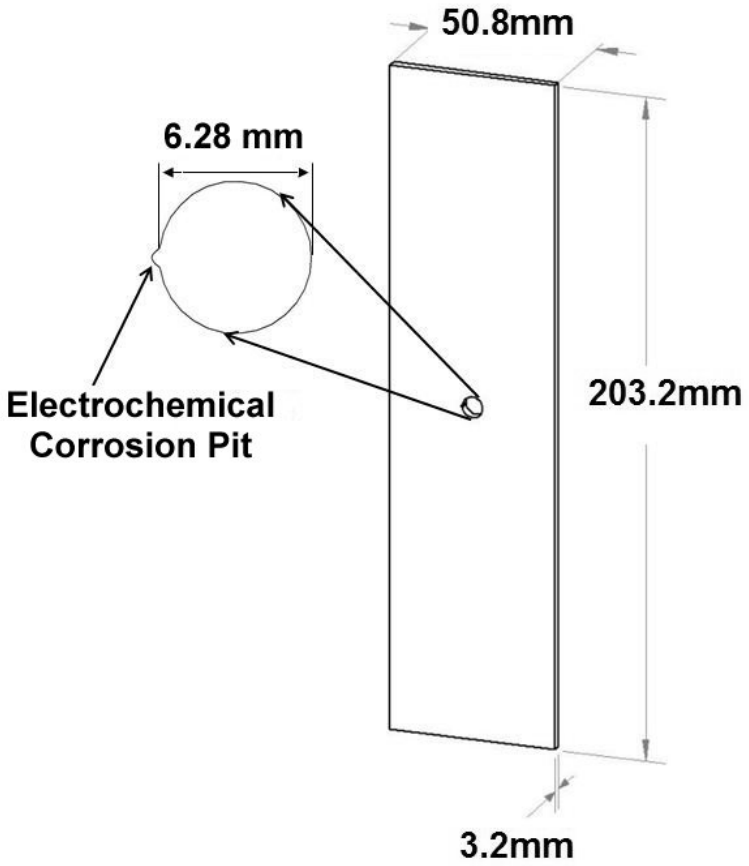

Figure 3.1: Diagram of the uni-axial test specimen with dimensions. Cut from 7075-T6 Aluminum plate using a water-jet by the AFIT Machine shop.

geometries, they require different taping configurations. The through pit shape was created by placing two 2.0 mm wide strips of tape approximately 0.25 mm apart on the edge of the hole perpendicular to the loading direction. The corner pits shape was created by placing a single 2.0 mm wide strip of tape with a 0.21 mm hole drilled in the center over the edge of the hole perpendicular to the loading direction. The hole was aligned so that it was centered over the edge between the front face and the bore of the hole [4]. An example of both tape scenarios is shown in Fig. 3.2.

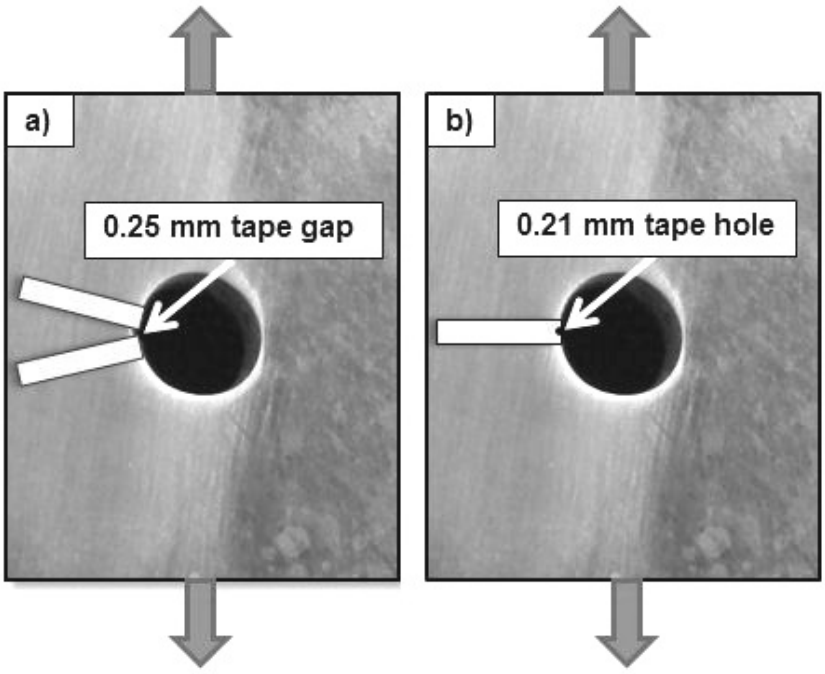

Figure 3.2: a) Tape placement for creating a through pit. b) Tape placement for creating a corner pit. The arrows show the loading direction for each specimen.

Once the tape was applied and allowed to settle for several hours, the areas in which corrosion was not desirable were coated with XP 2000 Stop-off lacquer. The lacquer was applied in a circular shape with a radius of approximately 2 cm around the hole in a single coat and allowed to dry for 24 hours. Once cured, a small plastic cylinder was secured to one side of painted region using silicone caulking. This plastic cylinder acted as a container for the corrosion reaction. The caulking was used to both seal and secure the cylinder to the painted surface. To prevent any of the solution from leaving through the hole, a 2.5 cm piece of tape was applied to the side of the hole that was opposite the lacquer coating. As a result, the only areas exposed to the corrosive solution were the areas that would become the corrosion pits. The caulking was allowed to cure for 24 hours before completing the reaction.

A solution of $0.1MAlCl_3 + 0.86MNaCl + HCl$ (pH =2) was used to corrode the aluminum specimen. The chemical reaction was driven by a 0.6 VDC potential provided by a DC power supply. The positive output lead was clipped to the non-coated portion of the specimen, and the negative output lead was clipped to a platinum electrode that was submerged in the corrosive solution. During the reaction, hydrogen bubbles would form over the corrosion site and act as an insulator, ultimately slowing or stopping the reaction. A small brush or pipette was used to circulate the solution to remove the bubbles so that the reaction could continue at an acceptable rate. After approximately, 6 – 9 minutes, the corrosion pit reached the desired size and reaction was stopped. The solution was removed using pipette and the plastic cylinder, lacquer, and tape were also removed from the specimen to expose the newly formed corrosion pit. Figure 3.3 shows the two types of pits formed during the reaction. The specimen was then rinsed with deionized water and dried thoroughly. The corrosion pits were measured using the Zeiss optical microscope. These pit sizes were used in the calculations to approximate the stress intensity ranges for each specimen. The initial pit size and approximated stress intensity range for each specimen are shown in Table 3.3.

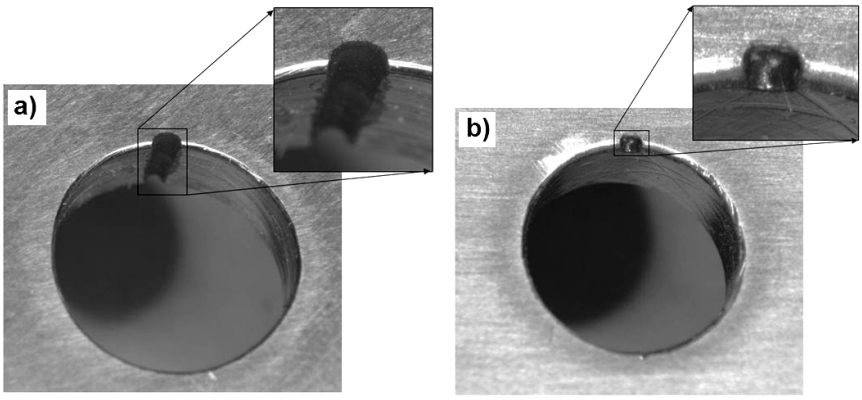

Figure 3.3: a) Example of through pit. b) Example of corner pit.

The specimens were labeled with a three letter code. The first letter refers to the current set of specimens. The second letter refers to either air (A) or salt (S) environments. Finally, the third letter refers to the type of pit; either through (l) or corner pit (S). One specimen is referred to as H13. This is a specimen that was previously prepared by Sabelkin.

Table 3.3: Specifications for the uni-axial test specimens. ΔK values are computed by Eq. 3.1.

Specimen	**Pit Radius (mm)**	**Pit Type**	**Environment**	**ΔK**	**Max σ (MPa)**	**Min σ (MPa)**
H13*	0.31	Through	Air	3.0	68.1	34.1
SAl-01	0.39	Through	Air	4.0	84.2	42.1
SAl-02	0.38	Through	Air	5.0	106.2	53.1
SAl-03	0.35	Through	Air	3.5	76.5	38.2
SAl-04	0.29	Through	Air	4.0	93.0	46.5
SAS-01	0.31	Corner	Air	4.0	91.6	45.8
SAS-02	0.43	Corner	Air	5.0	102.9	51.5
SAS-03	0.37	Corner	Air	3.5	76.5	38.2
SAS-04	0.47	Corner	Air	3.0	59.8	29.9
SAS-05	0.51	Corner	Air	3.75	74.3	37.2
SSl-01	0.27	Through	Saltwater	4.0	95.7	47.9
SSl-02	0.34	Through	Saltwater	5.0	110.6	55.3
SSl-03	0.31	Through	Saltwater	3.5	79.9	40.0
SSl-04	0.31	Through	Saltwater	3.0	68.4	34.2
SSl-05	0.30	Through	Saltwater	2.75	55.4	27.7
SSS-01	0.37	Corner	Saltwater	4.0	85.7	42.9
SSS-02	0.36	Corner	Saltwater	5.0	108.6	54.3
SSS-03	0.37	Corner	Saltwater	3.5	75.3	37.7
SSS-04	0.37	Corner	Saltwater	3.0	64.8	32.4
SSS-05	0.42	Corner	Saltwater	3.75	81.1	40.6

*Denotes a specimen previously prepared by Sabelkin.

3.3 Test Procedures

Testing procedures involved taking a prepared specimen and subjecting it to cyclical loading (R= 0.5 & 0.1) in an MTS machine until the fatigue crack either initiated and grew to a length of 17 mm or until 1 million cycles occurred without fatigue crack initiation. Unlike the previous AFIT research, the specimens were not initially subjected to a small

load for a number of cycles to cause a pre-crack. Instead, the specimens with corrosion pits were subjected the same cyclic load during the entire experiment. This was done to determine if the initiation from a machined crack and from a corrosion pit occur differently. Initially, the experimentally applied loads were calculated using closed form solutions from Tweed et al. shown in Eq. 3.1 where a is the crack length, c is radius of the hole, w is the width of the specimen, F_{min} and F_{max} are the minimum and maximum applied loads respectively, and ΔK_1 is the stress intensity range for mode I loading. [20]. This equation used the crack length, other geometric properties and applied loads to calculate the approximate stress intensity factor for the radial through crack originating from a circular hole with a radial circular pit (Fig. 3.4).

$$\Delta K_I = 0.5 * (3 - \frac{a}{c+a}) * (2.243 * (1 - \frac{a}{c+a}^{3}) * \frac{F_{max}(1 - \frac{F_{min}}{F_{max}})}{wt} * \sqrt{\pi a} \qquad (3.1)$$

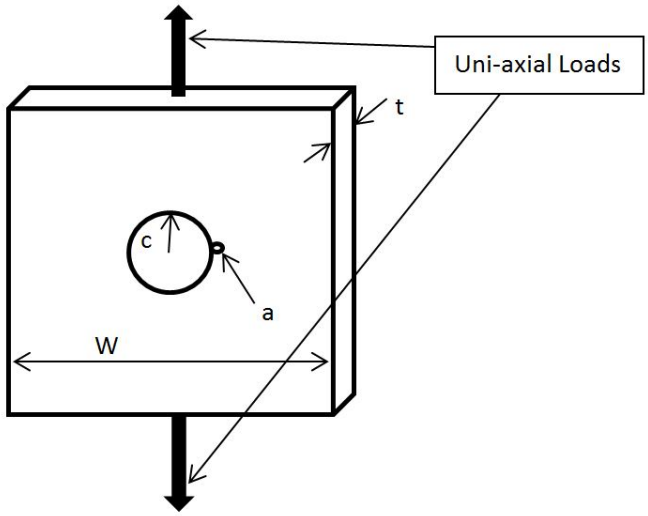

Figure 3.4: The circular hole with one radial crack at the hole boundary in an infinite plane geometry for which Eq. 3.1 determines the stress intensity factor.

This equation was used because there was no method to calculate the stress intensity factor for the experimental geometry at the time of testing. However, it was thought to be accurate enough to give approximate values to be used in the calculation of the experimental loads. The results from the equation differed from the actual values computed from the finite element analysis (FEA). These results are discussed in the Finite Element Analysis section of this thesis. After the stress intensity calculations for the experimental geometry were completed, the stress intensity factors were modified to represent the actual values. These values are shown in Table 3.3 along with the experimental loads.

With the loading situation controlled by the MTS system, the crack growth must be monitored through external equipment. Since the crack growth can be quite small, a high fidelity and high magnification camera was used. A Pixelink camera and software package were used to photograph and measure the crack growth as the number of cycles progressed. The test setup showing the camera and the specimen in the grips of the MTS machine is shown in Fig. 3.5. The Pixelink software uses the pixels in the image to calculate a length of an object in the image. To calibrate the software, the camera was setup in front of the machine so that the specimen was in focus and a picture of the hole was taken. The hole was photographed so that the dimensions of the hole could be verified by external means. The software was then calibrated so that the number of pixels across the diameter of the hole corresponded to the actual length of the hole. Care was taken so that the camera was not moved during the testing. Additionally, the camera and software were re-calibrated each time a new specimen was tested. Additionally, an incandescent light bulb was used to provide light for the picture. The angle at which the light hit the surface of the specimen could be changed to expose cracks in their infancy. Incorrect lighting could make these cracks impossible to see until they reached a significant length.

When the crack reached a length of approximately 17 mm, the test was stopped and the specimen was considered to have failed. This was done to preserve the fracture surfaces. If

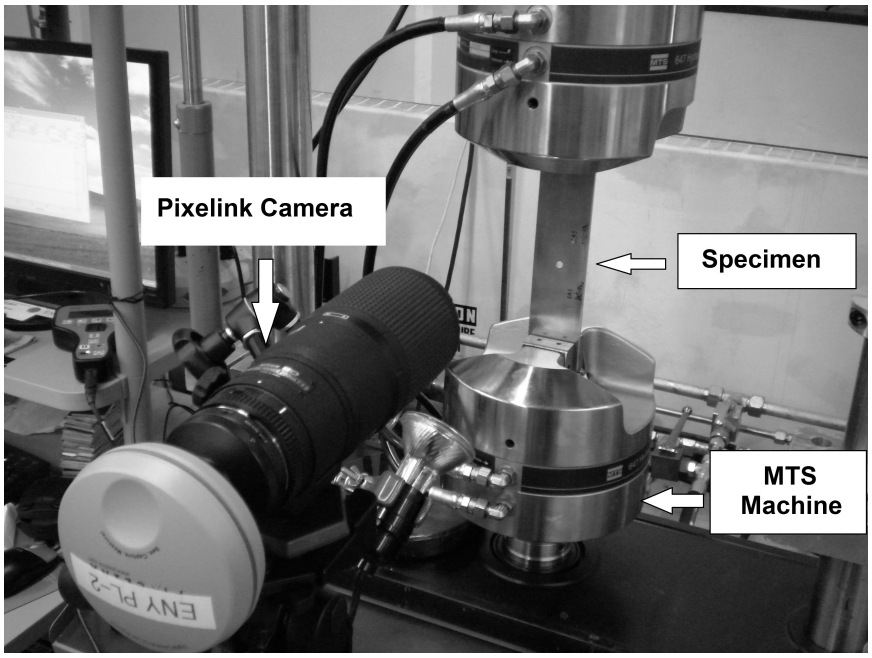

Figure 3.5: The setup used to propagate and measure fatigue cracks. The camera and associated software was used to measure the length of the crack as the number of cycles progressed. All testing occurred in the AFIT Mechanics of Materials Laboratory.

the crack were allowed to grow to a longer length, the fracture surfaces could be damaged from the two halves colliding into one another. The fracture surfaces were removed from the whole of the specimen using a band saw. This was done so that the surfaces could be examined using both an optical light microscope and a scanning electron microscope (SEM). Since some of the specimens were tested in laboratory air and others were tested in a 3.5% saltwater solution, special chambers were required to contain the saltwater during testing. The saltwater chambers used are shown in Fig. 3.6.

These steel chambers sandwich the test specimen and the two halves are bolted together and sealed with rubber gaskets to ensure a water tight seal. Once the chambers were secured, the saltwater was added through the holes in the top of the chambers until

Figure 3.6: The water tight chamber used to expose the specimens to a saltwater environment while still allowing the crack growth to be monitored. The hole in the top of the chamber is used to fill them with saltwater.

they are full. The clear polycarbonate front and back plates allowed the crack growth to be photographed and monitored throughout the experiments.

Additionally, specimens were not just subjected to the applied loads for an extended period of time. Instead, the loading cycles involved subjecting the specimen to the desired experimental stresses for 5000 cycles. After these 5000 cycles, marker band cycles were introduced to the specimen. These marker bands are 25 cycles with the lower stress limit at 10% the normal stress value followed by 50 cycles of the normal stress values. These 75 cycles are then repeated 10 times to create 10 sets of marker bands. The variation in loading changes the way the crack propagates through the material. As a result, the fracture surface resulting from marker band loading looks different from that caused by normal loading. Thus, when using the SEM, the crack growth for each 5000 cycles can accurately be measured [4, 22, 33]. Marker bands also provides a method to keep track of

coordinates on the fracture surface when examining it under extremely high magnification. An example of these marker bands is shown in Fig. 3.7

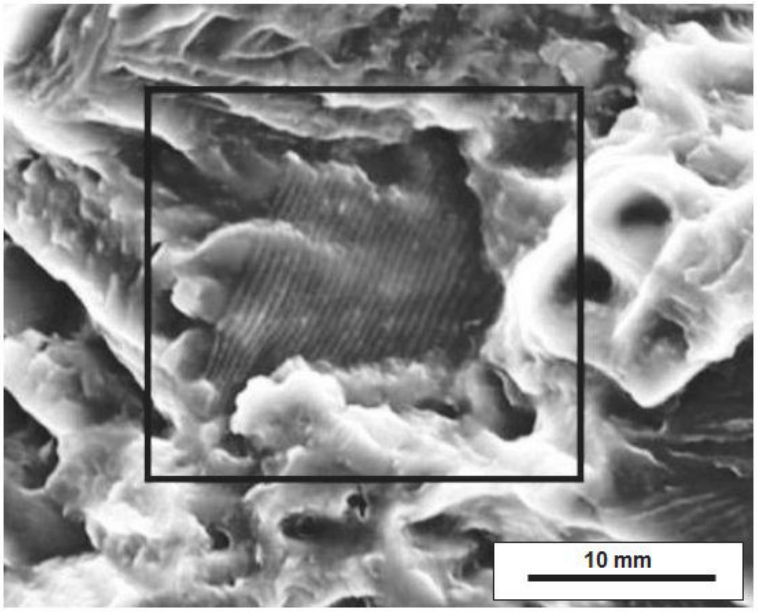

Figure 3.7: Black Box: Example of marker bands produced by changing the ΔK loading conditions in an aluminum specimen. Notice the contrast between the marker bands and the surrounding material.

3.4 Finite Element Modeling

As previously discussed, there is a closed form solution for calculating the stress intensity factor of a crack that originates from a hole in a flat plate as given in 3.1. The current research specimens are similar to this geometry. However, in addition to a crack, the present study examined a corrosion pit on the edge of a hole. As a result, the validity of Eq. 3.1 was unknown for the present study. To determine if this equation could be used to approximate the stress intensity factor of the test specimens, specimens were analyzed through finite element analysis (FEA).

Dassault Systems Abaqus is widely used FEA code [11]. However, like all modeling programs, Abaqus still requires a number of assumptions to be declared by the user. The author assumed the following throughout the modeling procedures:

- The aluminum material was isotropic and homogeneous.
- The mechanical properties of the aluminum alloy were constant (E=71.1 GPa, ν=0.33).
- The pits are a uniform shape with smooth edges and no irregularities.
- There were no other flaws of any kind in the specimens and the crack initiated from the corrosion pit.
- The applied load was completely perpendicular to the crack growth direction.
- There is no variation in the applied loads.
- Specimens in a plane stress condition.

A model of a uni-axial specimen was created in two dimensions using the Abaqus graphical user interface. To test the validity of the assumptions made for modeling, the initial model involved a very simple case; a flat plate with a centered hole like the specimen shown in Fig. 3.8.

The dimensions for this model matches the specimen shown in Fig. 3.1 without the corrosion pit. The test consisted of loading the specimen in tension in the longitudinal direction to determine the stress concentration factor (K_t) caused by the hole. After refining the mesh of CPS4R plane stress elements in a convergence study, the K_t value matched within 1% of the published values from Dowling [12]. This convergence occurred when the mesh density approached 0.4 elements/mm^2. The plot of this convergence study as well as the final meshed model are shown in Appendix A, Fig. A.1 and Fig. A.2. The

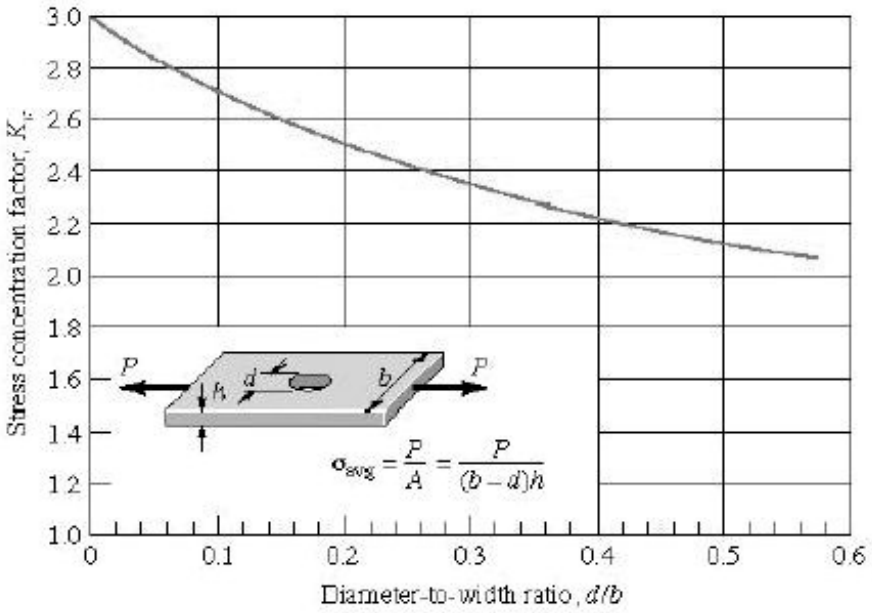

Figure 3.8: Specimen geometry and governing equations used as the reference for the finite element model of the stress concentration caused by the circular hole, [12]. The model approached the calculated reference value within 1% after mesh refinement.

general procedure involved first refining the mesh away from the hole until it converged to the calculated nominal stress value. From there, the mesh size surrounding the hole was further refined until the stress converged on the value that made the K_t approach the correct value. The K_t is simply the ratio of the stress near the hole to the nominal stress in the plate. This test determined which mesh and boundary condition settings are required for the more complex cases involving a crack and a pit.

The next step to develop a finite element model involved modeling a horizontal crack from the edge of the hole to determine whether or not the finite element model approached the closed form solution. The same refinement procedures were used as in the stress concentration factor scenario and the convergence plot and final mesh are shown in Fig. A.3 and Fig. A.4, Appendix A. It is especially important that the mesh near the crack be refined so that accurate results are achieved, as shown in Simandjuntak's study [38]. The

stress intensity factor from the FEA model was within 2% of the value given by Eq. 3.1 given the same loading and geometric conditions. This convergence occurred when the mesh density approached 1.4 elements/mm^2. It is important to note that Abaqus returns a the K_{max} value [18]. The ΔK values must be calculated using eq. 3.2 ($R = 0.5$).

$$\Delta K = K_{max} * (1 - R) \tag{3.2}$$

The minor differences in the results between the closed form and FEA solution is likely a result of the assumptions of the equation. The equation assumes infinitely wide plates, or a situation in which the size of the crack/hole are small enough when compared to the width of the specimen that the plate could be considered infinitely wide. The experimental specimens do not fulfill these assumptions. As a result, slight deviation from the equation is expected.

After successful completion of a two-dimensional model of a hole with a horizontal crack, the mesh and element settings were applied to a model consisting of a crack originating from a corrosion through pit on a circular hole to mimic the actual geometry of the specimens. Since the calculation of the stress intensity factor requires a sharp point, the pit was modeled so that a small sharp crack extended from the middle of the pit perpendicular to the load direction. This configuration mimicked the actual geometry very closely. To keep the results consistent, the total length of the pit and the small crack was equal to the total length of the crack used in the crack-only FEA model. The pit diameter in the model was set at 0.30 mm because this is the average value of the experimentally created pits. The pits used in the models were assumed smooth, i.e. uniform half-circles to reduce the complexity of the FEA model. The ΔK values for this model matched identically to the results from the crack only model of the same overall crack length and load conditions. In other words, the pit was not a factor in the determination of the stress intensity factor in Abaqus. Instead, the main geometric factor in determining the stress intensity factor

was the total flaw length. Since there was no difference in the results of the two models, the crack-only model was used to determine the ΔK values for the specimens because it was less computational intensive. To determine the initial stress intensity values of each specimen, the initial pit lengths were assumed to be the length of the crack in the Abaqus model. The results for the initial ΔK values are shown in Table 3.4. The table shows the expected value of the closed form solution as well as the corresponding results of the FEA models. Additionally, the convergence plot and final mesh are shown in Fig. A.5 and Fig. A.6, Appendix A. After the initial conditions for each specimen was modeled, different crack lengths during the growth of the crack from the pit were modeled. Then, interpolation was used to fill in the values between these data points. This was done because it would be inefficient and time consuming to create an Abaqus model for each of the crack sizes throughout the experiments. These values are discussed in the figures of chapter 5.

Table 3.4: ΔK values predicted by the closed form solution and the ΔK values produced by Abaqus for through pit specimens.

Specimen	**Predicted ΔK,** $MPa * \sqrt{m}$	**Abaqus Model, mm**	**Total Flaw Size, mm**
SAl-02	5.0	4.9	0.38
SAl-03	3.4	3.5	0.35
SAl-04	4.0	3.9	0.29
H13	3.0	3.0	0.31
SSl-01	4.0	3.9	0.27
SSl-02	5.0	4.9	0.34
SSl-03	3.5	3.6	0.31
SSl-04	3.0	3.0	0.31
SSl-05	2.75	2.74	0.30

After the through-pit specimens were successfully modeled, the next step involved modeling the corner pit specimens. Aside from the obvious geometry differences, the models differ because the corner pit models must use three dimensional geometry as the pit does not go all the way through the specimen. Rather, the pits go no more than halfway through the thickness. Three dimensional modeling requires a great deal more effort, when

compared to two dimensional modeling, because the model must be partitioned into small, simple three dimensional regions [18]. This is done because Abaqus is not able to mesh complex shapes, like a hole with a crack, using its automatic meshing techniques. As a result, significant user input is required to create geometrical regions that are suitable for hexagonal mesh elements which then must be meshed by hand using the bottom-up meshing technique. Abaqus does have the ability to mesh complex shapes using tetrahedral elements. However, these elements are not suitable for use in the region of a crack [18, 32].

Creating a three dimensional version of the through pit model provided a simple case to determine which meshing methods are most accurate for three dimensional modeling. Since the through pit model had fairly simple geometry, meshing the model with solid C3D8R elements was easily accomplished using the built in Abaqus meshing algorithms. There was no significant difference between the results of the three dimensional and two dimensional through pit models, ceteris paribus.

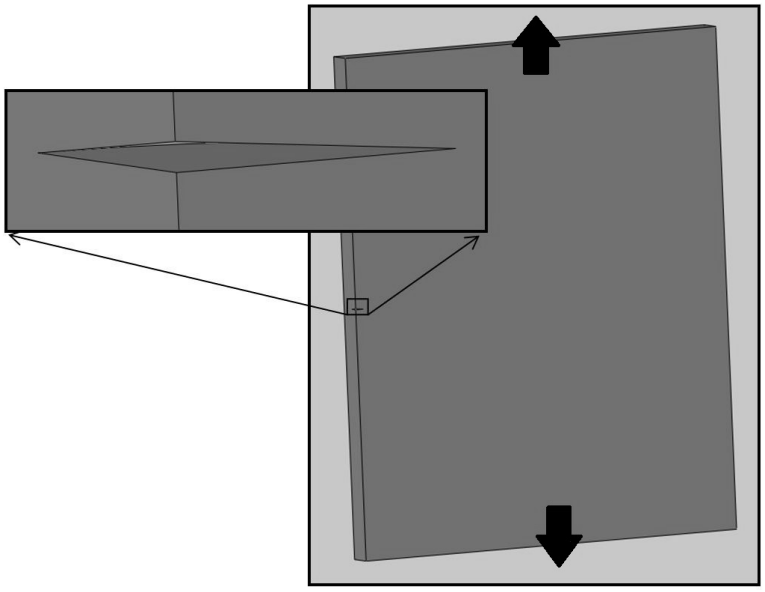

Figure 3.9: The original corner crack model created using Solidworks. This model was too complex for Abaqus to create a reliable mesh. The arrows indicate the loading directions.

Unfortunately, the meshing/modeling techniques used in the three dimensional through-pit model did not carry over to the corner-pit model because the corner crack proved to be much more complex in terms of meshing than the straight through crack. It took several iterations of corner crack model until a reliable model was created. The first step was to create a model that had a closed form solution available to compare the model to the equation's results. The first attempt involved importing a full corner crack model from Solidworks, Fig. 3.9, and attempting to mesh the part in Abaqus.

Due to the complex nature of the physical corner crack, an appropriate mesh could not be created. The next attempt involved modeling the plate as a top half and a bottom half each containing a corner crack partition. In other words, there is no physical crack modeled, but instead, there is a region that was allowed to separate from one another while the rest of the surface was not allowed to separate, Fig. 3.10. This technique is referred to as creating a seam [18]. The convergence study for this model is shown in Fig. A.5, Appendix A.

As a result, Abaqus views the region as a crack, but does not have any difficulty meshing the simple geometry. Additionally, the model obeyed the following conditions: $\frac{a}{t}, \frac{a}{b} < 0.5$ as described by the geometry in Fig. 3.11.

$$K = \frac{2}{\pi} * \frac{P}{4 * b * t} * \sqrt{\pi * a} \tag{3.3}$$

Since, the conditions of the equation were met by the FE model, the solution approached the exact closed form solution from Dowling within 1%. The values converged only after significant refinement of the mesh near the crack. The convergence study data is shown in Fig. A.5, Appendix A.

The corner crack model acted as a proof of concept for completing a corner pit model. Instead of creating a three dimensional corner pit in Abaqus, the corner pit was assumed to

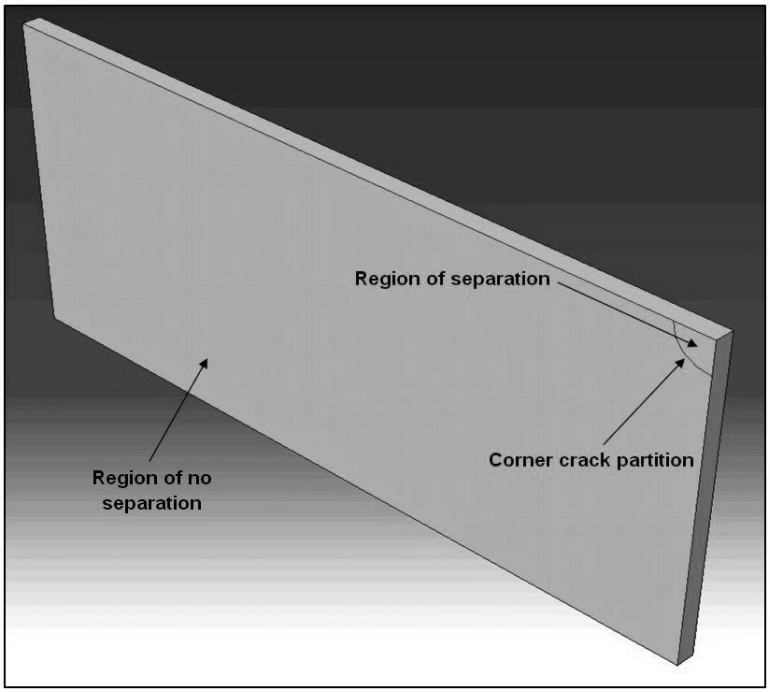

Figure 3.10: One half the symmetrical model for the corner crack example created in Abaqus. Notice the different regions of separation around the crack. This model had a geometry that could easily be meshed by Abaqus automatically.

be a quarter circular crack on the edge of a hole. Since Abaqus uses the total length of the flaw to calculate the stress intensity values, this is a valid assumption. The corner pit model was created as two halves that mirror one another along the crack growth plane. Each half was approximately 5 mm tall; much shorter than the actual experimental specimens. They were shortened to reduce the number of total elements and, subsequently, the computing power required to run the model simulations. The width and the thickness of the model matched those of the test specimens (50.8 mm wide and 3.2 mm thick). Once these two halves were created, they were bonded using the interference tools in Abaqus. The model was made so that the corrosion pit partitions were allowed to separate from one another, but the rest of the bonded surfaces were not allowed to move with respect to each other. This

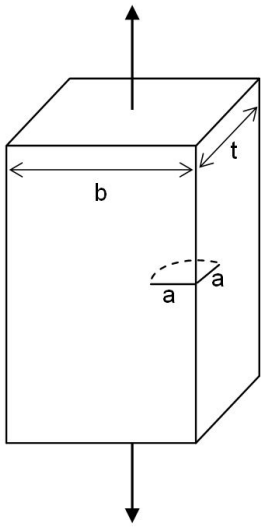

Figure 3.11: Geometry that is described by Eq. 3.3. It is important to note that eq. 3.3 is only valid when the crack is small compared to both the thickness and the width of the specimen. [12]

is the same seam method that was employed for the corner crack example model. Figure 3.12 illustrates the various different regions in the finite element model.

Even with all of the assumptions and simplifications used in the model, the meshing process was still far from simple. First, the model required a great deal of partitions throughout the model (especially near the crack region) because of the complex geometry associated with the hole-crack interaction. The model was partitioned until the region around the crack became a small cube with a height and width approximately equal to the radius of the crack. This cube region containing the crack required using the bottom-up meshing technique to manually mesh the volume. Once these regions were meshed by hand, the remainder of the model could be meshed automatically using the swept mesh of C3D8R elements as shown in Fig. 3.13. The convergence study for this model is shown in Fig. A.5, Appendix A.

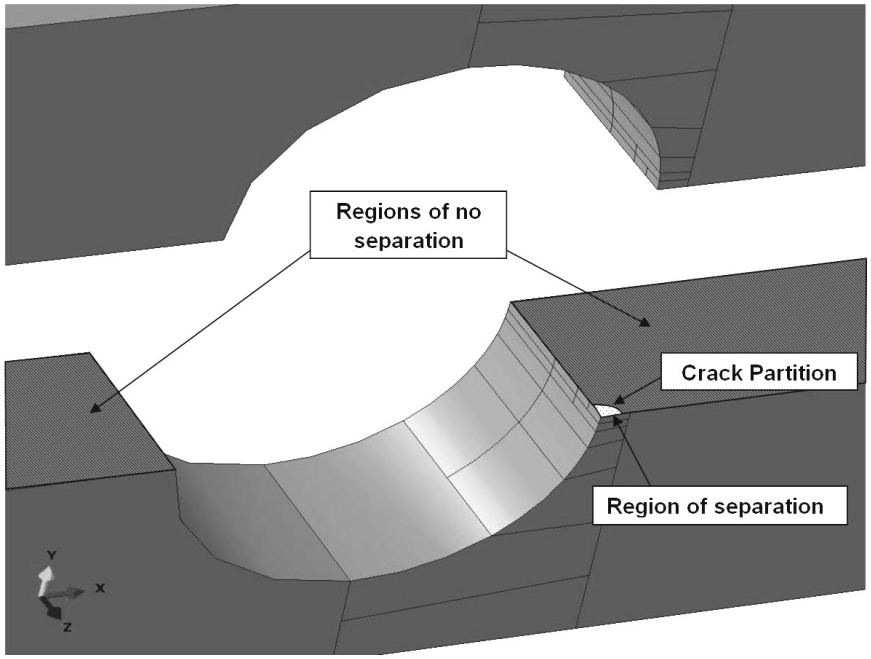

Figure 3.12: The two halves which make up the corner pit finite element model. Notice the regions of separation where the corrosion pit exists and the regions of no separation everywhere else on the surfaces. Also, notice the number of partitions required to simplify the geometry.

The working model was then used to model each corner-pit specimen. This way, the accurate ΔK values could be determined for each pit size and loading condition (Table 3.5) and this data could be compared against the previous research data. To determine the stress intensity factor as the crack grew, several iterations of models were made. Each iteration had a different crack length. Once enough iterations were modeled, the data was interpolated to fill in the un-modeled data points.

This incremental modeling was done because it would be impractical to model every iteration of the crack growth for each specimen. Figure 3.14 shows the stress intensity factor as the size of the corner crack changed. As the corner crack increases in size, the aspect ratio of the crack changes. This means that the width of the crack, c, grows faster

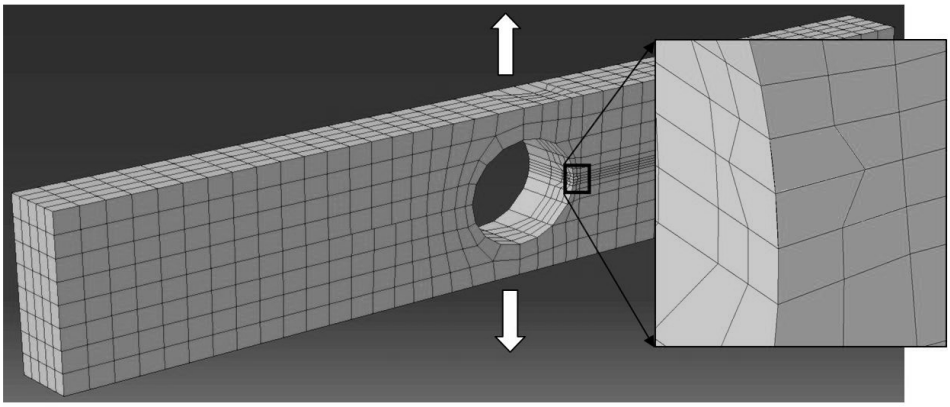

Figure 3.13: The final mesh of the corner pit model. Notice the number of partitions and the finer mesh in the regions of the pit (black box).

Table 3.5: ΔK values predicted by the closed form solution from Dowling and by Abaqus for corner pit specimens.

Specimen	**Predicted dK,** $MPa * \sqrt{m}$	**Abaqus Model, mm**	**Total Flaw Size, mm**
SAS-01	4.0	2.11	0.31
SAS-02	5.0	2.35	0.43
SAS-03	3.5	1.62	0.37
SAS-04	3.0	1.6	0.47
SAS-05	3.75	1.93	0.51
SSS-01	4.0	2.02	0.37
SSS-02	5.0	2.16	0.36
SSS-03	3.5	1.63	0.37
SSS-04	3.0	1.54	0.37
SSS-05	3.75	1.91	0.42

*Note: The large discrepancy between the predicted and Abaqus values lie in the fact that the predicted values were calculated assuming a through pit because 3.1 is not applicable for corner pits.

than the length of the crack, a. So, during the initial stages of crack growth, a/c becomes smaller. This was observed in the experiments because the crack would appear on the side of the specimen with the corner pit and, a short number of cycles later, the crack appeared on the opposite side of the specimen. This is only possible if the length of c increased

faster than the length of a during the early stages of crack growth. Fig. 4.13 illustrates this where a typical experimental growth of a corner pit is shown. Similarly, this change in aspect ratio explains the sharp increase of the stress intensity range in Fig. 3.14 at lower a values because the crack's width is increasing faster than its length. When the crack length reaches the thickness of the specimen, the stress intensity range follows a more linear trend as dictated by Eq. 3.1.

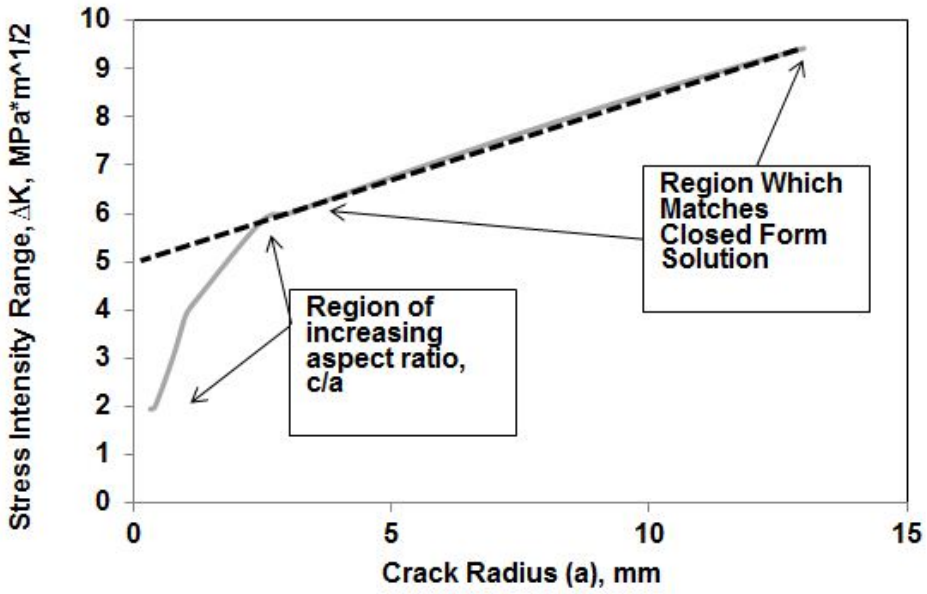

Figure 3.14: Plot showing the change in ΔK as the corner crack grew. Since the corner crack did not grow symmetrically in the experiments, the aspect ratio was changed until the crack resembled as through crack. The dashed line represents the closed form solution while the solid line represents the finite element values.

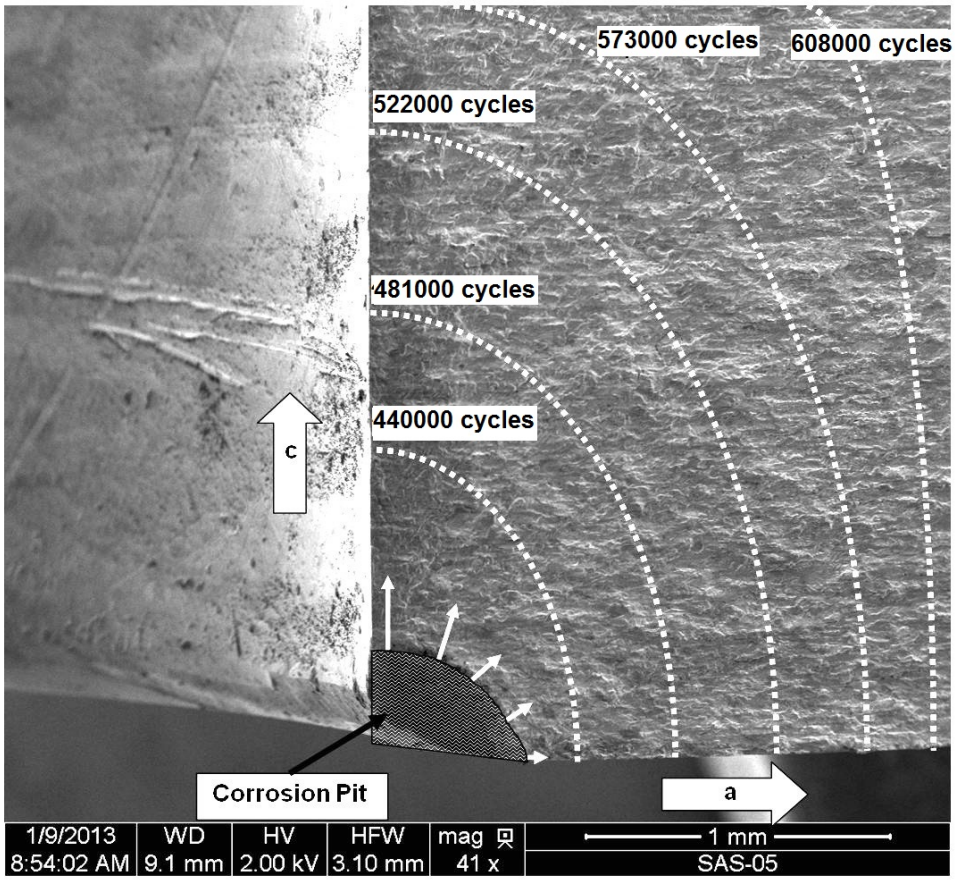

Figure 3.15: SEM photograph illustrating the changing aspect ratio, a/c, during the corner crack growth. This was shown during the experiments because the crack appeared on the opposite side of the corner pit after the crack initially appeared on the corner pit side.

IV. Results and Discussion

4.1 Chapter Overview

This chapter presents the results from all the experiments. The results for the uni-axial specimens with through pits are discussed in section 4.2. The results, for the uni-axial specimens with corner pits are discussed in section 4.3. Results for these experiments include plots relating the stress intensity range to the number of cycles required for a fatigue crack to initiate, plots of the crack growth rate as a function of stress intensity range, as well as the interpretation of the SEM images with regard to fatigue crack initiation.

4.2 Results of Specimens with Through Pits

Testing for the uni-axial specimens with through pits occurred smoothly except for the specimen SAl-01. This specimen had incorrect loads applied and as a result, its results were disregarded. Crack initiation and growth occurred for ΔK's of 3.5, 3.9, and 4.9 when exposed to air and for ΔK's of 2.74, 3.0, 3.6, 3.9, and 4.9 when exposed to a saltwater environment. The specimen H13 ($\Delta K = 3.0$, through pit) did not initiate after 1 million cycles in the air environment so this particular experiment was terminated. The crack length versus the number of cycles for the specimens that did have crack initiation and growth are shown in Figs. B.1-B.7 (Appendix B). Similarly, the $\frac{da}{dN}$ vs. ΔK curves are shown in Figs. B.8-B.14 (Appendix B). The $\frac{da}{dN}$ vs. ΔK curves were derived from the experimental data. During the experiments, the crack length was measured after every 5751 load cycles and, as a result, the crack length had reasonable resolution. The crack length was plotted with respect to the number of cycles and a polynomial trend line was applied using Microsoft Excel. The trend line determined onset of crack growth with more accuracy than the camera monitoring technique. This is because during some experiments the cracks would be undetectable until they reached a sizable length of up to $1mm$. As a

result, the trend line was used to detect when the crack first initiated giving a more accurate estimate of the crack initiation than the camera data alone. Additionally, the crack growth rate curves were calculated by using the derivative of the trend line from the crack length plot. This was done because a $\frac{da}{dN}$ curve is by definition the rate of change of a crack length vs. cycles curve. Since the trend line of the crack length eliminated some of the data scatter, the derivate of this line further reduced the data scatter that is inherent in manual experimental measurements. This data was used to plot the cycles until initiation vs. ΔK as shown in Fig. 4.1. The combined $\frac{da}{dN}$ data for all of the through pits specimens is shown in Fig. 4.11. In this figure, the data points are from the current experiments, while the trend lines represent the data for the notched specimens in the Misak et al experiments [28].

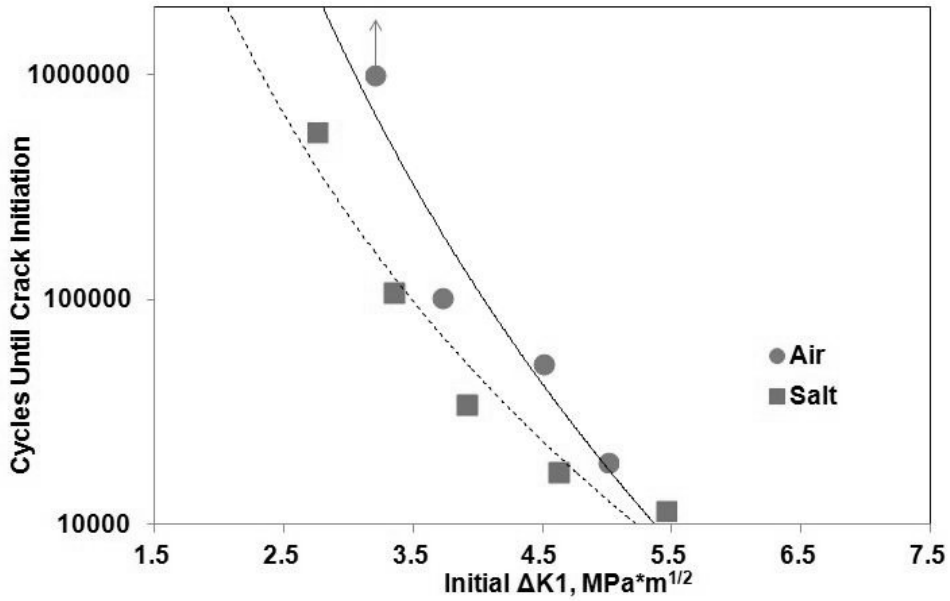

Figure 4.1: Plot of the cycles until initiation vs. the stress intensity factor for the through pit specimens exposed to both air and saltwater (3.5 %) environments. (Power function trendlines)

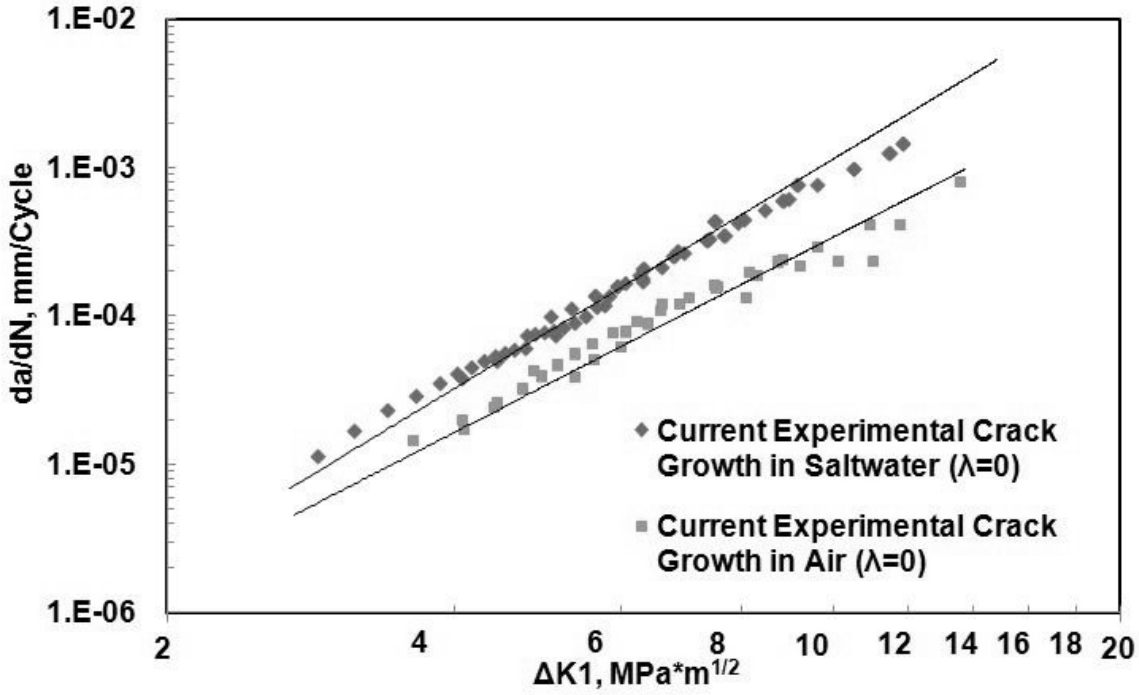

Figure 4.2: The crack growth rate of the through-pit specimens as a function of the stress intensity range. The crack rates are very similar throughout the entire life span of the fatigue crack. The trend lines are from the previous Misak et. al data and the data points represent the current research data [28].

4.3 Results of Specimens with Corner Pits

All of the corner pit experiments occurred without any irregularities. In air, crack initiation occurred for ΔK values of 2.18, 1.93 and 2.35. Fatigue cracks did not initiate in the specimens with ΔK values of 1.60 and 1.62 after 1 million cycles, as a result, the experiments were terminated before failure. The crack growth plots for the specimens that did have crack growth in air are shown in Figs. C.1, C.3 and C.2. In the saltwater solution, initiation occurred for ΔK of 1.91, 2.02, and 2.16. Fatigue crack initiation did not occur in specimens with a ΔK less than 1.91. The crack growth plots are shown in Fig. C.4, C.5, and C.6 (Appendix C). Additionally, the da/dN vs. ΔK plots for the specimens that had

crack growth are shown in Fig. C.3, C.7-C.12 (Appendix C). These plots were developed using the same trend line techniques that are described in the previous section. Figure 4.3 shows the cycles until initiation for the experimental stress intensity ranges. Figure 4.12 is a compilation of all of the crack growth rate data for the corner pit specimens. In this figure, the data points are from the current experiments, while the trend lines represent the data for the notched specimens in the Misak et al experiments [28].

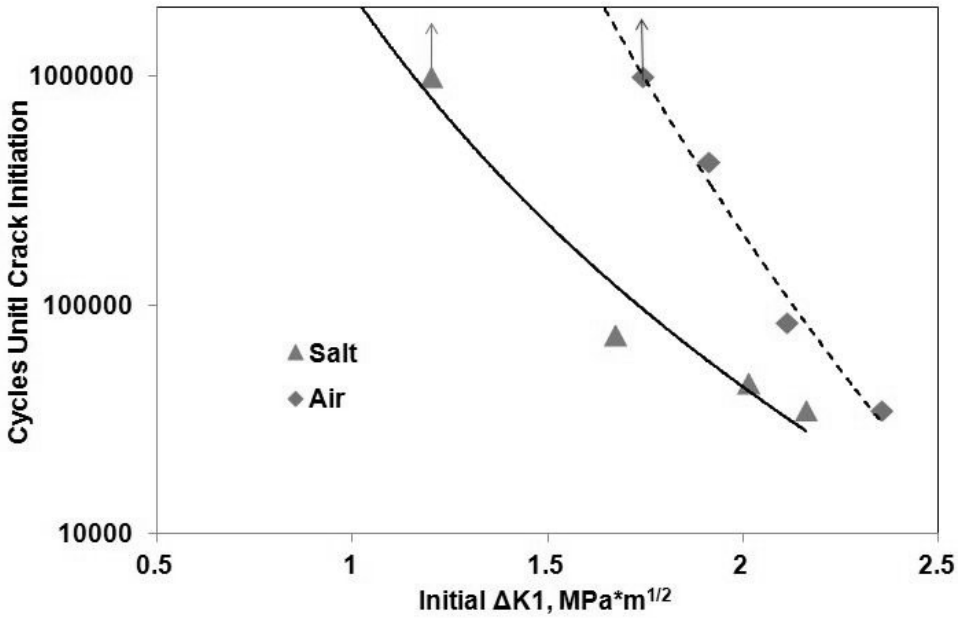

Figure 4.3: Plot of the cycles until initiation vs. the stress intensity factor for the corner pit specimens exposed to both air and salt environments. (Power function trend lines)

4.4 Microscopy Results

After the experiments were completed, the test specimens were cut so that the two halves (above and below the crack) could be separated. From here, the actual pit size could be measured with the SEM and/or optical microscopes because the entire pit was visible for examination. Examples of both through pits and corner pits are shown in Fig. 4.5 and

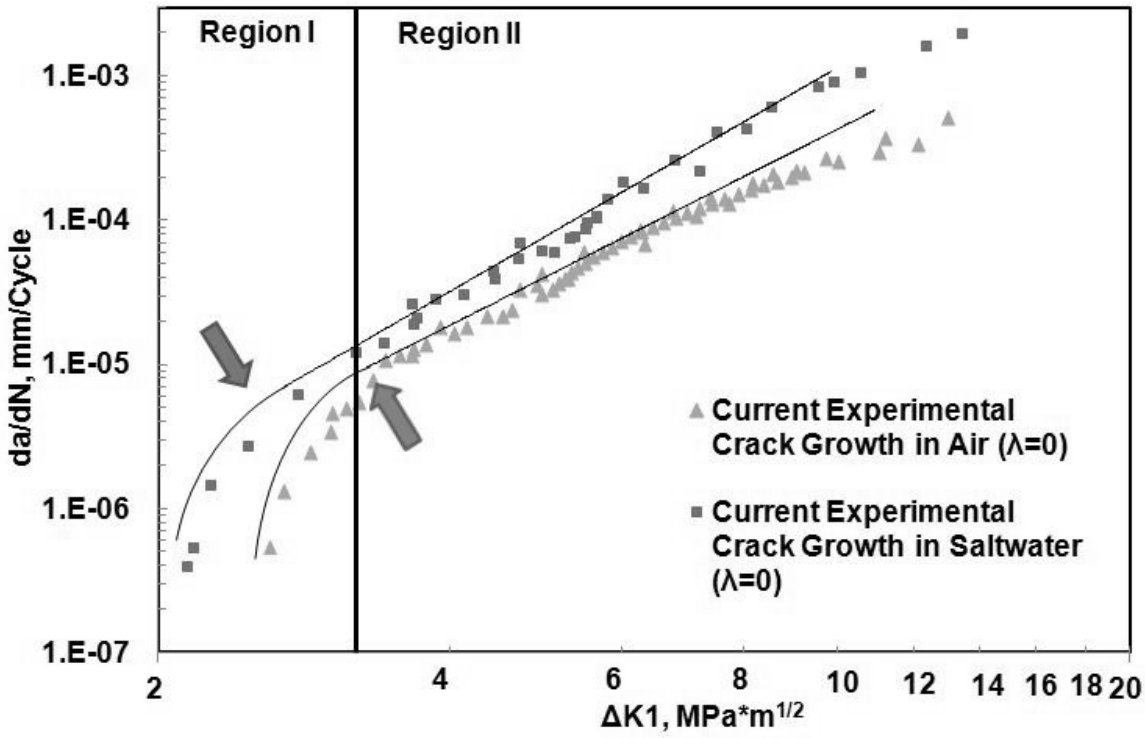

Figure 4.4: Plot showing comparison of previous crack growth data with current crack growth data for all of the corner pit specimens. The trend lines are from the previous Misak et. al data and the data points represent the current research data [28]. The arrows shows when the crack reaches the width of the specimen. The threshold values of ΔK for crack growth saltwater is 1.90 and in air is 2.17.

the measurements are shown in Fig. 4.6 and 4.7, respectively. Since the pits have irregular geometries, several measurements along the length of the pit were taken. The average pit size from each specimen was used in the corresponding Abaqus model to determine the stress intensity factor prior to any fatigue loading. These updated ΔK values replaced the values previously calculated from the closed form stress intensity solutions in the various plots and tables. While the microscopes were crucial in determining the initial conditions

of the specimens, it was also invaluable in studying the way fatigue cracks initiated and grew.

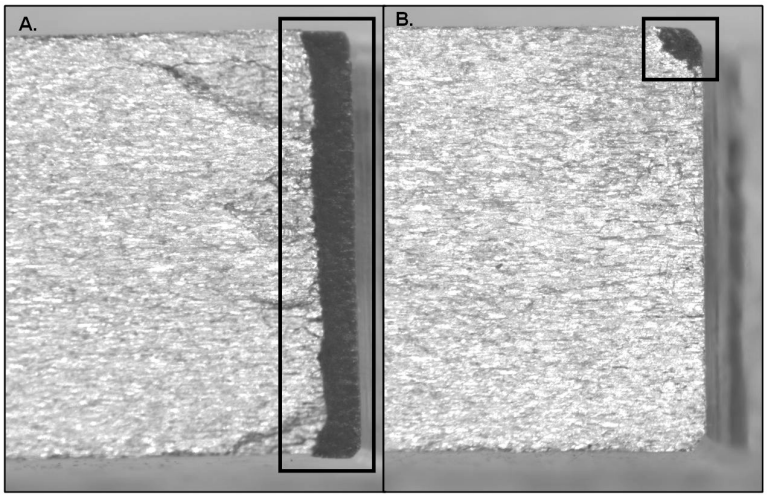

Figure 4.5: A.) Top view of a through pit (box) after the specimen was split into two halves along the fatigue crack. B.)Top view of a corner pit (box) after the specimen was split into two halves along the fatigue crack. Both pictures taken using a Zeiss optical microscope at 25x magnification.

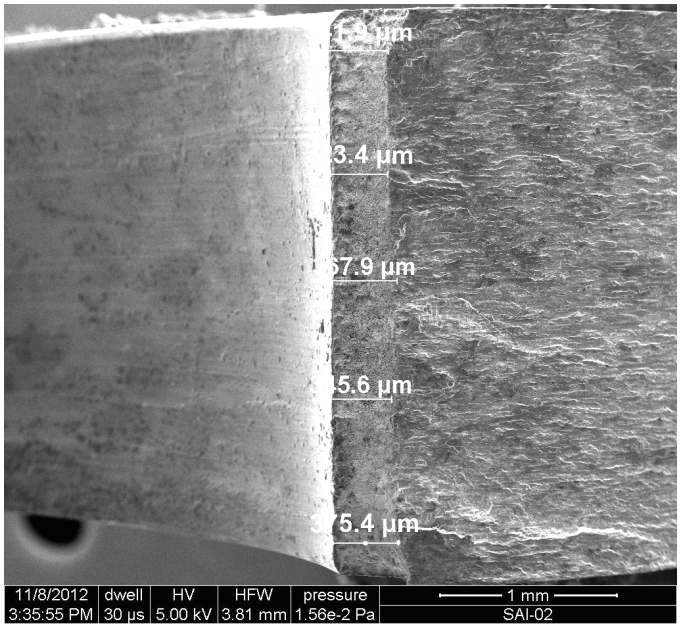

Figure 4.6: Top view of the through pit specimen SAI-02 using the SEM. Measurements of the pit were taken at several positions so that an average pit size could be calculated. These actual pit sizes were plugged into the Abaqus models as the initial crack size.

Using the SEM the crack initiation from the corrosion pit could be studied with significantly more detail when compared to using an optical microscope. For through pit specimens, the crack initiation occurred in a fairly uniform manner despite having multiple initiation sites. In other words, micro cracks generally formed in several different locations. Each of the micro cracks would grow for a short time and after a number of cycles, these micro cracks coalesced into a single crack front that continued to propagate until the end of the fatigue loading. The marker bands were used to determine when one part of the fracture surface initiated before another part. The area that initiated first will have marker bands before any other initiation region. One area of initiation is shown in Fig. 4.8. The crack began near the left most set of marker bands and continued to grow towards the right. These small areas of initiation occurred along the corrosion pit and eventually formed into

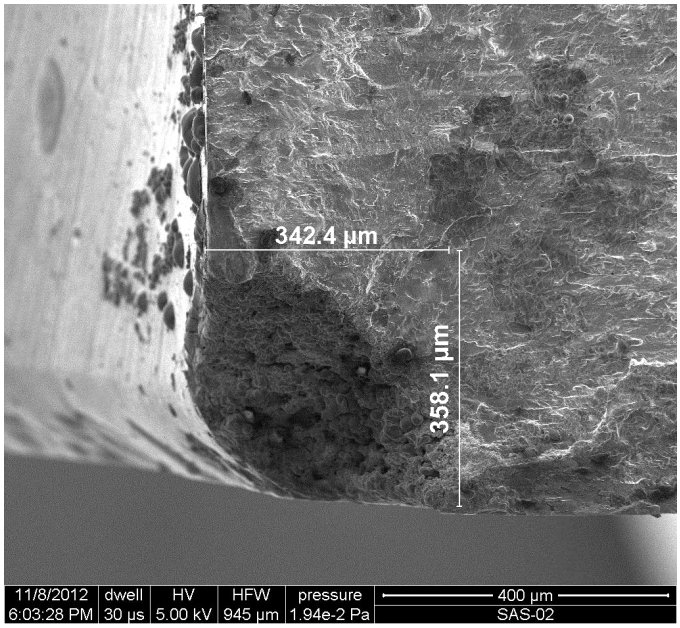

Figure 4.7: Top view of the corner pit specimen SAS-02 using the SEM. Measurements of the pit were taken at a point that represented the average radius of the pit. These actual pit sizes were plugged into the Abaqus models as the initial crack size.

one continuous crack front. As a result, the initiation and early stages of crack growth are very similar those same stages in the machine notch specimens from the Misak et al. study [28].

The SEM was crucial in determining the crack initiation in the corner pit specimens. Due to the geometry of the corner pit, there are many fewer possible crack initiation sites than for a through pit specimen. Consequently, the crack initiation site can be narrowed down to a fairly specific region. Since the crack initiated in a concentrated area, the crack forms a unified crack front with fewer load cycles than a through pit specimen. This is shown by the marker bands outline in Fig. 4.9.

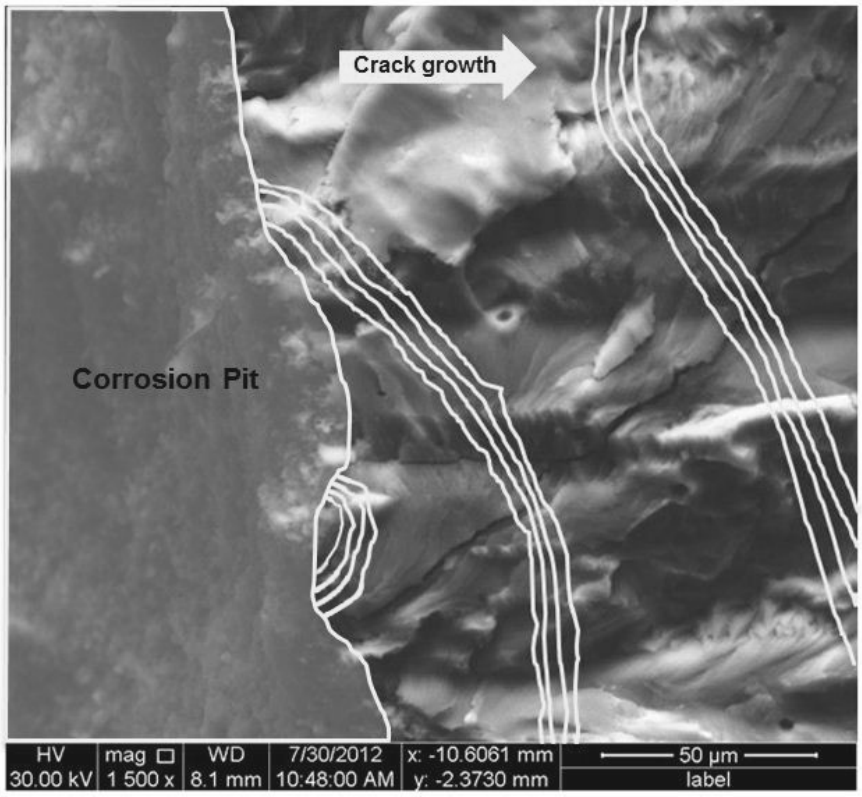

Figure 4.8: SEM photograph showing one area of crack initiation in a through pit specimen. The white lines highlight different sets of marker bands as the number of fatigue cycles increases during the experiments. The sets of maker bands appear at 418000, 424000, and 430000 cycles respectively from left to right.

4.5 Discussion of Results

As expected, as the stress intensity factor increases, the cycles until crack initiation decreases. Also, the specimens that are exposed to saltwater (3.5%) develop fatigue cracks in fewer cycles than their counterparts that are only exposed to laboratory air. This is true for both through and corner pit specimens as shown in Fig. 4.10.

The crack growth rates of each set of specimens compared to the machine-notched specimens in the Misak et al study was also an important result [28]. Fig. 4.11 shows the

crack growth rates for both the through pit specimens and the previously tested machine-notched specimens.

There is virtually no difference between the crack growth rates of two types of flaws. This is evident from the lack of difference between the data points (current experiment) and the trend lines (Misak et al experiments). Also, this figure shows that the growth rate for those specimens exposed to saltwater is higher than their counterparts tested in a laboratory air environment. These results are a slight surprise because it was expected that the process of coalescing the micro cracks into a uniform crack front would slow the crack growth rate initially when compared to the machine notched specimens. This is because the machine-notched specimens have a smooth surface for a uniform crack front to initiate and grow. The lack of difference is likely due to the fact the while the through pit surfaces were irregular, they were not irregular enough to cause a detectable difference in the growth rate results. The same cannot be said for the corner pit specimens.

Fig. 4.12 shows the crack growth rates at various stress intensity factors for the current experimental corner pit data and the Misak et al data [28]. The current data is represented by the data points and the previous data is represented by the trend lines. This figure shows that the growth rates of the corner pit specimens are smaller than the machine-notched specimens at low stress intensity values. This makes sense because the crack front must grow from the quarter circular pit to a crack front the width of the specimen as shown in Fig. 4.13.

Since the crack front is initially a quarter circular shape, it requires a number of cycles to grow into a full thickness through crack. As a result of these extra cycles, the crack growth rate is initially slower than the machine-notched specimens. Once the crack front extends across the thickness of the specimen, crack grow rate matches closely to the machine notch specimens. This is expected because by this point in the fatigue life, the two

sets of specimens have the same crack front geometry. The slower crack growth can also be attributed to a smaller number of possible initiation sites along the pit when compared to the machined specimens. This is simply because the corner pit has less surface than the machined notch or the through pit.

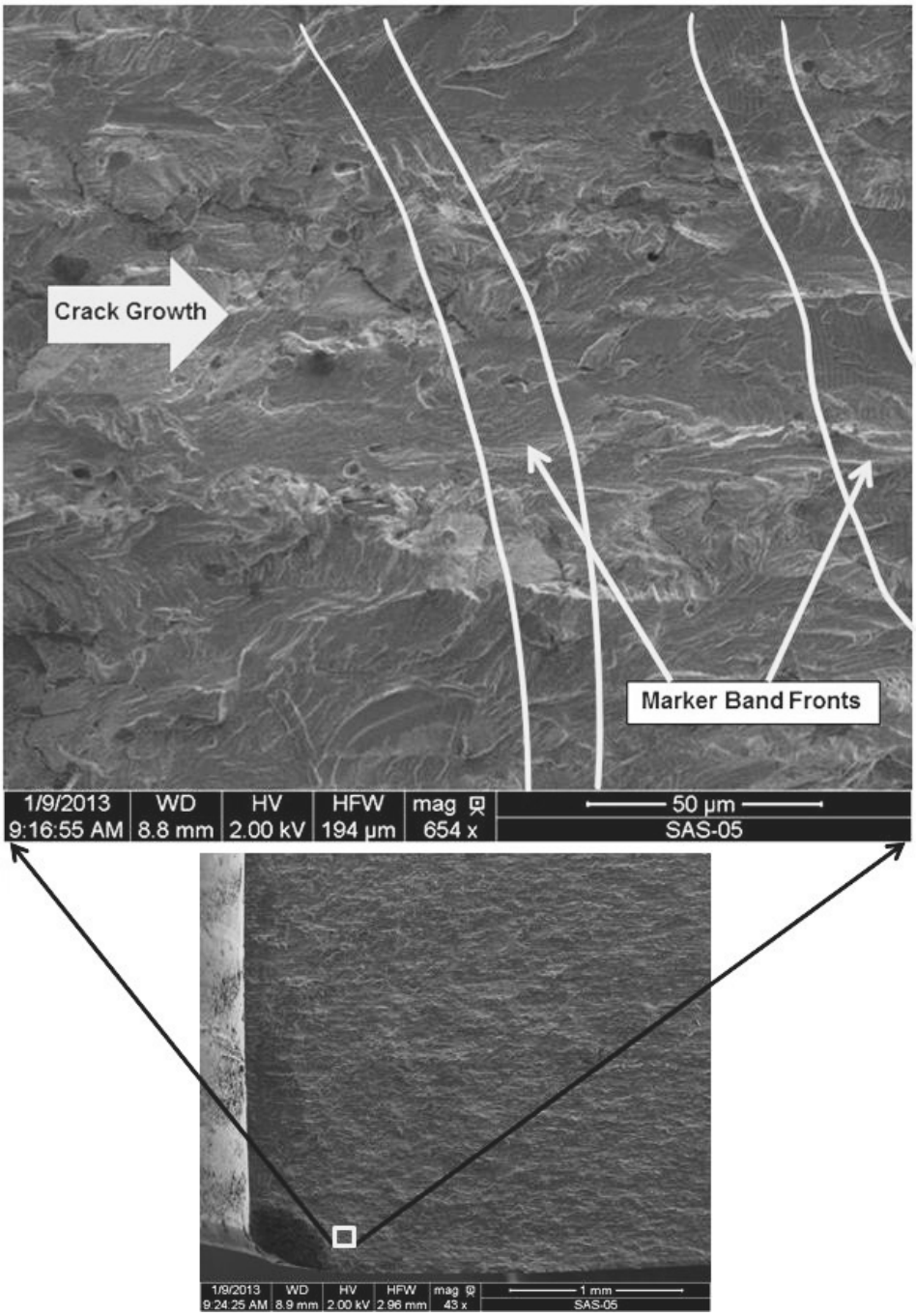

Figure 4.9: SEM photograph showing the how the crack front is unified in the early stages of crack growth. This is due to the limited number of initiation sites and the corner pit geometry. The marker bands appear at 430000 and 436000 cycles respectively from left to right.

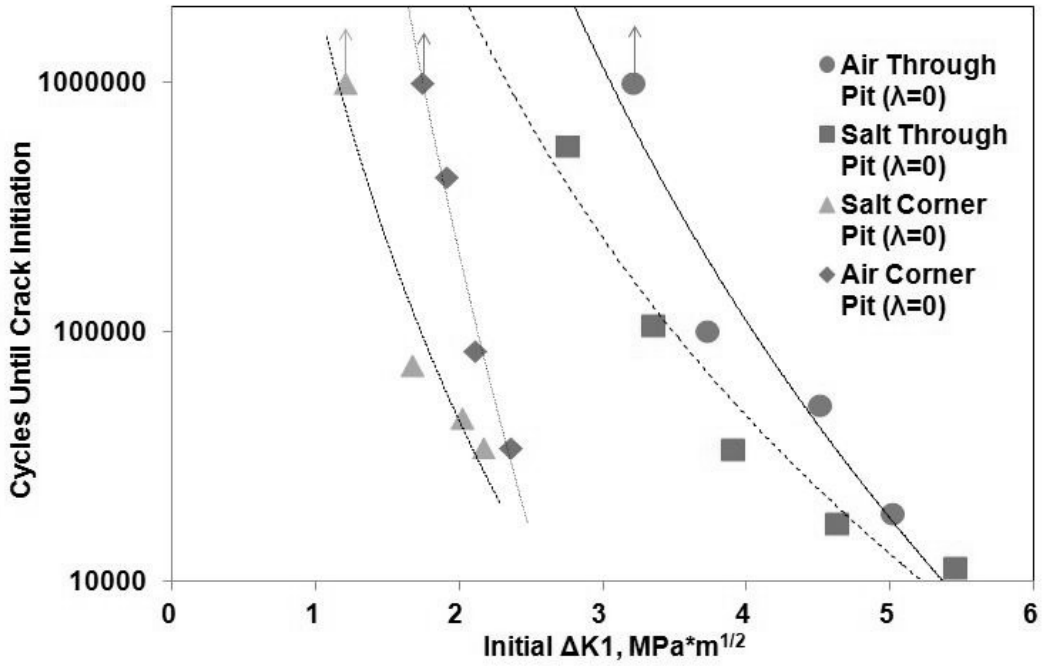

Figure 4.10: Plot showing the cycles required for fatigue crack initiation for all experimental specimens. Saltwater exposure reduced the time to produce fatigue crack for both through and corner pit specimens.

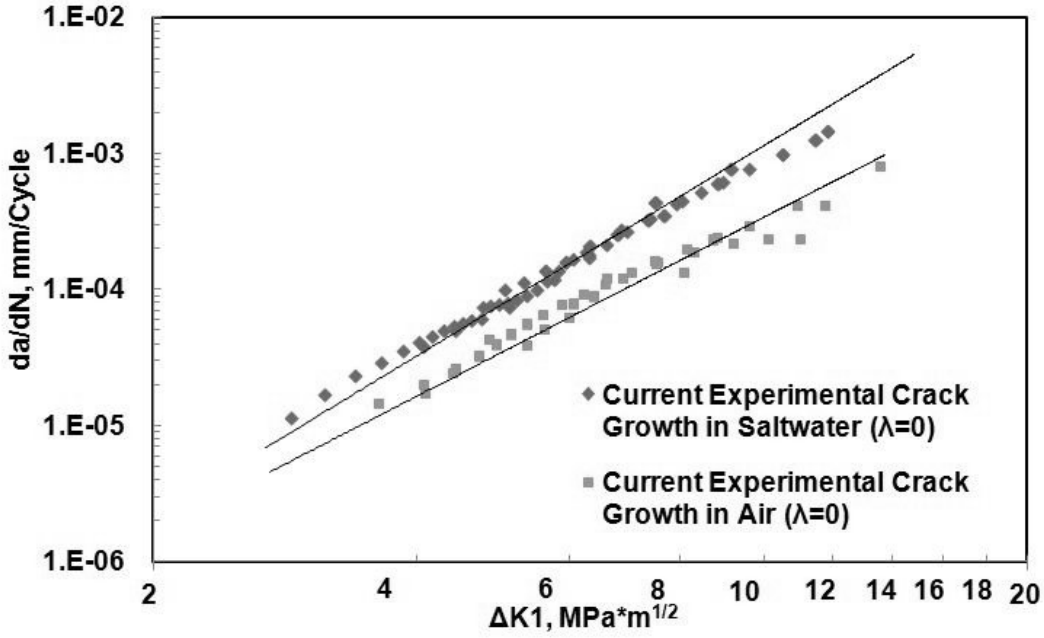

Figure 4.11: The crack growth rate of the through-pit specimens as a function of the stress intensity range. There is little variation from the pitted specimens (data points) and the machined specimens (trend lines). The trend lines are from the previous Misak et. al data and the data points represent the current research data [28].

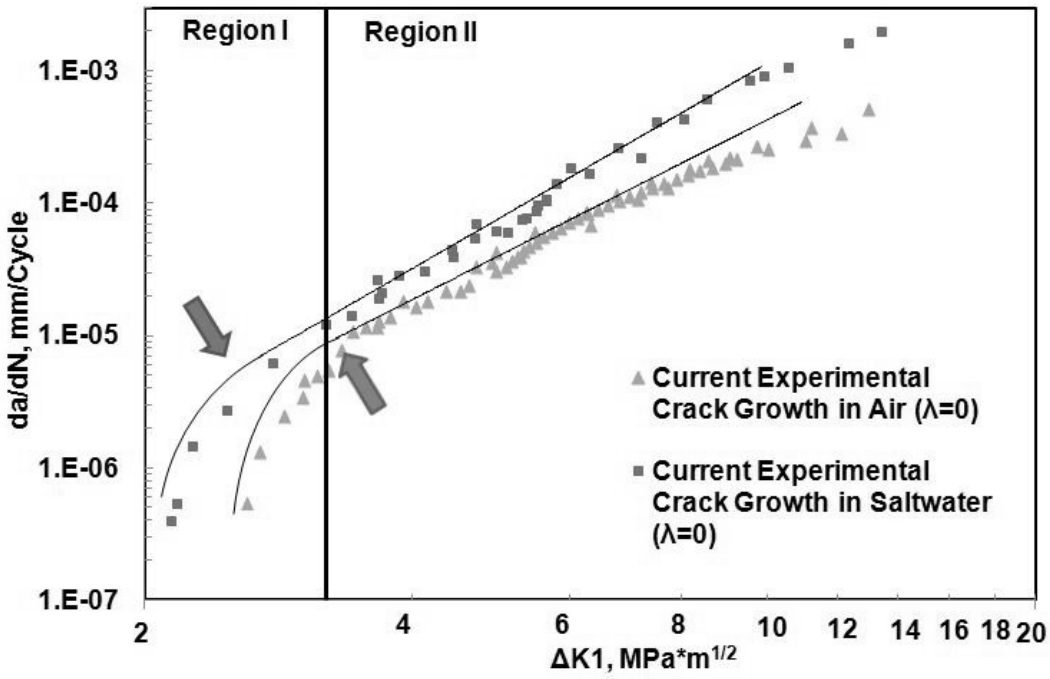

Figure 4.12: Plot showing the crack growth rate data for all of the corner pit specimens. The data points represent the corner pit specimens and the trend lines represent the machine notch specimens.

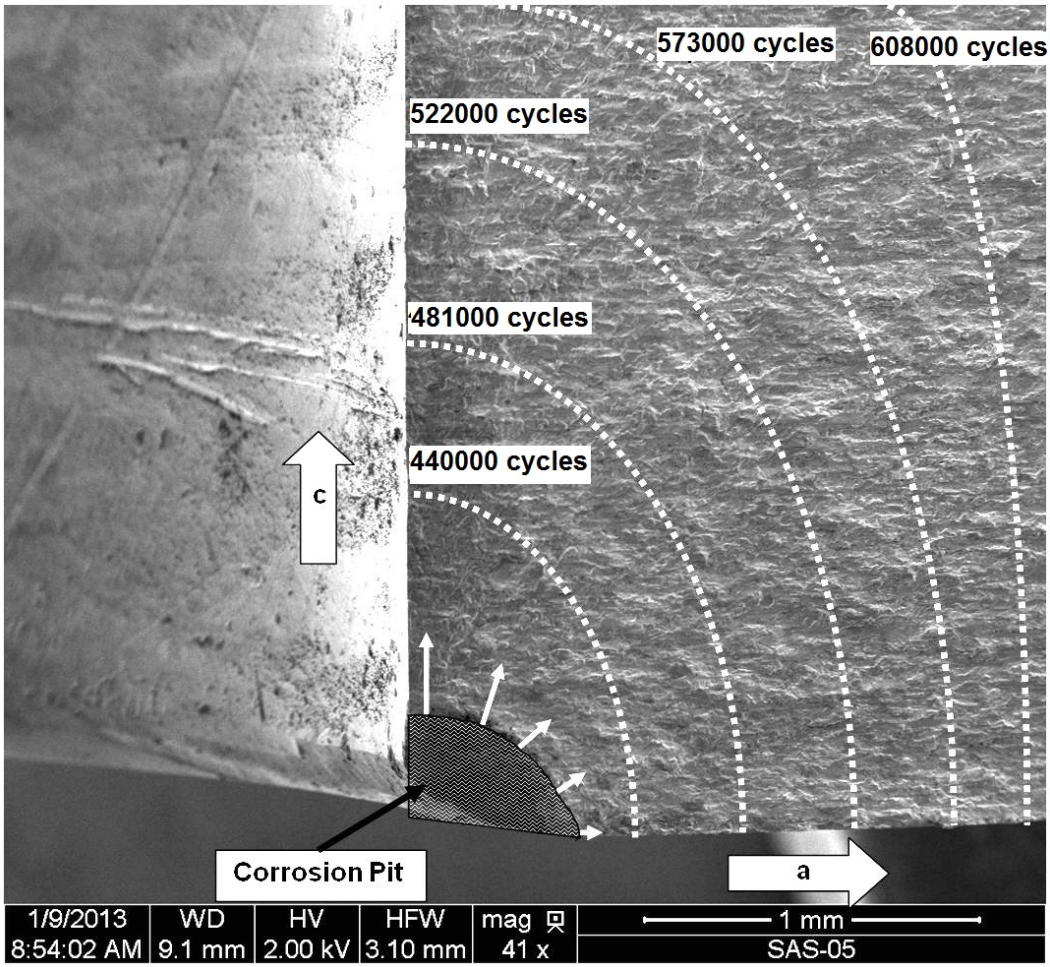

Figure 4.13: SEM photograph illustrating the changing aspect ratio, a/c, during the corner crack growth. The growth of the crack from the pit to a full width crack front required a number of fatigue cycles resulting in slower initial crack growth.

V. Conclusions and Recommendations

5.1 Conclusions

This work investigated the fatigue crack initiation in 7075-T6 test specimens with through and corner corrosion pits that were exposed to both laboratory air and saltwater (3.5%) environments. These specimens were fatigued to a 17 mm long crack using a uni-axial MTS load frame. From these experiments, the crack initiation and fatigue crack growth rates were determined. These results were compared to the crack initiation and fatigue crack growth rates of test specimens with machined flaws. Additionally, the SEM was used to examine the fracture surfaces closely to determine the mechanisms of crack initiation for the fatigued specimens. Along with experimental procedures, finite element models were created to predict the stress intensity range (ΔK) for the test specimens both iniatially and as the crack growth progressed. This was done, in part, to confirm the validity of Eq. 5.1 for through pit specimens and to determine the ΔK values for the corner pit specimens since no closed form solution exists.

Conclusions determined by the results of the study invloving uniaxial fatigue loading (tension-tension, 20 Hz, R=0.5) include:

- A corrosive environment (3.5% saltwater) reduces the fatigue crack growth rate of through pit specimens under cyclic uni-axial load by an average of 30% and corner pit specimens by an average of 20% when compared to through and corner pit specimens exposed to laboratory air.

- A corrosive environment decreases the cycles required for crack initiation in both types of corrosion pits, i.e. through and corner pit. The reduction is up to 67% for through pits and the reduction is up to 59% for corner pits.

- Using Eq. 5.1 is not an appropriate method for approximating the ΔK values of the corner pit specimens until the crack front width equals the width of the specimen, i.e. this equation is only valid for $a > 1.1t$, if $\frac{a}{t}$=0.1.

$$\Delta K_I = .5 * (3 - \frac{a}{c+a}) * (2.243 * (1 - \frac{a}{c+a}^{3}) * \frac{F_{max}(1 - \frac{F_{min}}{F_{max}})}{wt} * \sqrt{\pi a} \qquad (5.1)$$

- Abaqus FEA provides an accurate method for modeling corner pit specimens given the proper assumptions. It is also accurate for through pit specimens, but it is unnecessary due to the validity of Eq. 5.1. The Abaqus values and equation values agree within 1%.

- Using marker bands is an accurate method for determining crack growth characteristics, especially during the early stages of crack growth.

- There is no significant difference between the crack growth rate of through pit and machined-notch specimens.

- Corner pit specimens initially have a slower crack growth rate than machined notch specimens. When the crack front reaches the thickness of the specimen, the two crack growth rates become equal.

5.2 Recommendations

Due to the variability that is inherent in materials testing, further testing on the fatigue crack growth from corrosion pits in 7075-T6 Al should be conducted. There are a wide range of test variables that could be altered that would also provide useful information with regard to the fatigue life of aluminum alloys with flaws.

Additionally, further refinement should be conducted with the Abaqus modeling. The use of an external meshing program would be useful to create models with geometries that more closely represent the geometry of the test specimens.

Appendix A: Finite Element Data

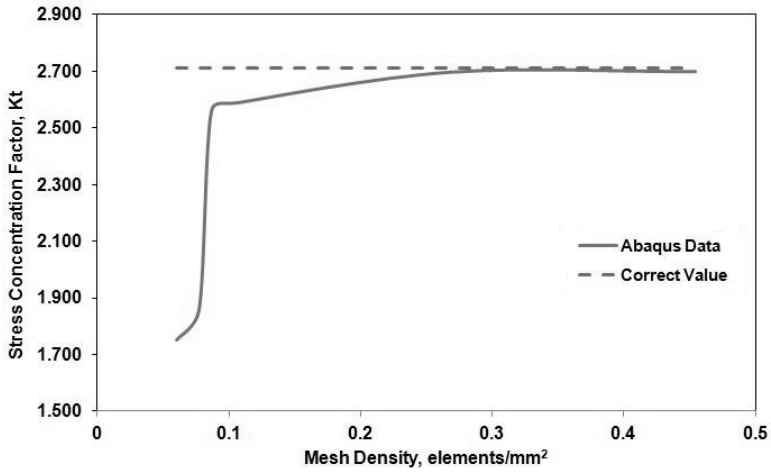

Figure A.1: Plot showing the convergence of the stress concentration value for the uniaxial specimen with centered hole under tensile loading. Value matches the theoretical value from Dowling within 1%.

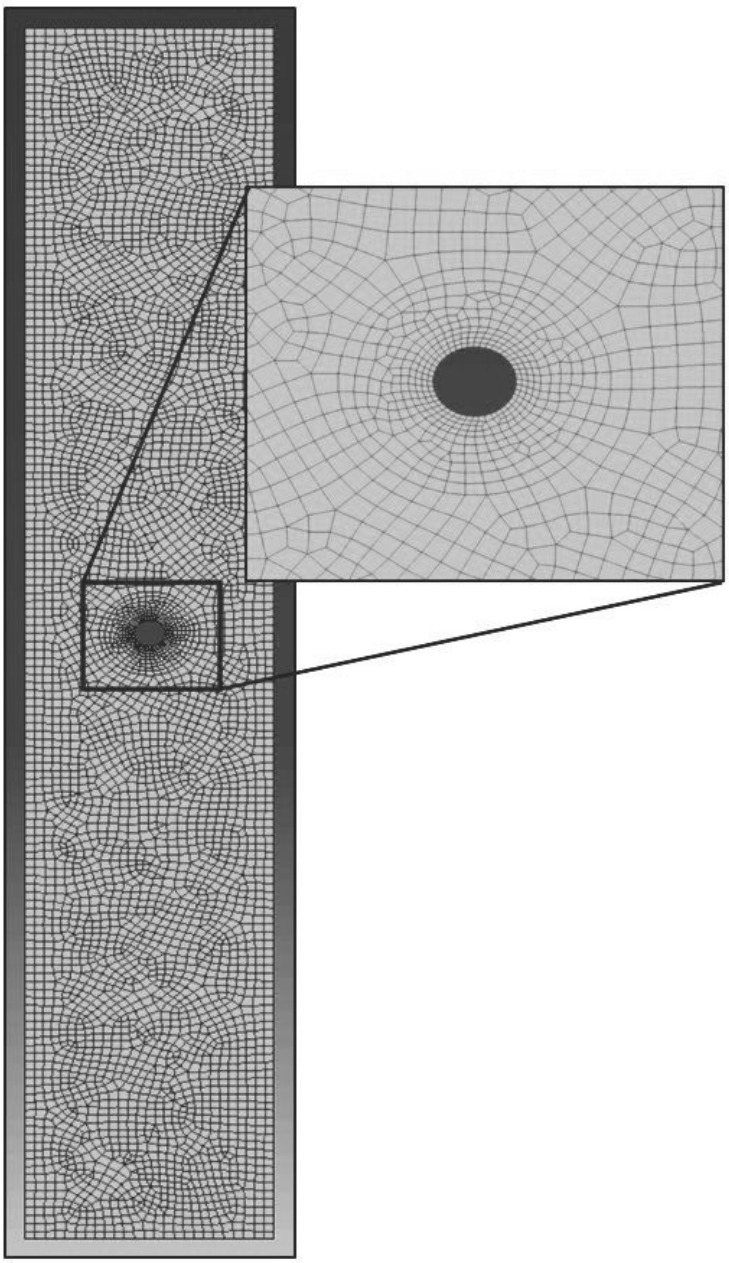

Figure A.2: Mesh created by Abaqus for the uniaxial specimen with only a hole. Notice how the mesh is more refined near the hole when compared to the other sections of the model. This gave accurate stress concentration values. The mesh consists of 2D quad elements.

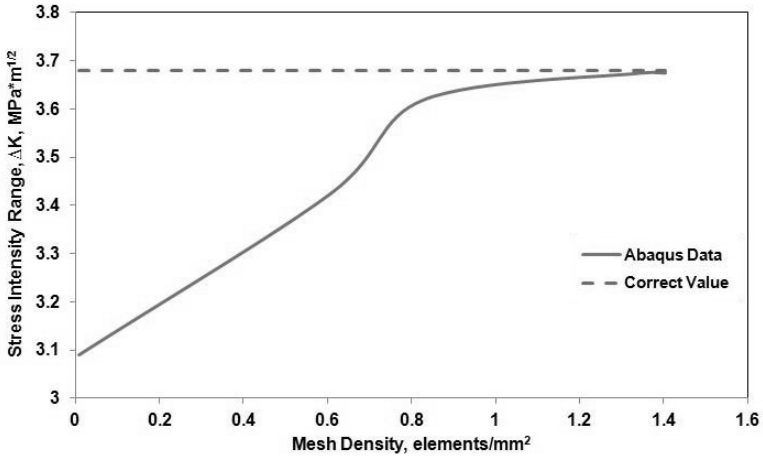

Figure A.3: Plot showing the convergence of the stress intensity range for the uniaxial specimen with a horizontal crack growing from the hole. This value matched the equation value closely, but there was some discrepancy. Likely, due to differences in geometry.

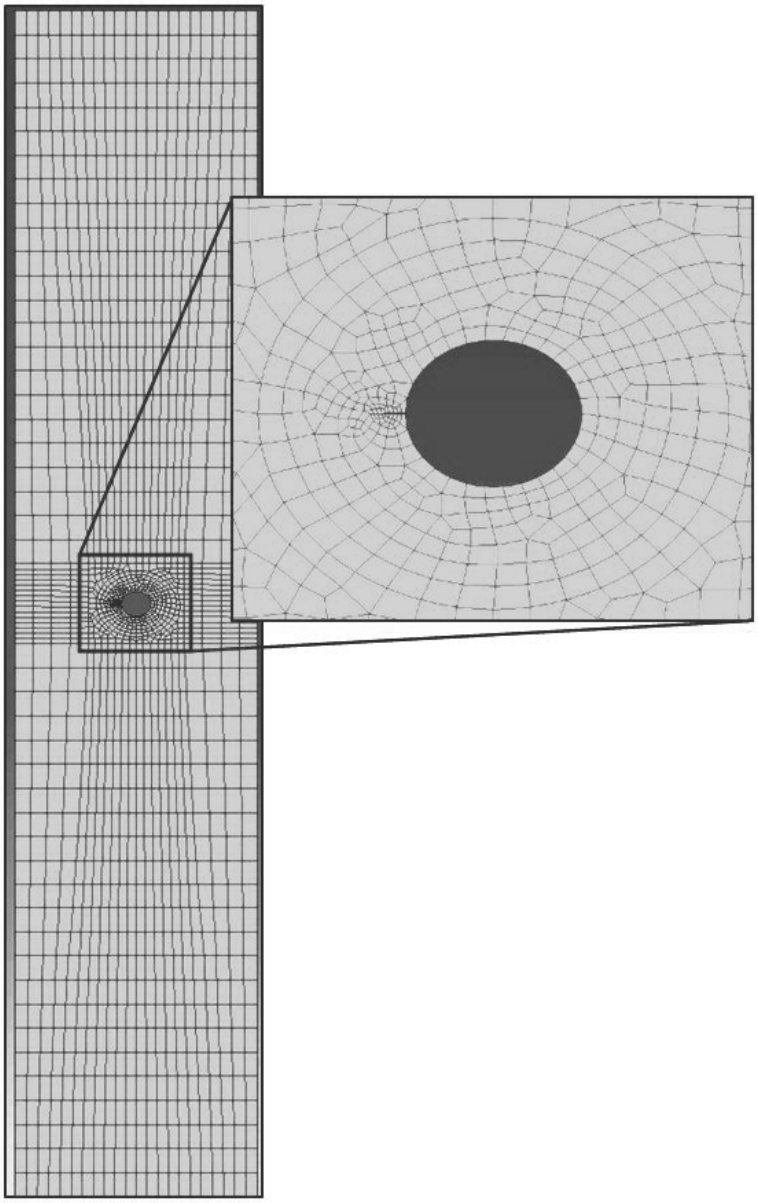

Figure A.4: Mesh created by Abaqus for the uniaxial specimen with a crack on a hole. Worthy of note is that the mesh is more refined near the crack tip when compared to the other sections of the model. This gave accurate stress intensity values. The mesh consists of 2D quad elements.

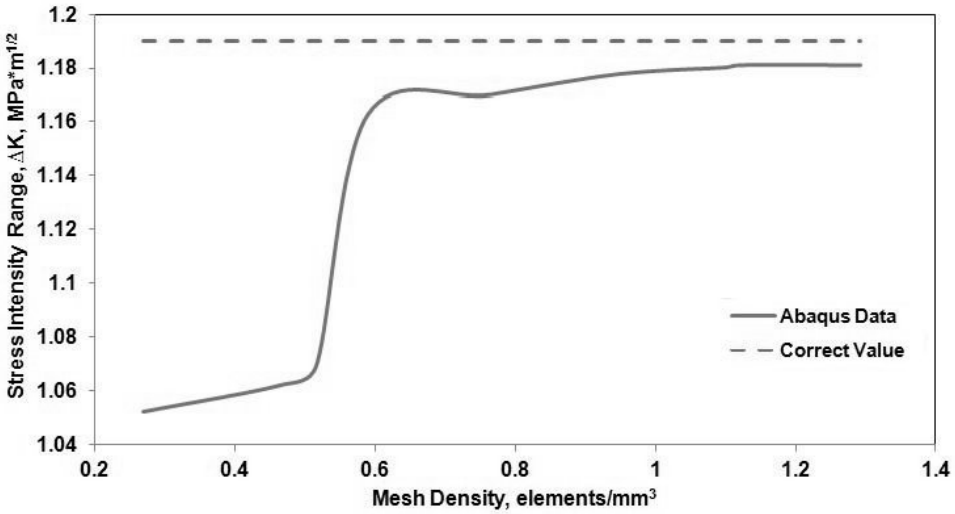

Figure A.5: Plot showing the convergence of the uniaxial corner crack specimen. This specimen was used to test the mesh settings and modeling technique. Its results could be compared to a closed form solution.

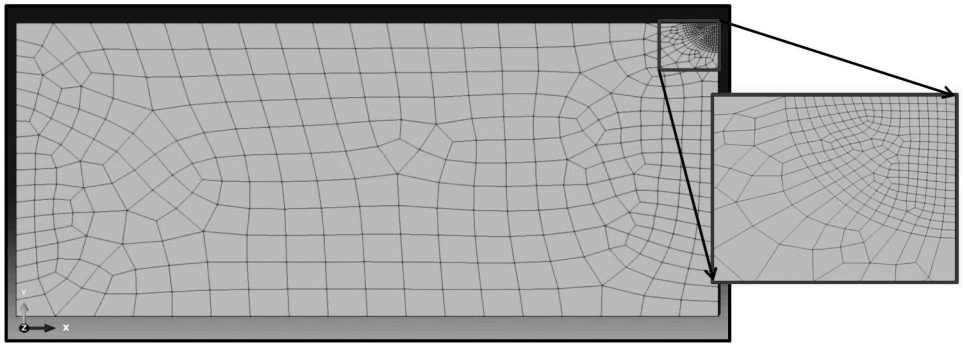

Figure A.6: FE model of the quarter circular corner crack used to determine the necessary settings to achieve accurate results. A very refined mesh near the tip (box) was necessary for accurate $K1$ results. Far from the crack required less refinement. This model acheived a K1 value at $< 1\%$ of the closed form solution of the same geometry.

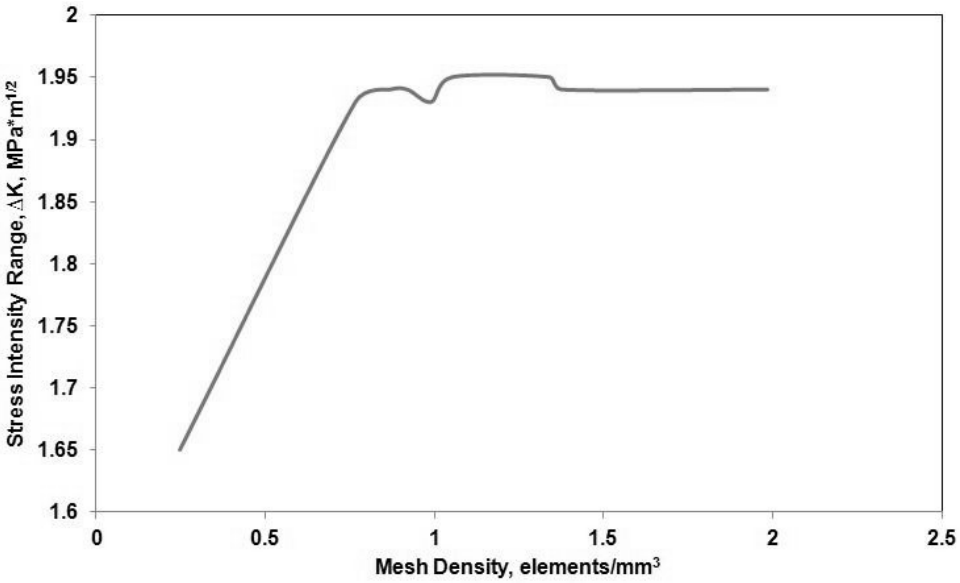

Figure A.7: Plot showing the convergence of the uniaxial corner pit specimen. There is no closed form solution for comparison.

Appendix B: Crack Growth Plots for Through Pit Specimens

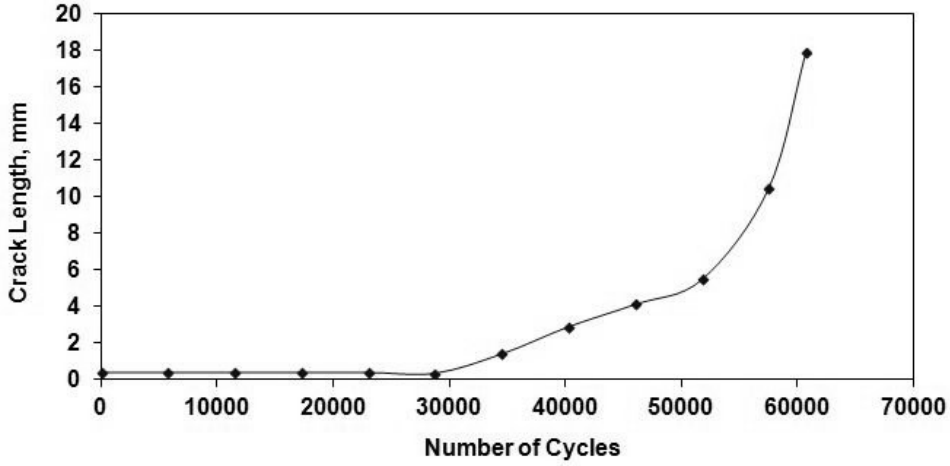

Figure B.1: Plot of the crack length vs. the number of cycles during fatigue testing for the SAl-02 specimen. Specifics about this test are shown in Table 3.3.

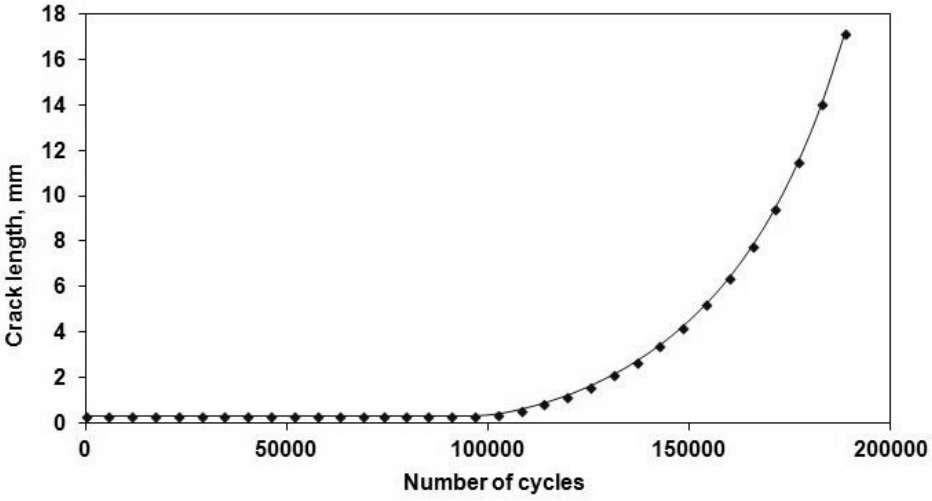

Figure B.2: Plot of the crack length vs. the number of cycles during fatigue testing for the SAl-03 specimen. Specifics about this test are shown in Table 3.3.

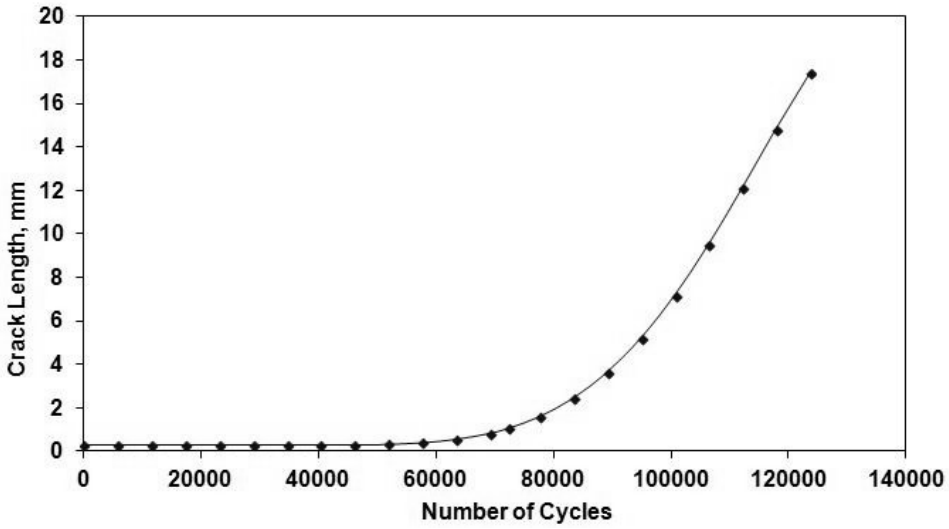

Figure B.3: Plot of the crack length vs. the number of cycles during fatigue testing for the SAl-04 specimen. Specifics about this test are shown in Table 3.3.

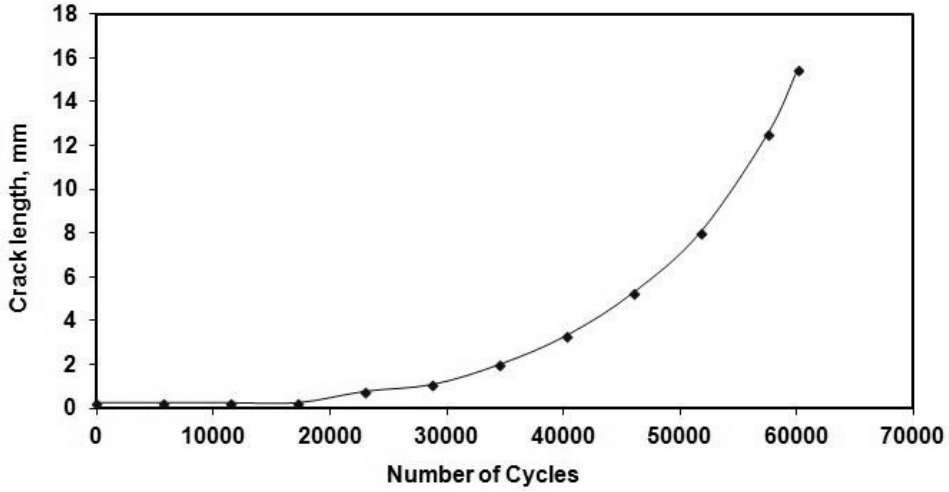

Figure B.4: Plot of the crack length vs. the number of cycles during fatigue testing for the SSl-01 specimen. Specifics about this test are shown in Table 3.3.

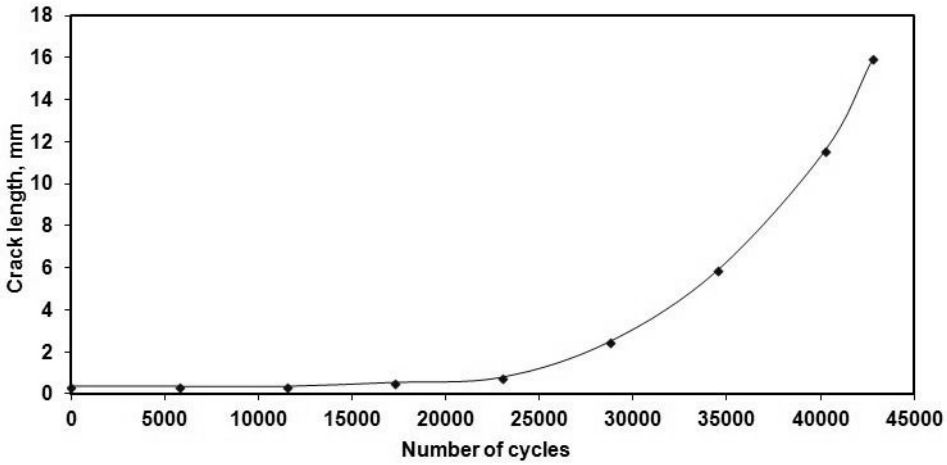

Figure B.5: Plot of the crack length vs. the number of cycles during fatigue testing for the SSl-02 specimen. Specifics about this test are shown in Table 3.3.

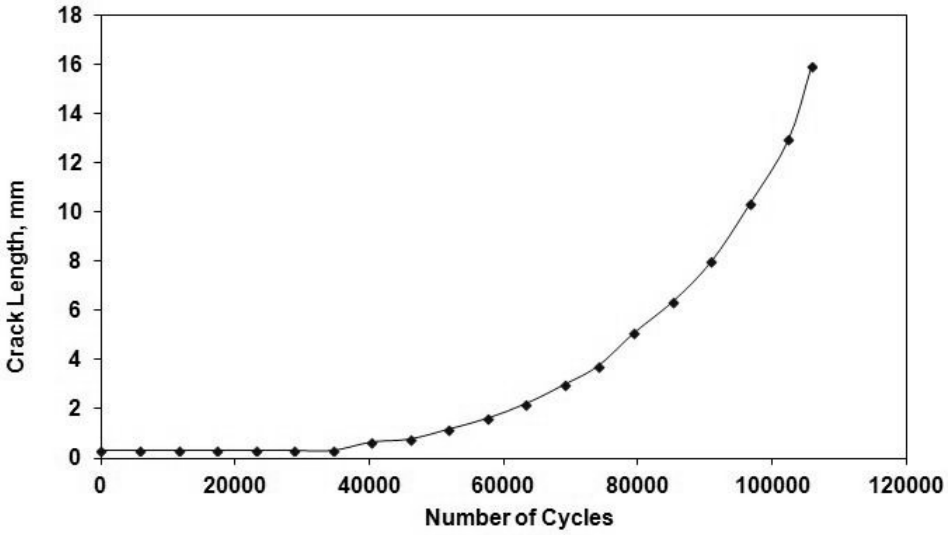

Figure B.6: Plot of the crack length vs. the number of cycles during fatigue testing for the SSl-03 specimen. Specifics about this test are shown in Table 3.3.

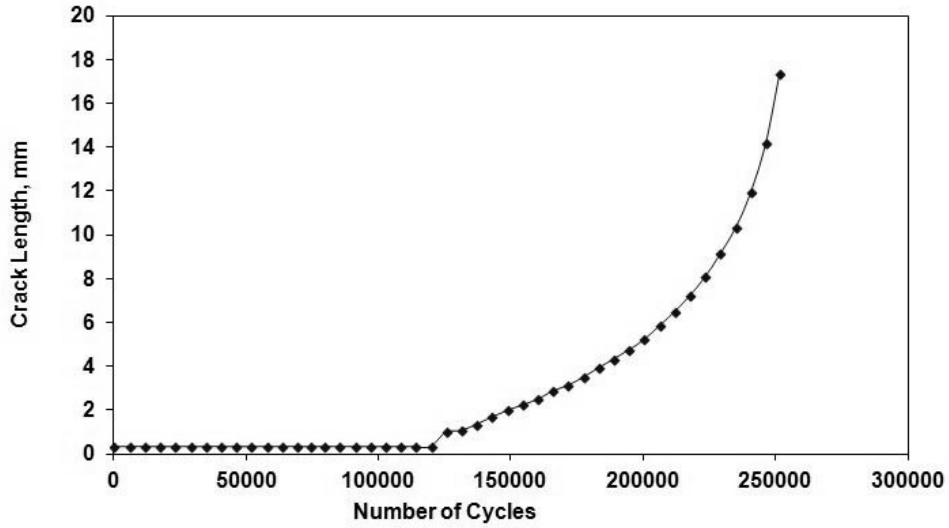

Figure B.7: Plot of the crack length vs. the number of cycles during fatigue testing for the SSl-04 specimen. Specifics about this test are shown in Table 3.3.

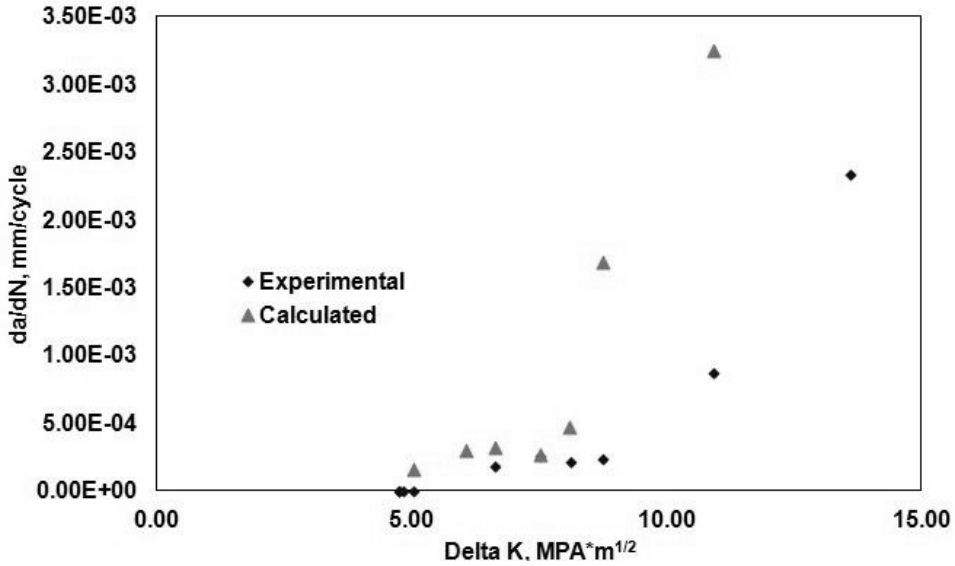

Figure B.8: Rate of crack growth vs. the stress intensity factor for SAl-02. Specifics about this test are shown in Table 3.3.

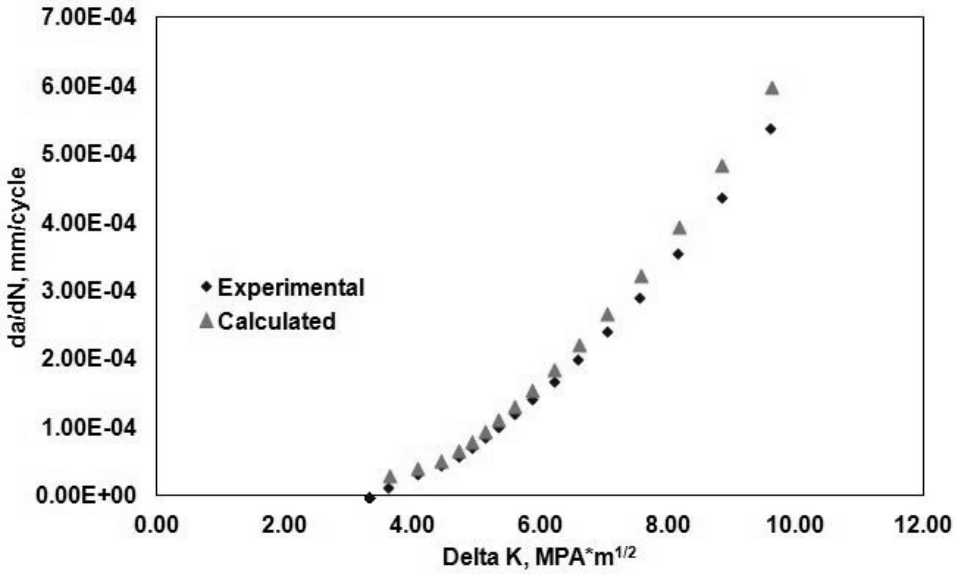

Figure B.9: Rate of crack growth vs. the stress intensity factor for SAl-03. Specifics about this test are shown in Table 3.3.

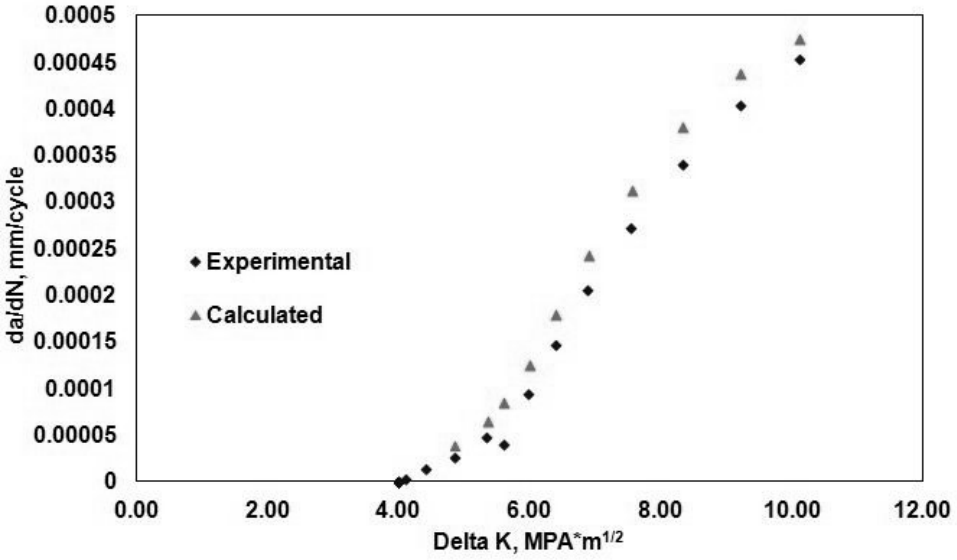

Figure B.10: Rate of crack growth vs. the stress intensity factor for SAl-04. Specifics about this test are shown in Table 3.3.

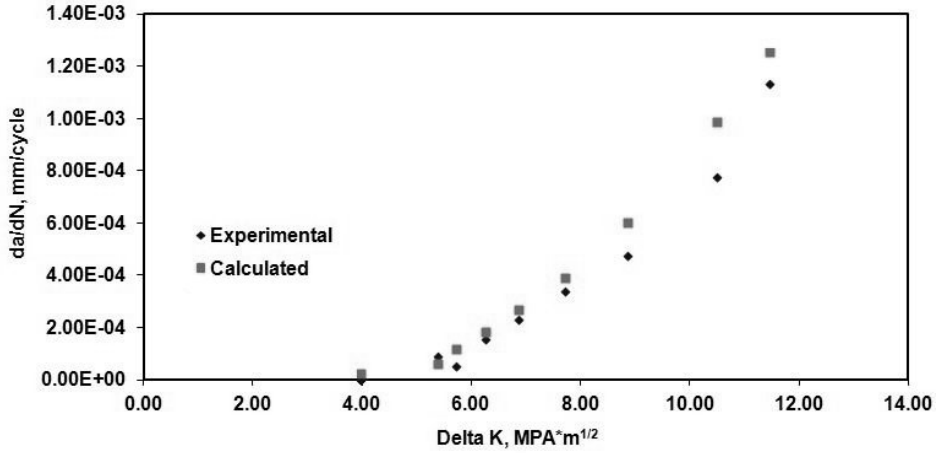

Figure B.11: Rate of crack growth vs. the stress intensity factor for SSl-01. Specifics about this test are shown in Table 3.3.

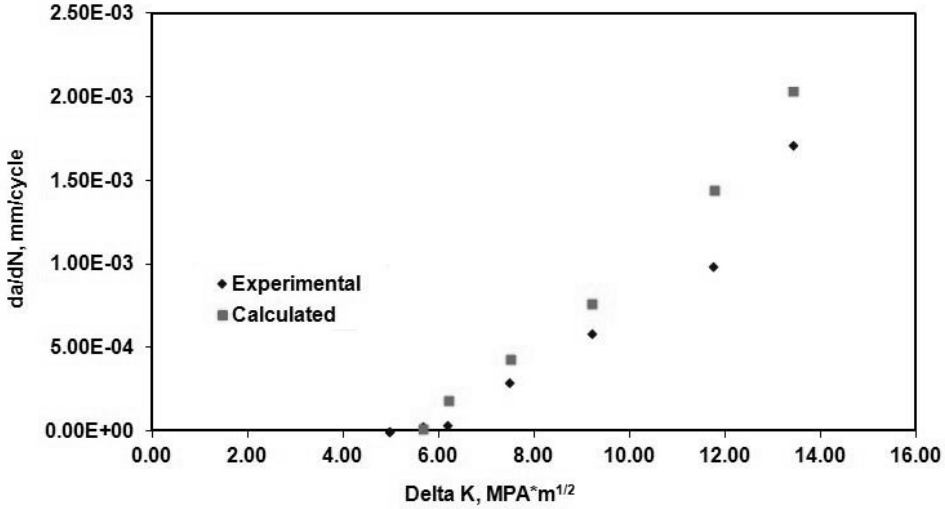

Figure B.12: Rate of crack growth vs. the stress intensity factor for SSl-02. Specifics about this test are shown in Table 3.3.

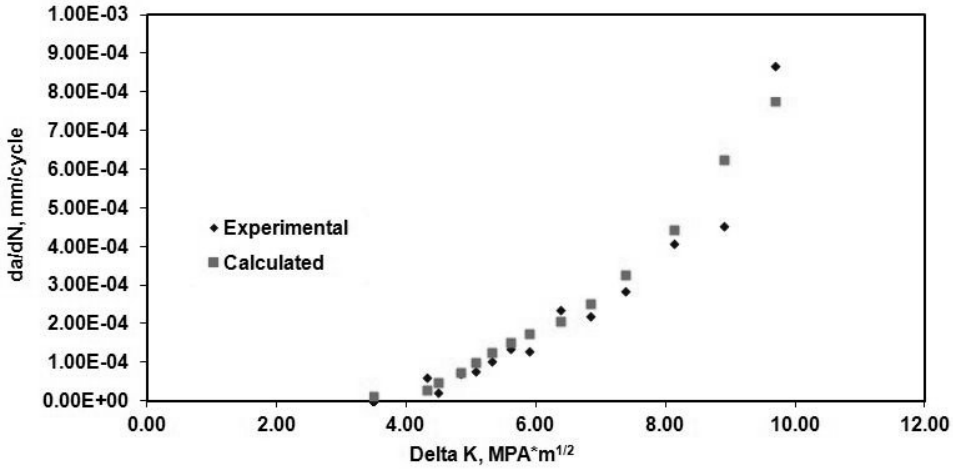

Figure B.13: Rate of crack growth vs. the stress intensity factor for SSl-03. Specifics about this test are shown in Table 3.3.

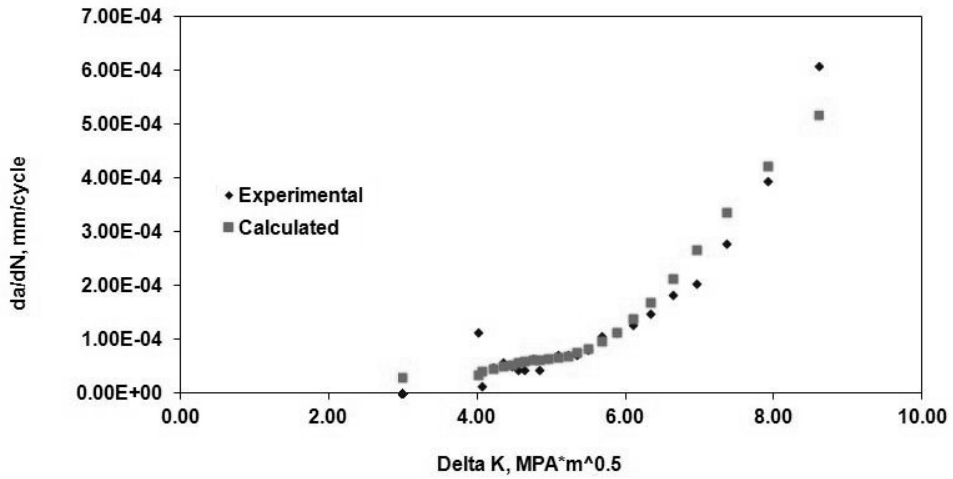

Figure B.14: Rate of crack growth vs. the stress intensity factor for SSl-04. Specifics about this test are shown in Table 3.3.

Appendix C: Crack Growth Plots for Corner Pit Specimens

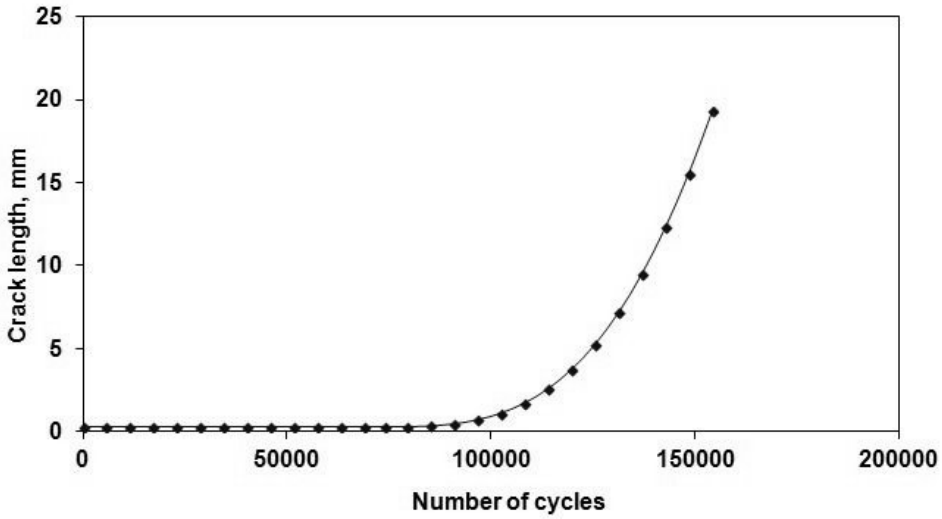

Figure C.1: Plot of the crack length vs. the number of cycles during fatigue testing for the SAS-01 specimen. Specifics about this test are shown in Table 3.3.

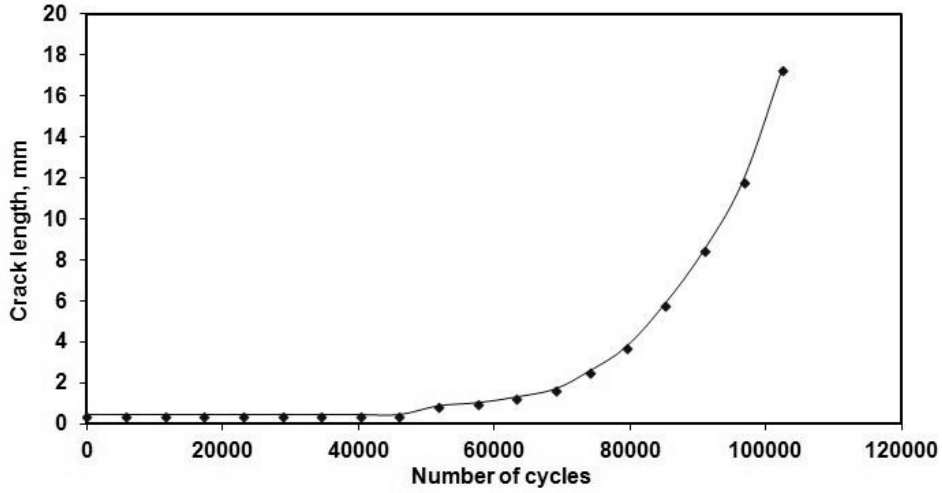

Figure C.2: Plot of the crack length vs. the number of cycles during fatigue testing for the SAS-02 specimen. Specifics about this test are shown in Table 3.3.

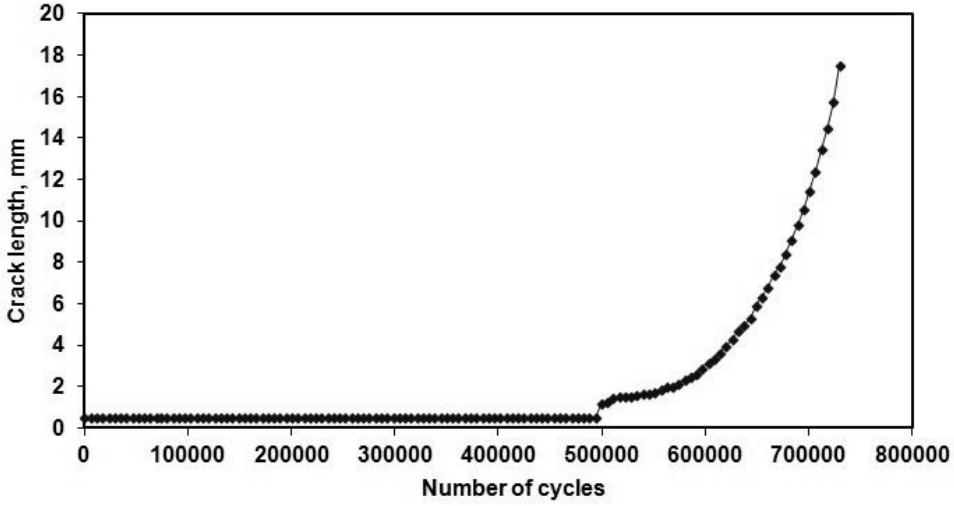

Figure C.3: Plot of the crack length vs. the number of cycles during fatigue testing for the SAS-05 specimen. Specifics about this test are shown in Table 3.3.

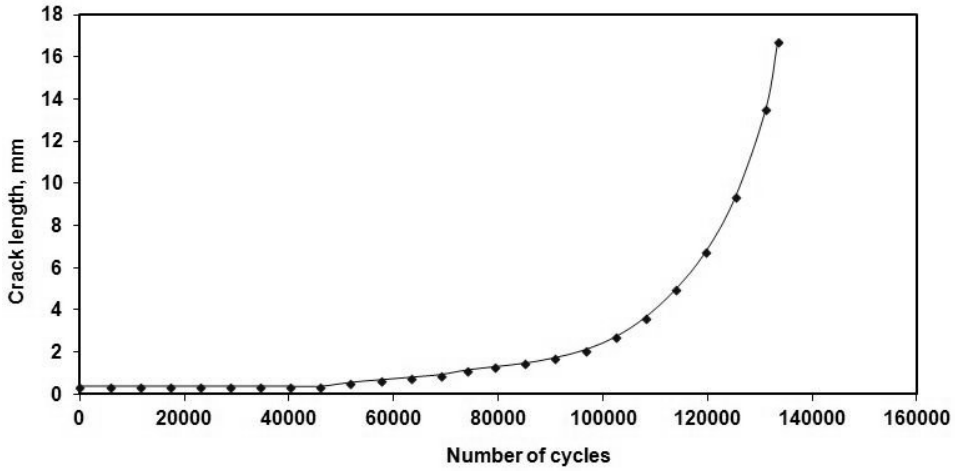

Figure C.4: Plot of the crack length vs. the number of cycles during fatigue testing for the SSS-01 specimen. Specifics about this test are shown in Table 3.3.

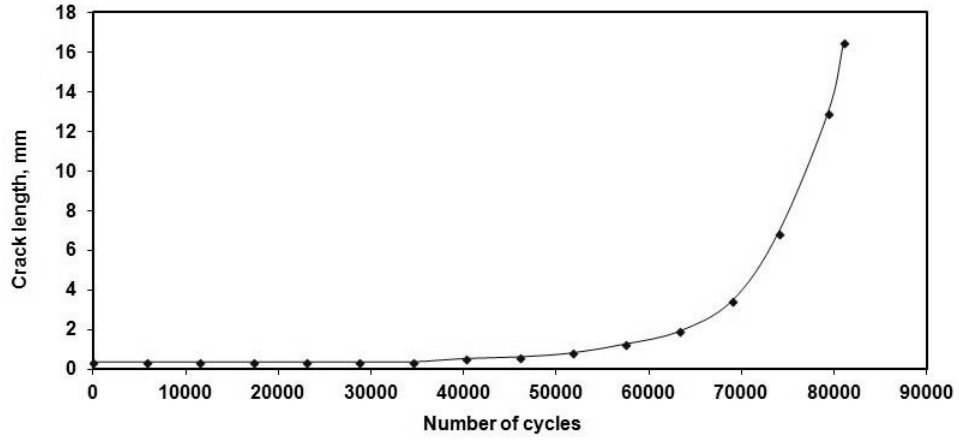

Figure C.5: Plot of the crack length vs. the number of cycles during fatigue testing for the SSS-02 specimen. Specifics about this test are shown in Table 3.3.

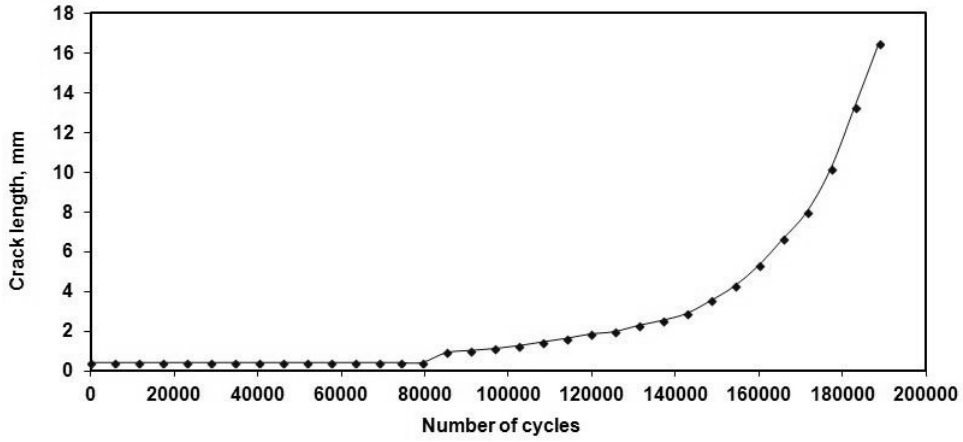

Figure C.6: Plot of the crack length vs. the number of cycles during fatigue testing for the SSS-05 specimen. Specifics about this test are shown in Table 3.3.

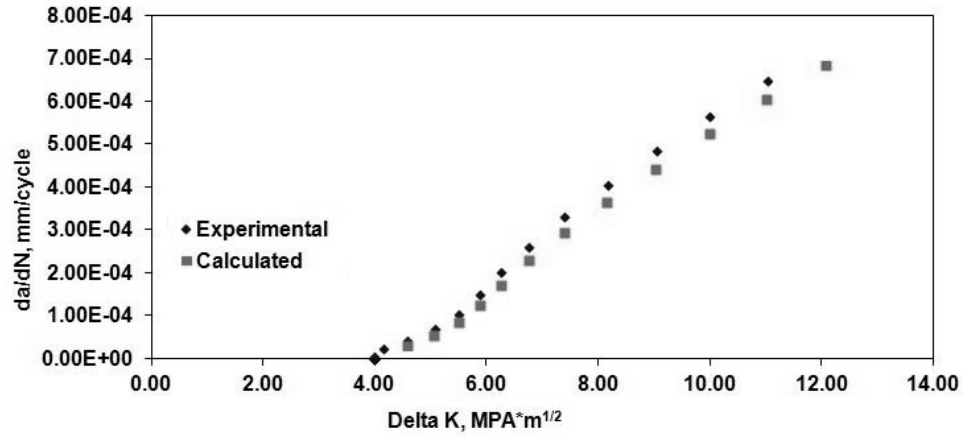

Figure C.7: Rate of crack growth vs. the stress intensity factor for SAS-01. Specifics about this test are shown in Table 3.3.

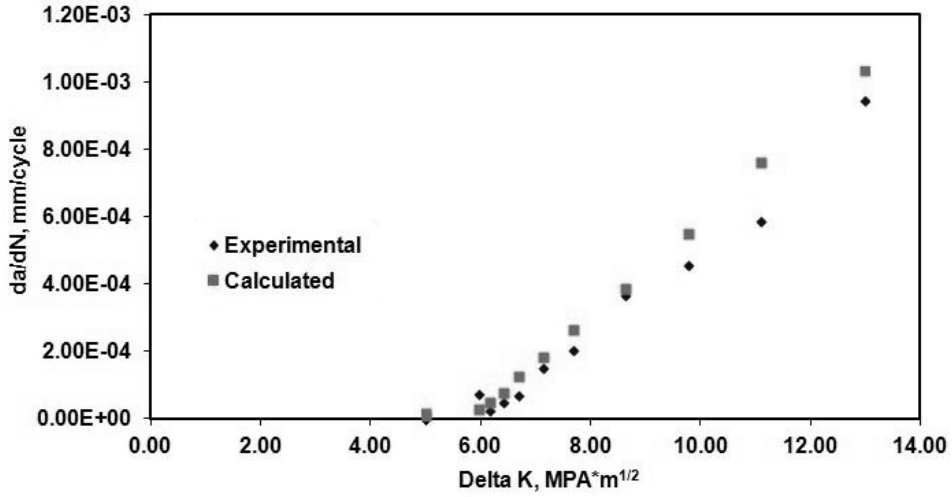

Figure C.8: Rate of crack growth vs. the stress intensity factor for SAS-02. Specifics about this test are shown in Table 3.3.

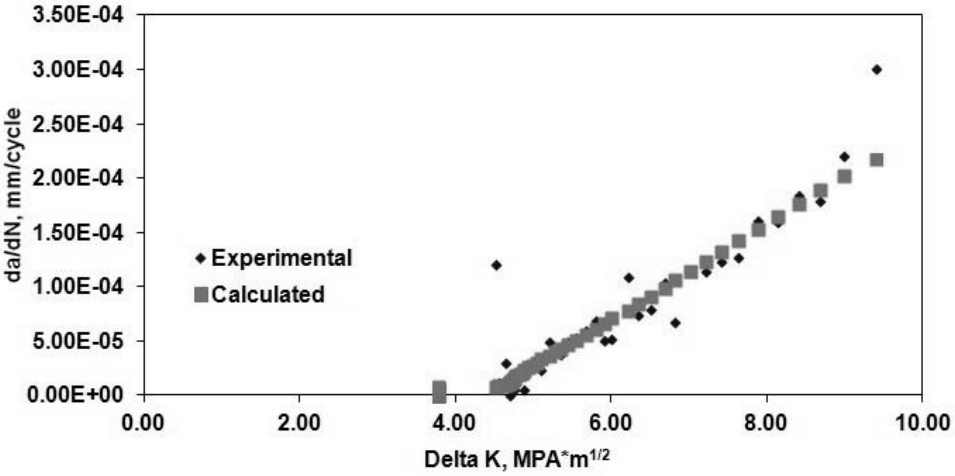

Figure C.9: Rate of crack growth vs. the stress intensity factor for SAS-05. Specifics about this test are shown in Table 3.3.

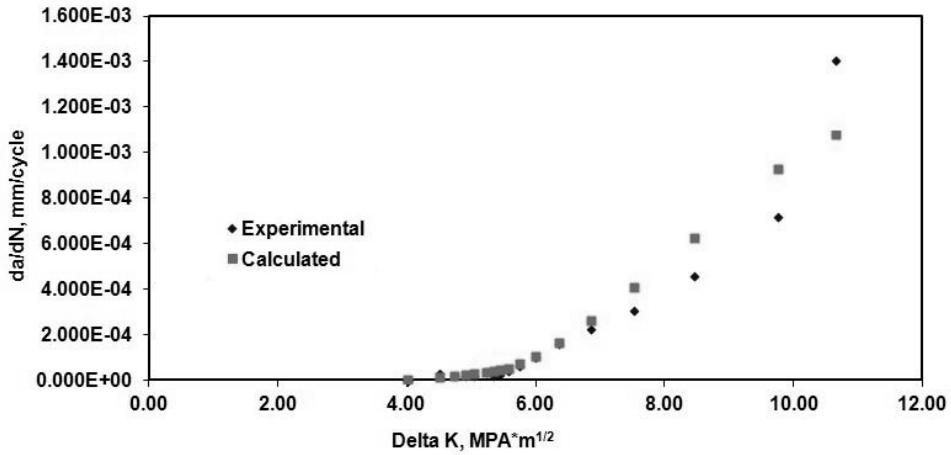

Figure C.10: Rate of crack growth vs. the stress intensity factor for SSS-01. Specifics about this test are shown in Table 3.3.

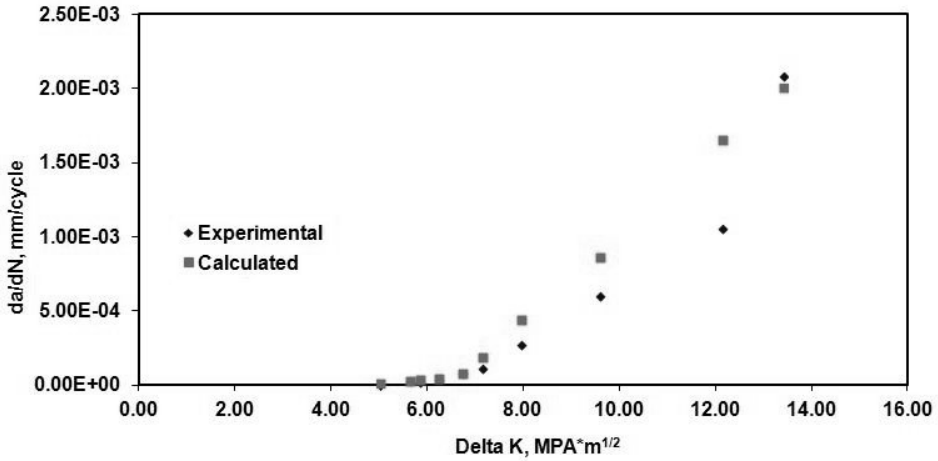

Figure C.11: Rate of crack growth vs. the stress intensity factor for SSS-02. Specifics about this test are shown in Table 3.3.

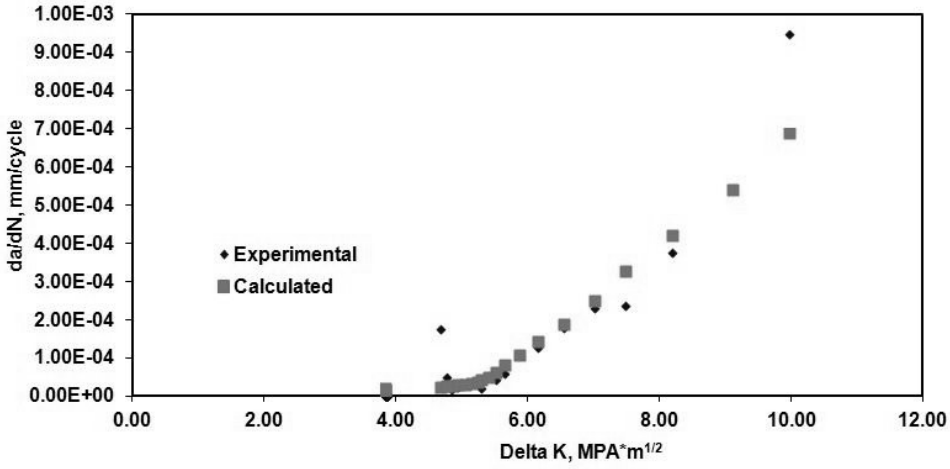

Figure C.12: Rate of crack growth vs. the stress intensity factor for SSS-05. Specifics about this test are shown in Table 3.3.

Appendix D: SEM Photographs After Experimentation

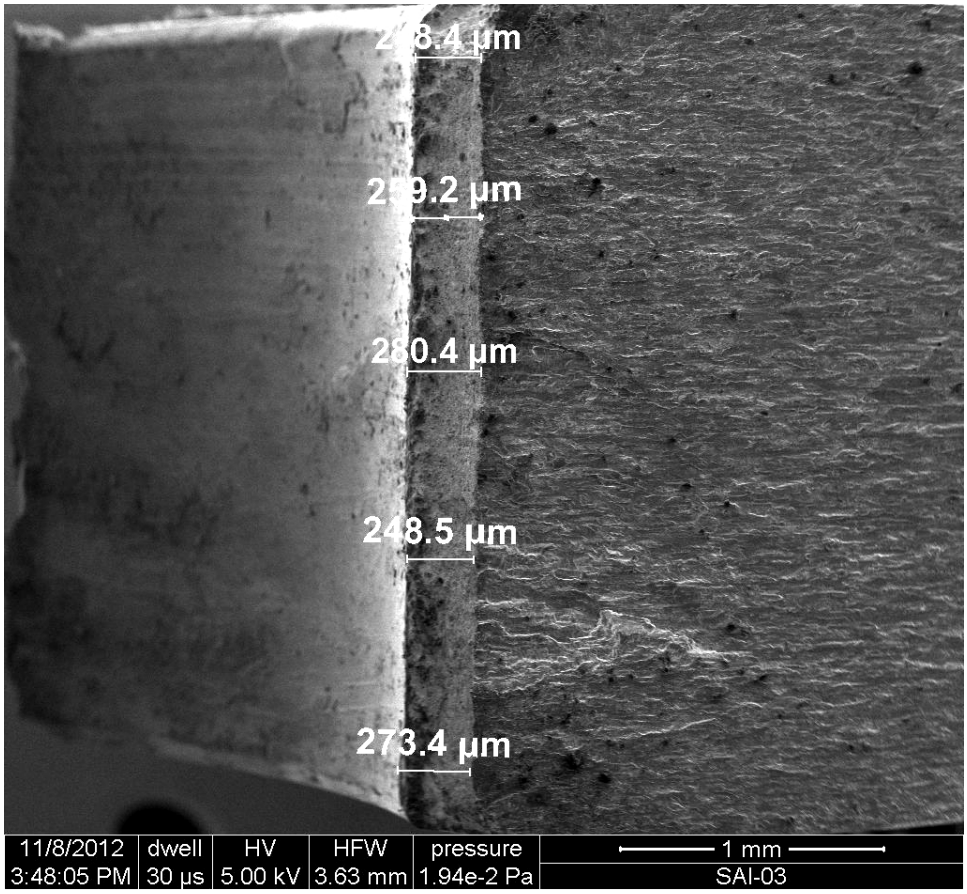

Figure D.1: Top view of the through pit specimen SAl-03 using the SEM. Measurements of the pit were taken at several positions so that an average pit size could be calculated. These actual pit sizes were plugged into the Abaqus models as the initial crack size.

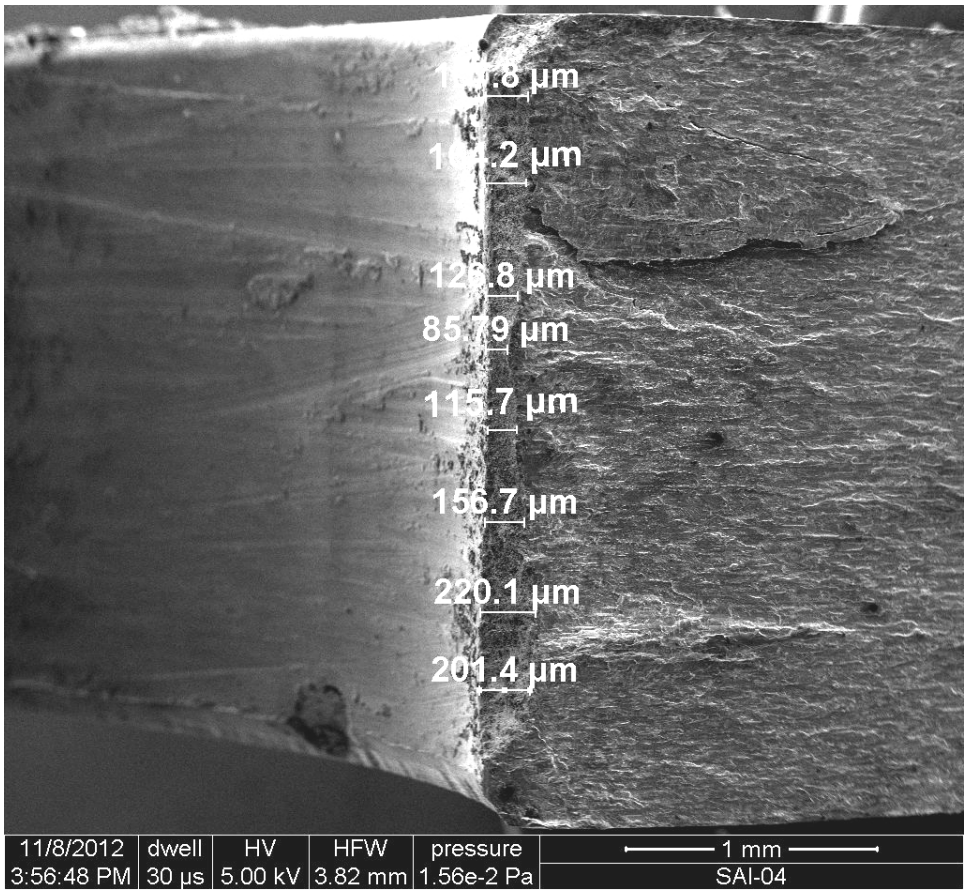

Figure D.2: Top view of the through pit specimen SAl-04 using the SEM. Measurements of the pit were taken at several positions so that an average pit size could be calculated. This specimen required more measurements because the pit was very irregular. These actual pit sizes were plugged into the Abaqus models as the initial crack size.

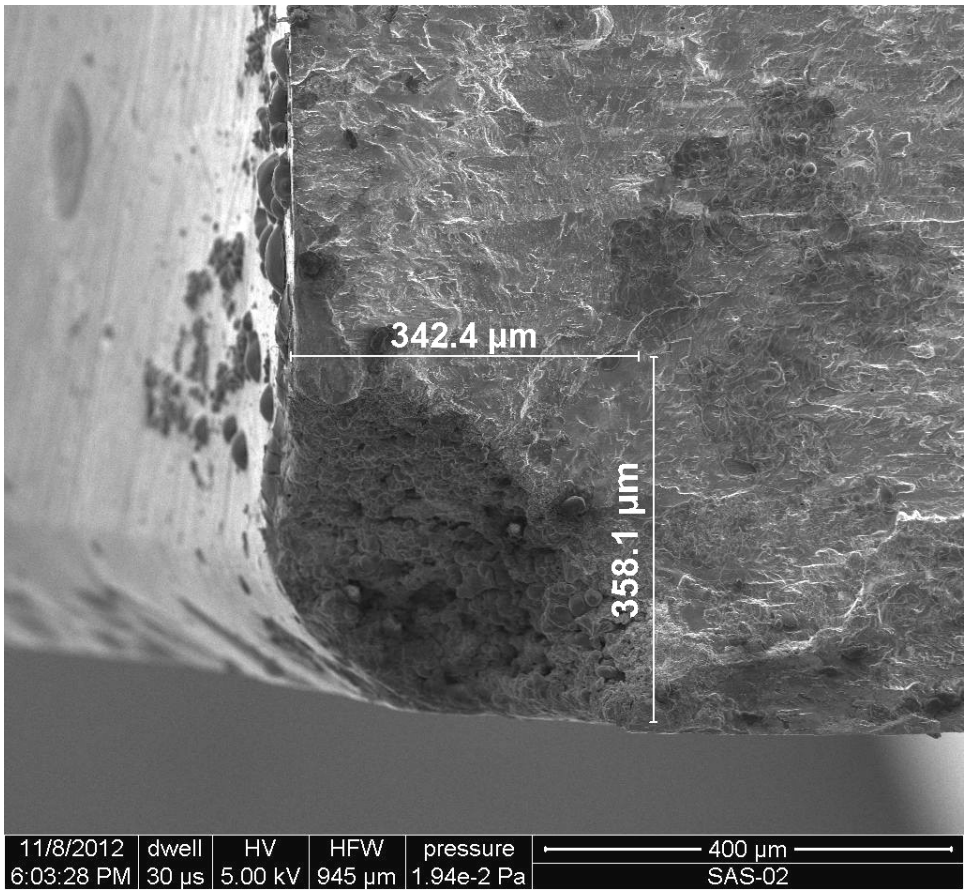

Figure D.3: Top view of the corner pit specimen SAS-02 using the SEM. Measurements of the pit were taken at several positions so that an average pit size could be calculated. These actual pit sizes were plugged into the Abaqus models as the initial crack size.

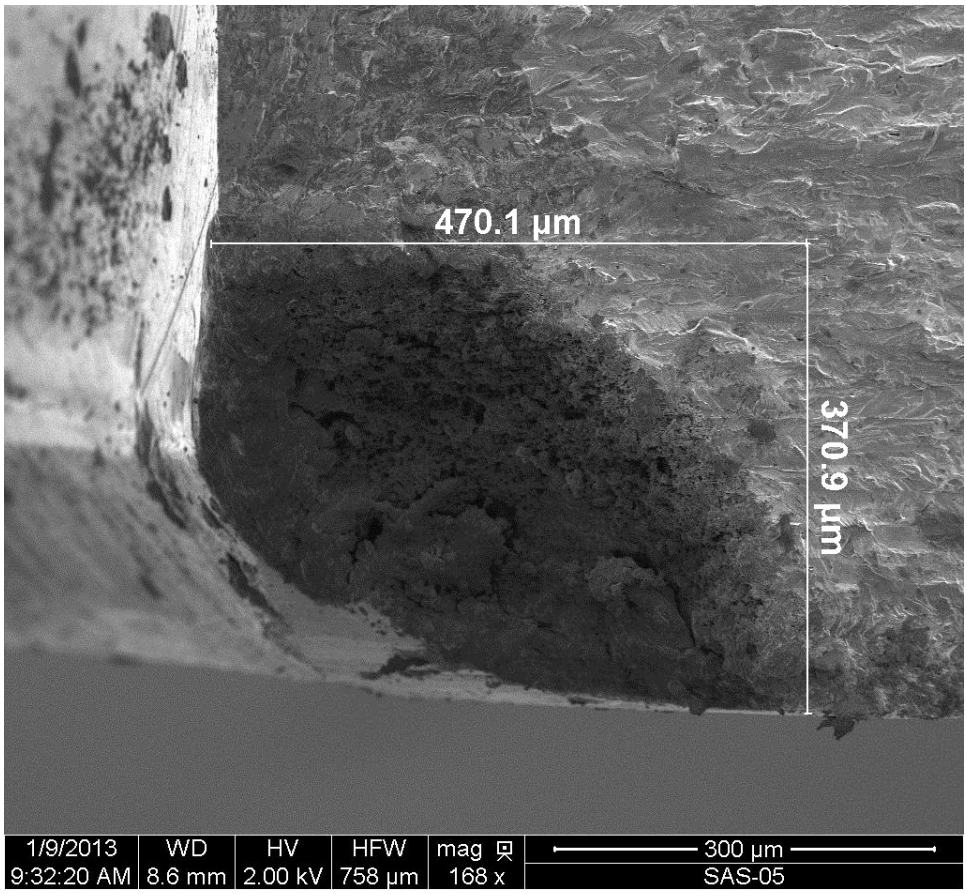

Figure D.4: Top view of the corner pit specimen SAS-05 using the SEM. Measurements of the pit were taken at several positions so that an average pit size could be calculated. These actual pit sizes were plugged into the Abaqus models as the initial crack size.

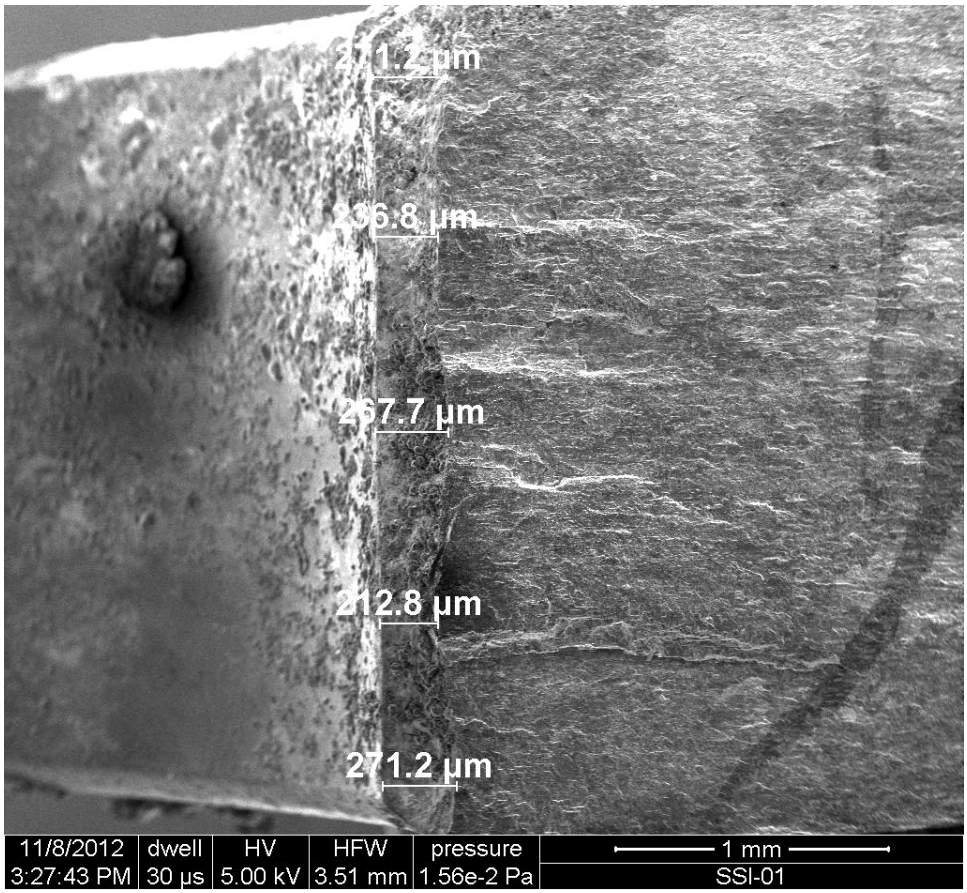

Figure D.5: Top view of the through pit specimen SSl-01 using the SEM. Measurements of the pit were taken at several positions so that an average pit size could be calculated. These actual pit sizes were plugged into the Abaqus models as the initial crack size.

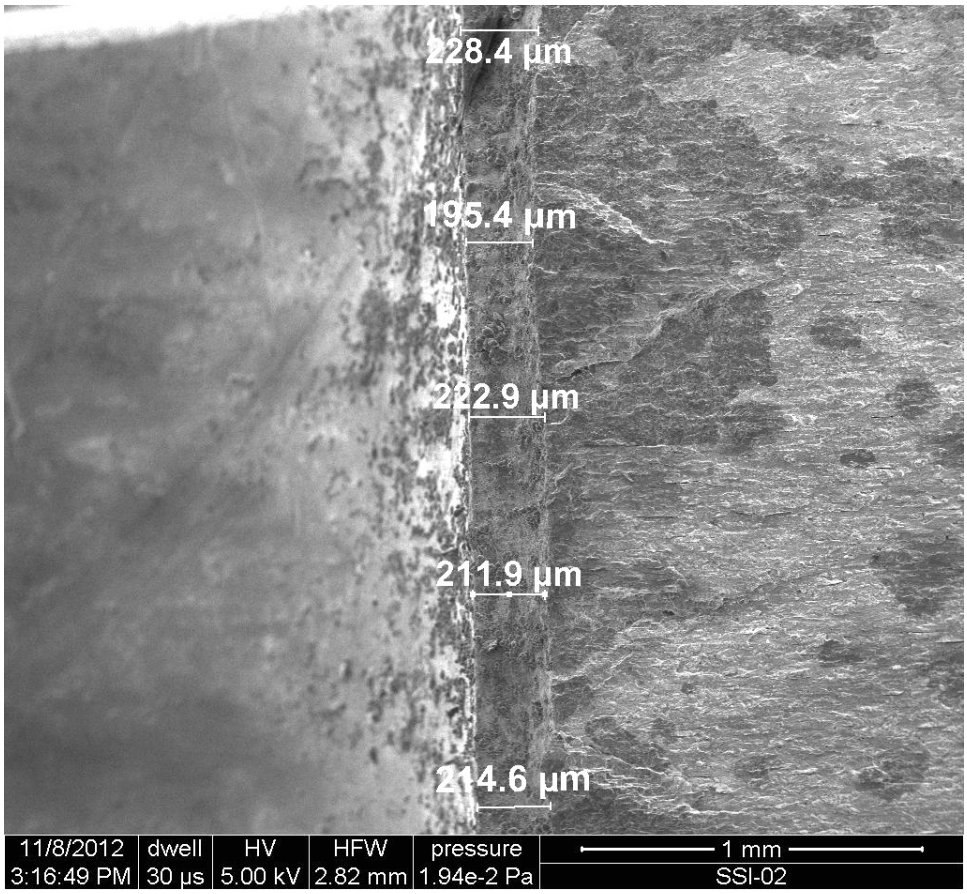

Figure D.6: Top view of the through pit specimen SSl-02 using the SEM. Measurements of the pit were taken at several positions so that an average pit size could be calculated. These actual pit sizes were plugged into the Abaqus models as the initial crack size.

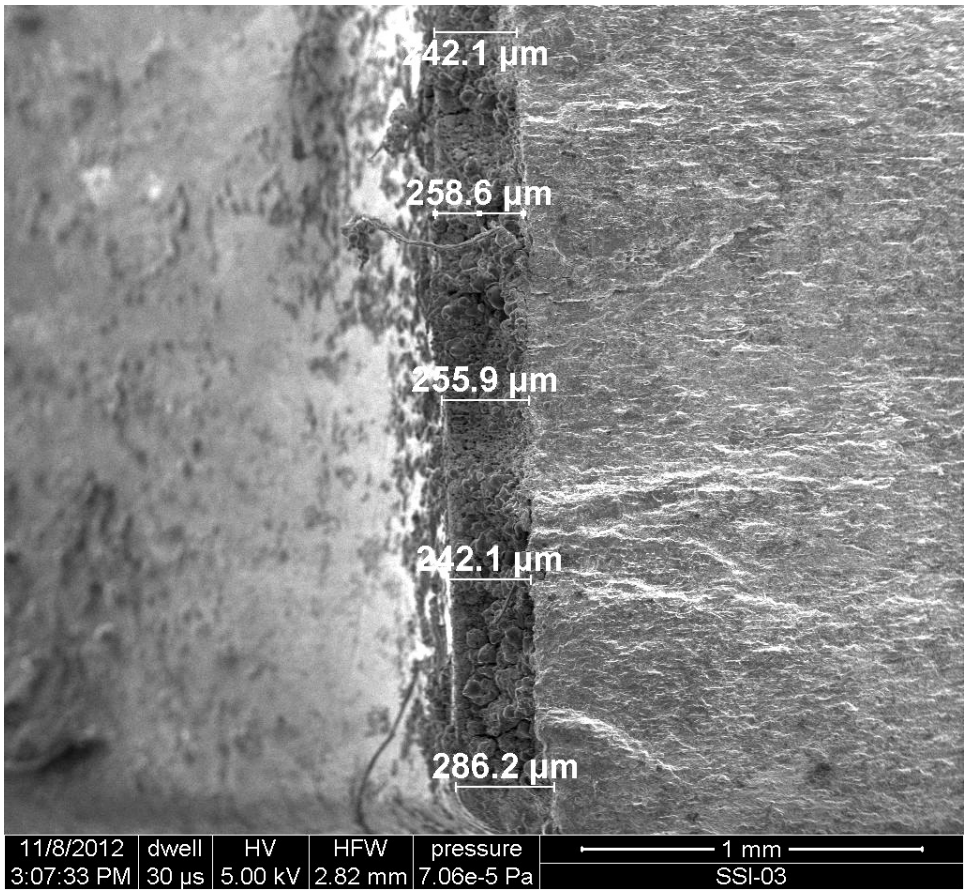

Figure D.7: Top view of the through pit specimen SSl-03 using the SEM. Measurements of the pit were taken at several positions so that an average pit size could be calculated. These actual pit sizes were plugged into the Abaqus models as the initial crack size.

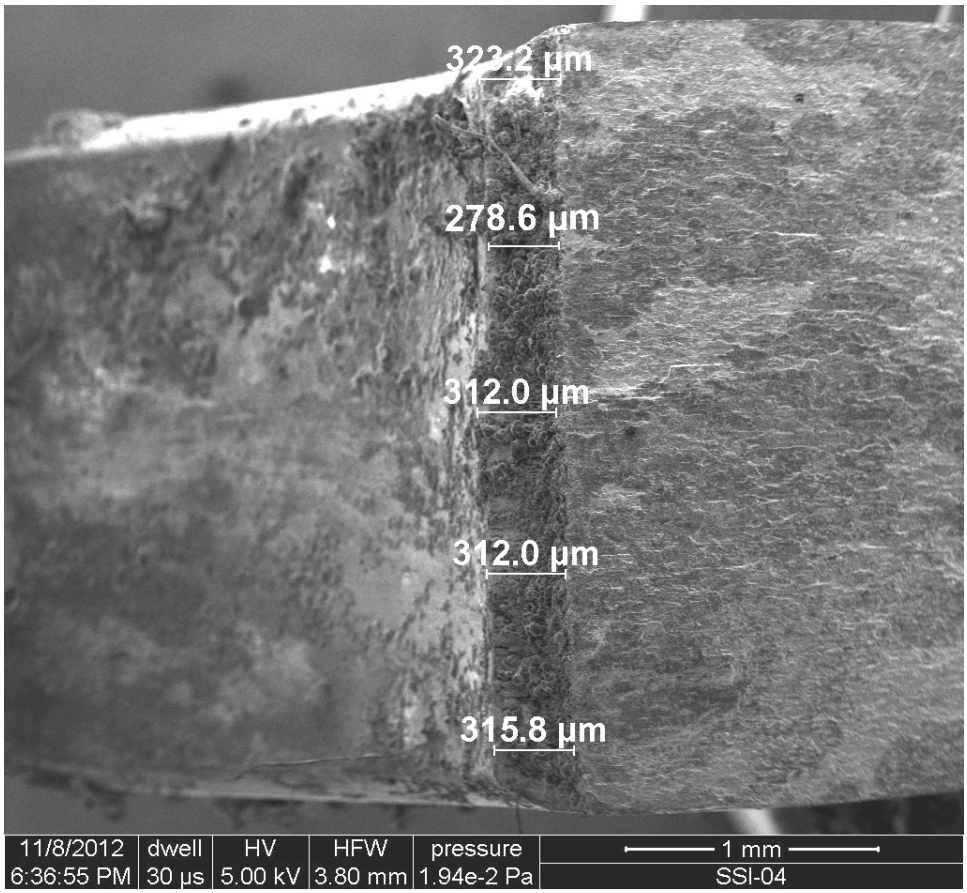

Figure D.8: Top view of the through pit specimen SSl-04 using the SEM. Measurements of the pit were taken at several positions so that an average pit size could be calculated. These actual pit sizes were plugged into the Abaqus models as the initial crack size.

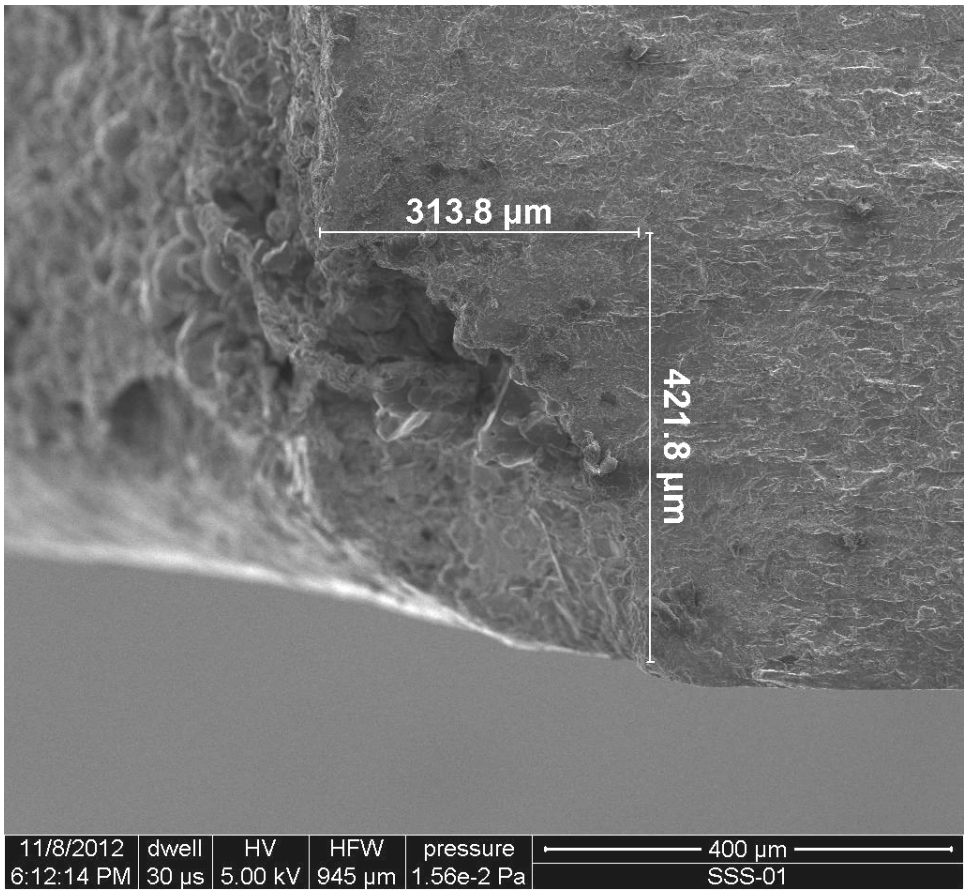

Figure D.9: Top view of the corner pit specimen SSS-01 using the SEM. Measurements of the pit were taken at several positions so that an average pit size could be calculated. These actual pit sizes were plugged into the Abaqus models as the initial crack size.

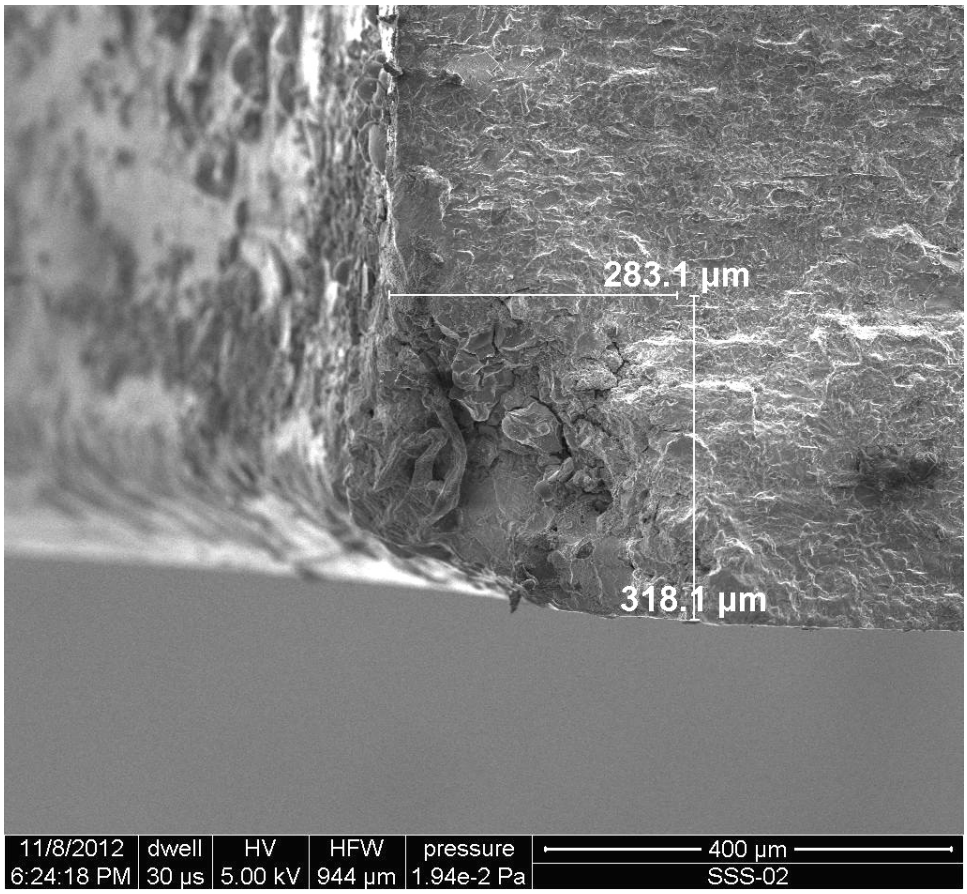

Figure D.10: Top view of the corner pit specimen SSS-02 using the SEM. Measurements of the pit were taken at several positions so that an average pit size could be calculated. These actual pit sizes were plugged into the Abaqus models as the initial crack size.

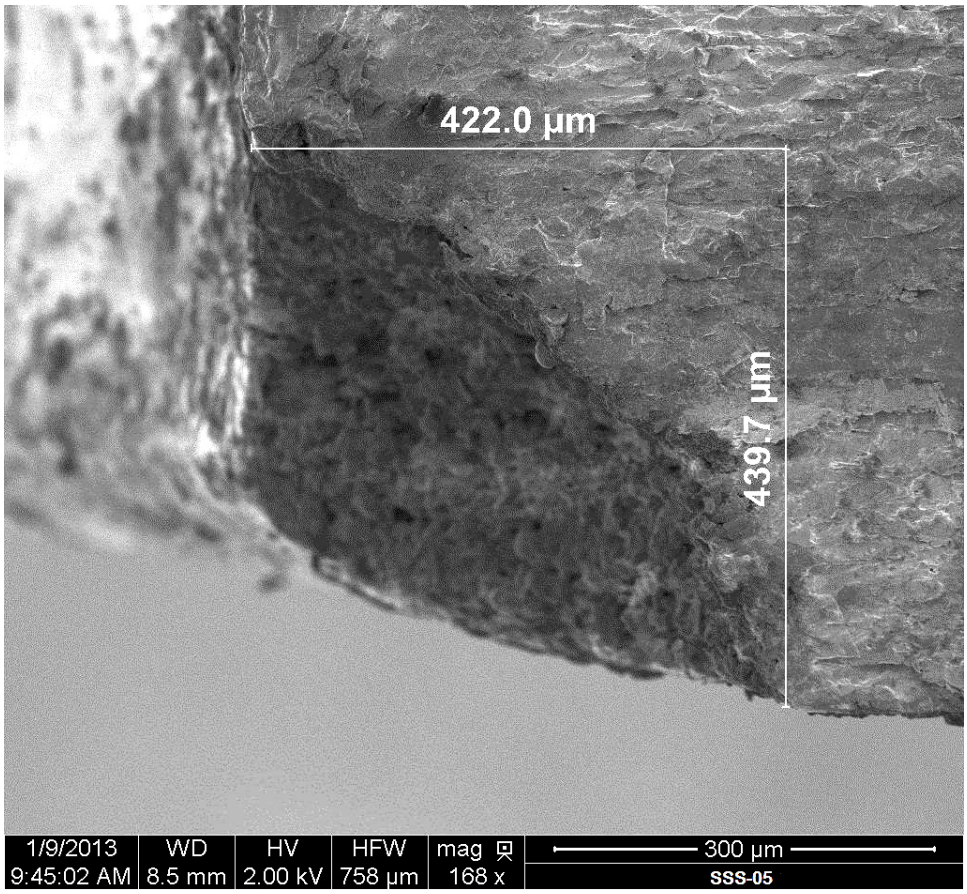

Figure D.11: Top view of the corner pit specimen SSS-05 using the SEM. Measurements of the pit were taken at several positions so that an average pit size could be calculated. These actual pit sizes were plugged into the Abaqus models as the initial crack size.

Bibliography

[1] Anderson, T.L. *Fracture Mechanics: Fundamentals and Applications*. Taylor and Francis, 2005.

[2] Bathias, C. and P.C. Paris. *Gigacycle Fatigue in Mechanical Practice*. Marcel Dekker, 2005.

[3] Bolotin, V. V. *Mechanics of Fatigue*. Boca Raton: CRC, 1999.

[4] Burns, J.B. "The Effect of Initiation Feature and Environment on Fatigue Crack Formation and Early Propagation in Al-Zn-Mg-Cu." *PhD Dissertation, University of Virginia*, 2010.

[5] Burns, J.T., J.M. Larsen, and R.P. Gangloff. "Driving forces for localized corrosion-to-fatigue crack transition in AlZnMgCu". *Fatigue and Fracture of Engineering Materials and Structures*, 34(0):745 – 773, 2011. ISSN 1460-2695.

[6] Burns, J.T., J.T. Larsen, and R.P. Gangloff. "Effect of Corrosion Severity on Fatigue Evolution in Al-Zn-Mg-Cu". *Corrosion Science*, 52:498–508, 2010. ISSN 0010-938X.

[7] Castro, P.M.S.T., P.F.P. Matos, G.P. Moreira, and L.F.M. Silva. "An overview on fatigue analysis of aeronautical structural details: Open hole, single rivet lap-joint, and lap-joint panel". *Materials Science and Engineering A*, 468-470:144–157, 2007. ISSN 0921-5093.

[8] Chen, G.S., K.C. Wan, M. Gao, R.P. Wei, and T.H. Flournoy. "Transition from pitting to fatigue crack growth modeling of corrosion fatigue crack nucleation in a 2024-T3 aluminum alloy". *Materials Science and Engineering*, 219(1-2):126–132, 2002.

[9] Chlistovsky, R.M., P.J. Heffernan, and D.L. DuQuesnay. "Corrosion-fatigue behaviour of 7075-T651 aluminum alloy subjected to periodic overloads". *International Journal of Fatigue*, 29:1941–1949, 2007. ISSN 0142-1123.

[10] Clark, G. "A Review of Australian and New Zealand Investigations on Aeronautical Fatigue During the Period April 2005 to March 2007". *Air Vehicles Division Defence Science and Technology Organisation*, 2007. ISSN DSTO-TN-0747.

[11] Cooke, R.D., D.S. Malkus, and M.E. Plesha. *Concepts and Applications of Finite Element Analysis*. John Wiley and Sons Inc., 2001.

[12] Dowling, N.E. *Mechanical Behavior of Materials. 3rd ed.* Pearson, 2007.

[13] DuQuesnay, D.L., P.R. Underhill, and H.J. Britt. "Fatigue crack growth from corrosion damage in 7075-T6511 aluminium alloy under aircraft loading". *Dept of Mechanical Engineering, Royal Military College of Canada*, 1996.

[14] Endo, M. and A.J. McEvily. "Prediction of the behavior of small fatigue cracks". *Materials Science and Engineering: A*, 468-470(0):51 – 58, 2007. ISSN 0921-5093.

[15] Forman, R.G. "Study of Fatigue Crack Initiation From Flaws Using Fracture Mechanics Theory". *AFFDL, WPAFB, OH*, 1968.

[16] Forman, R.G. and L.A. James. "Flaw growth behavior of 2124-T851 aluminum plate load in short transverse grain direction". *Materials Technology Branch Report*, 1975.

[17] Gangloff, R.P. "Environmental Cracking- Corrosion Fatigue". *Corrosion Tests and Standards Manual ASM International*, 1–20, 2004.

[18] Hibbitt, Karlsson, and Sorensen. *Abaqus/Standard User's Manual, Version 6.11*. Hibbitt, Karlsson & Sorensen, 2011.

[19] Jones, Kimberli and D.W. Hoeppner. "Prior corrosion and fatigue of 2024-T3 aluminum alloy". *Corrosion Science*, 48(10):3109–3122, 2006.

[20] Kachanov, M., B. Shafiro, and I. Tsukrov. *Handbook of Elasticity Solutions*. Kluwer Academic Publishers, 2003.

[21] Kachanov, M., B. Shafiro, and I Tsukrov. *Handbook of Elasticity Solutions*. Dordrecht: Kluwer Academic, 2003.

[22] Kim, S., J.T. Burns, and R.P. Gangloff. "Fatigue crack formation and growth from localized corrosion in AlZnMgCu". *Engineering Fracture Mechanics*, 76(0):651–667, 2009. ISSN 0013-7944.

[23] Koch, G.H. and E.L. Hagerdorn. "Effect of Pre-existing Corrosion of Fatigue Cracking of Aluminum Alloys 2024-T3 and 7075-T6". *Air Force Research Laboratory, WPAFB, OH*, 1995.

[24] Lados, D.A. and P.C. Paris. "Parameters and key trends affecting fatigue crack growth: A tribute to Professor Arthur J. McEvily's contributions". *Materials Science and Engineering: A*, 468-470(0):70 – 73, 2007. ISSN 0921-5093.

[25] Lee, Y. and S.G. Dorman. "Effect of chromate primer on corrosion fatigue in aluminum alloy 7075". *Procedia Engineering*, 10:1220–1225, 2011. ISSN 1877-7058.

[26] Lukas, P. and L. Kunz. "Small cracksnucleation, growth and implication to fatigue life". *International Journal of Fatigue*, 25(0):855–862, 2003. ISSN 0142-1123.

[27] Lynch, S.P. "Progression markings, striations, and crack-arrest markings on fracture surfaces". *Materials Science and Engineering: A*, 468-470(0):74–80, 2007. ISSN 0921-5093.

[28] Misak, H.E., V.Y. Perel, V. Sabelkin, and S. Mall. "Corrosion Fatigue Crack Growth Behavior of 7075-T6 under Biaxial Tension-Tension Cyclic Loading Condition". *Engineering Fracture Mechanics*, –, 2013. ISSN 0013-7944.

[29] Molent, L., S.A. Barter, P. White, and B. Dixon. "Damage tolerance demonstration testing for the Australian F/A-18". *International Journal of Fatigue*, 31:1031–1038, 2009. ISSN 0142-1123.

[30] Nan, Z.Y., S. Ishihara, and T. Goshima. "Corrosion fatigue behavior of extruded magnesium alloy AZ31 in sodium chloride solution". *International Journal of Fatigue*, 38:1181–1188, 2008. ISSN 0142-1123.

[31] Pao, P.S., P.S. Gill, and C.R. Feng. "On fatigue crack initiation from corrosion pits in 7075-T7351 aluminum alloy". *Scripta Materialia*, 43:391–396, 2000.

[32] Puso, M.A. and J. Solberg. "A stabilized nodally integrated tetrahedral". *International Journal for Numerical Methods in Engineering*, 67(6):841–867, 2006. ISSN 1097-0207.

[33] Ragazzo, C Hertzberg and R. Jaccard. "A Method for Generating Fatigue Marker Bands Using a Constant K_{max} Test Procedure." *Journal of Testing and Evaluation*, 23(1):8, 1995.

[34] Raju, L.S. and J.C. Newman Jr. "Finite Element Analysis of Corner Cracks in Rectangular Bars". *NASA Technical Memorandum*, TM-98070:1–47, 1987.

[35] Ro, Y., S.R. Agnew, G.H. Bray, and R.P. Gangloff. "Environment-exposure-dependent fatigue crack growth kinetics for AlCuMg/Li". *Materials Science and Engineering A*, 468-470:88–97, 2007. ISSN 0921-5093.

[36] Roberge, P.R. *Corrosion Engineering: Principles and Practice*. McGraw-Hill, 2008.

[37] Sankaran, K., K. R. Perez, and K.V. Jata. "Effects of pitting corrosion on the fatigue behavior of aluminum alloy 7075-T6: modeling and experimental studies". *Air Force Research Laboratory, WPAFB,OH*, 2000.

[38] Sarinova, S., A. Hassan, P.J. Martyn, and D.J. Smith. "Fatigue crack closure of a corner crack: A comparison of experimental results with finite element predictions". *International Journal of Fatigue*, 27(8):914 – 919, 2005.

[39] Szklarska-Smialowska, Z. "Pitting corrosion of aluminum". *Corrosion Science*, 41(9):1743 – 1767, 1999. ISSN 0010-938X.

[40] various. *Corrosion Fatigue: Mechanics, Metallurgy, Electrochemistry, and Engineering*. ASM International, 1983.

[41] various. *Metals Handbook, Vol.2 - Properties and Selection: Nonferrous Alloys and Special-Purpose Materials*. ASM International, 1990.

[42] various. *Handbook of Damage Tolerant Design*. United States Air Force, 2012.

[43] Wang, Q.Y, N. Kawagoishi, and Q. Chen. "Effect of pitting corrosion on very high cycle fatigue behavior". *Scripta Materialia*, 49(7):711–716, 2003.

[44] Wei, R.P. and Q. Chen. "Microconstituent-Induced Pitting Corrosion in Aluminum Alloy 2024-T3". *NACE International*, 52(1):8 – 15, 1996. ISSN 0010-9312.

[45] White, P., S.A. Barter, and C. Wright. "Small crack growth rates from simple sequences containing underloads in AA7050-T7451". *Internation Journal of Fatigue*, 31(0):1865–1874, 2009. ISSN 0142-1123.

[46] Xu-Dong, L., W. Xi-Shu, R. Huai-Hui, C. Yin-Long, and M. Zhi-Tao. "Effect of prior corrosion state on the fatigue small cracking behaviour of 6151-T6 aluminum alloy". *Corrosion Science*, 55:26–33, 2012.

[47] Zhao, L.G., J. Tong, and J. Byrne. "Stress intensity factor K and the elastic T-stress for corner cracks". *International Journal of Fracture*, 109:209–225, 2001.

REPORT DOCUMENTATION PAGE

Form Approved
OMB No. 0704–0188

1. REPORT DATE *(DD–MM–YYYY)*	2. REPORT TYPE	3. DATES COVERED *(From — To)*
13–06–2013	Master's Thesis	Oct 2011–Jun 2013

4. TITLE AND SUBTITLE

Crack Initiation and Growth Behavior at Corrosion Pit in 7075-T6 High Strength Aluminum Alloy

5a. CONTRACT NUMBER

5b. GRANT NUMBER

5c. PROGRAM ELEMENT NUMBER

6. AUTHOR(S)

Hunt, Eric M., Second Lieutenant, USAF

5d. PROJECT NUMBER

5e. TASK NUMBER

5f. WORK UNIT NUMBER

7. PERFORMING ORGANIZATION NAME(S) AND ADDRESS(ES)

Air Force Institute of Technology
Graduate School of Engineering and Management (AFIT/EN)
2950 Hobson Way
WPAFB, OH 45433-7765

8. PERFORMING ORGANIZATION REPORT NUMBER

AFIT-ENY-13-J-01

9. SPONSORING / MONITORING AGENCY NAME(S) AND ADDRESS(ES)

Office of Corrosion Policy and Oversight
Mr. Richard A. Hays, Deputy Director
3000 Defense Pentagon
Washington, DC 20301
richard.hays@osd.mil

10. SPONSOR/MONITOR'S ACRONYM(S)

OSD

11. SPONSOR/MONITOR'S REPORT NUMBER(S)

12. DISTRIBUTION / AVAILABILITY STATEMENT

DISTRIBUTION STATEMENT A:
APPROVED FOR PUBLIC RELEASE; DISTRIBUTION UNLIMITED

13. SUPPLEMENTARY NOTES

14. ABSTRACT

Research on fatigue crack formation from two types corrosion pits tangent to a circular hole in a 7075-T6 aluminum alloy subjected to uni-axial loads ($R = 0.5, \lambda = 0$) in both an air and saltwater environment provides a method for exploring crack initiation and initial growth rates. This work focuses on a fracture mechanics approach to explore the transition from corrosion pit to crack growth. Specimens with a cylinder shaped through-pit tangent to a circular hole have a closed form solution to predict this ΔK that closely resembles the finite element solutions. Specimens with a semi-circular corner-pit tangent to hole lack a closed form solution and finite element modeling was used to determine ΔK of these specimens. Optical and electron microscopy provided an accurate way to measure and observe the crack growth rate ($\frac{da}{dN}$) and the cycles until initiation of the fatigue cracks. This research shows that corner-pit specimens initially have a slower crack growth rate than through-pit specimens due to the propagation of a quarter-circular crack front through the thickness of the sample. After initial crack growth, both corner-pit and through-pit samples have the same growth rate as their machine notched counterparts exposed air and saltwater environments.

15. SUBJECT TERMS

corrosion, fatigue crack initiation, corrosion pit, finite element analysis, fracture mechanics

16. SECURITY CLASSIFICATION OF:			17. LIMITATION OF ABSTRACT	18. NUMBER OF PAGES	19a. NAME OF RESPONSIBLE PERSON
a. REPORT	b. ABSTRACT	c. THIS PAGE			Dr. Shankar Mall (ENY)
U	U	U	UU	124	19b. TELEPHONE NUMBER *(include area code)* (937) 255-3636 x4587 shankar.mall@afit.edu